

Utah State University

DigitalCommons@USU

All Graduate Theses and Dissertations

Graduate Studies

5-2004

Development and Characterization of Eukaryotic Biomimetic Liposomes

Bradley Jay Taylor
Utah State University

Follow this and additional works at: <https://digitalcommons.usu.edu/etd>



Part of the [Bacteriology Commons](#), [Cell Biology Commons](#), and the [Microbial Physiology Commons](#)

Recommended Citation

Taylor, Bradley Jay, "Development and Characterization of Eukaryotic Biomimetic Liposomes" (2004). *All Graduate Theses and Dissertations*. 5508.
<https://digitalcommons.usu.edu/etd/5508>

This Dissertation is brought to you for free and open access by the Graduate Studies at DigitalCommons@USU. It has been accepted for inclusion in All Graduate Theses and Dissertations by an authorized administrator of DigitalCommons@USU. For more information, please contact digitalcommons@usu.edu.



DESIGN AND CHARACTERIZATION OF
EUKARYOTIC BIOMIMETIC LIPOSOMES

by

Bradley Jay Taylor

A dissertation submitted in partial fulfillment
of the requirements for the degree

of

DOCTOR OF PHILOSOPHY

in

Nutrition and Food Sciences

Approved:

UTAH STATE UNIVERSITY
Logan, Utah

2004

Copyright © Bradley Jay Taylor 2004
All Rights Reserved

ABSTRACT

Development and Characterization of
Eukaryotic Biomimetic Liposomes

by

Bradley Jay Taylor, Doctor of Philosophy

Utah State University, 2004

Major Professor: Dr. Marie K. Walsh
Department: Nutrition and Food Sciences

This study developed and characterized phospholipid vesicles, or liposomes, that mimic cell surfaces. Microemulsified liposomes contained biotinylated phosphatidylethanolamine, allowing them to be immobilized to avidin-coated glass. Laminin (LN), glycosphingolipids (GM1 and GM3), and *Escherichia coli*'s mechanosensitive channel of large conductance (EcoMscL) were embedded into liposome membranes. It was determined whether these embedded molecules exhibited their physiological roles of adhesion, cell recognition, and mechanosensation, respectively. Confocal laser scanning microscopy (CLSM) was employed to examine the interaction of fluorescently probed proteins, toxins, and bacteria with the immobilized microemulsified liposomes. Capture of individual and simultaneous multiple species of bacteria by GM1, GM3, or LN liposomes was quantified using ELISA and PCR.

Surface-bound liposomes were unilamellar and immovable, allowing removal of unincorporated probes and biomolecules. Liposomes remained intact and stable against

leakage of encapsulated sulforhodamine B for several months after immobilization.

Functional reconstitution of EcoMscL was examined using CLSM during modulations in the immersing solution.

Cholera toxin (β subunit) (CTB), bovine lactoferrin (BLF), and *E. coli* O157:H7 were co-localized proximate to the surface of GM1 liposomes. ELISAs determined *E. coli* O157:H7 and *Salmonella enteritidis* were captured on GM1 liposomes containing GM1 at 8.9 molar percent of total lipid. *Listeria monocytogenes* and *Listeria innocua* were not captured on the same liposomes.

PCR identified the capture of specific bacterial species from individual species and mixtures of several species on liposomes. Simultaneous assays with mixtures of multiple species showed that the receptor-associated binding of bacteria, described with PCR assays of an individual species, were independent of competitive microorganisms. *L. monocytogenes* and *L. innocua* were more frequently bound to LN liposomes than other liposomes, indicating LN promotes adhesion of both the pathogenic and a non-pathogenic strain of *Listeria*. *E. coli* O157:H7 was more frequently captured on GM1 liposomes than other liposomes, indicating a specificity for this bacteria. *S. enteritidis* bound to all liposomes, indicating a non-specific interaction.

Known eukaryotic biomolecules implicated in cell recognition, adhesion, and mechanosensation were embedded in a system of artificial bilayers immobilized on a solid support. Liposomes constitute a biomimetic capable of specifically interacting and capturing proteins, toxins, and bacteria in solution.

ACKNOWLEDGMENTS

I owe deep and sincere gratitude to Dr. Marie Walsh for her guidance, support, friendship, trust, and excellent competence. I extend my gratitude to the members of my committee, Drs. Bart Weimer, Donald McMahon, Timothy Gilbertson, and Charles Carpenter, for their expert advice in the course of my project and in preparation of this manuscript and other manuscripts. I thank Dr. Chris Corcoran for helping with the categorical data analysis. I acknowledge financial support received from the Gandhi fellowship, Western Dairy Center, Center for Microbial Detection and Physiology, and School of Graduate Studies at Utah State University. In addition, I acknowledge Dr. Lynn Ogden and the faculty of the Department of Food Science and Nutrition at Brigham Young University, who encouraged me and prepared me for graduate studies.

This goal would be yet unrealized were it not for the encouragement and support of my true love, Ie Mei. Her emotional and intellectual support cannot be underestimated. Without her constant enthusiasm and support at home, this study would surely be unfinished. We will look fondly back on the years in Logan and try to forget the sleepless nights with our preemies, Jackson Jay and Lance Logan. Though this time has been very enlightening and worthwhile, we hope life after school will be all the more fulfilling.

I am indebted to my parents, Anne and Jay Taylor, who taught their boys to work diligently at whatever we set out to accomplish. Mom and Dad, you have provided experiences, resources, opportunity, and love second to none. Your parenting efforts and prayers on my behalf are recognized and greatly appreciated. I hope to somehow express

the appreciation I feel for my deceased grandfather, Dr. Wayne Binns, who is an inspiration as a scientist and individual. Grandpa, thanks for making our stay in Cache Valley so comfortable and I hope to make you proud. Each of my grandparents is deserving of acknowledgment for their examples, direction, assistance, and love. Thanks to Ralph and Jane Binns for watching over us as surrogate parents during graduate school.

Many thanks to the many labmates who helped in developing the skills necessary to perform this work, critically evaluate it, and have a good time doing it. I especially thank David Taylor, Brian Pettee, Seung-Hee Nam, Andrea Hale, Wim Lippens, Paul Joseph, Seth Putnam, Karin Allen, Emily Harrington, Xie Yi, Lan-Szu Chou, and Marsha Hellquist. Each of you has contributed to this work. I acknowledge the faculty and staff of the Departments of Nutrition and Food Science; Biology; Animal, Dairy and Veterinary Science; and Statistics, who helped me along the way and treated me with respect and kindness throughout my tenure. There are many friends and family who are also acknowledged for their love and support.

Finally, I acknowledge the hand of The Master in all things. He has watched over my family. To Him I will be eternally grateful for affording us the many opportunities life has presented us, comforting us when we need comforting, and helping us develop our formula for happiness in this life and the life to come.

Bradley Jay Taylor

CONTENTS

	Page
ABSTRACT.....	iii
ACKNOWLEDGMENTS.....	v
LIST OF TABLES.....	xi
LIST OF FIGURES.....	xiii
LIST OF SYMBOLS, NOTATION, AND DEFINITIONS.....	xv
CHAPTER	
I. INTRODUCTION AND LITERATURE REVIEW	1
INTRODUCTION.....	1
LITERATURE REVIEW.....	5
Liposomes: Current Methodologies.....	5
Reconstituted EcoMscL and Glycolipids in Liposomes	9
Liposome Interaction and Binding Studies.....	10
Bacterial and Toxin Pathogenesis Initiated by Adhesion.....	11
Glycoproteins and Glycolipids.	13
Molecular Interactions Between Bacteria and Their Toxins with Host Cells.....	15
Pathogen Detection: Current Methodologies	23
Advances in Microscopy:	
Confocal Laser Scanning Microscopy.....	28
NULL HYPOTHESIS.....	29
RESEARCH OBJECTIVES.....	29
REFERENCES.....	30
II. IMMOBILIZATION OF BIOMIMETIC LIPOSOMES.....	39
ABSTRACT.....	39
INTRODUCTION.....	40
MATERIALS AND METHODS.....	45
Liposome Formulation Materials.....	45
Unilamellar Micoemulsified Liposome Formulations.....	45

Avidin and Microemulsified Liposome Immobilization.....	47
Immobilized Liposome Stability Determination.....	48
Fluorescent Labeling of Proteins.....	48
ELISAs for GM1 and LN Liposomes.....	48
Soluble Protein Binding Studies.....	50
Confocal Laser Scanning Microscopy.....	51
RESULTS AND DISCUSSION.....	52
Composition of Liposomes.....	52
Immobilized Liposome Formulations.....	53
Optimizing SRB Concentration.....	56
Characterization and Stability of Liposomes.....	57
Binding of Soluble Proteins.....	61
CONCLUSIONS.....	63
REFERENCES.....	64
III. CHARACTERIZATION OF IMMOBILIZED MICROEMULSIFIED LIPOSOMES CONTAINING ESCHERICHIA COLI'S MECHANOSENSITIVE CHANNEL OF LARGE CONDUCTANCE (MscL) USING CONFOCAL LASER SCANNING MICROSCOPY.....	78
ABSTRACT.....	78
INTRODUCTION.....	79
MATERIALS AND METHODS.....	82
Unilamellar Microemulsified Liposome Composition and Preparation.....	82
Immobilization and Stability of Liposomes.....	84
PCR, Cloning, and Sequencing of EcoMscL.....	84
<i>E. coli</i> Cell Growth and EcoMscL Induction.....	85
EcoMscL Fusion Protein Purification.....	86
Fluorescent Protein Labeling.....	87
Liposome Formulations Containing EcoMscL.....	87
Confocal Laser Scanning Microscopy.....	88

RESULTS.....	90
Unilamellar Microemulsified Liposome	
Composition and Preparation.....	90
Immobilization and Stability of Liposomes.....	90
PCR, Cloning, and Sequencing of EcoMscL	92
<i>E. coli</i> Cell Growth and EcoMscL Induction.....	92
Protein Fraction Purification.....	92
Fluorescent Labeling and Liposome Formulations	
of EcoMscL.....	93
Confocal Laser Scanning Microscopy.....	94
DISCUSSIONS AND CONCLUSIONS.....	97
REFERENCES.....	101
IV. BIOMIMETIC BINDING OF <i>ESCHERICHIA COLI</i> O157:H7, <i>SALMONELLA ENTERITIDIS</i> , <i>LISTERIA MONOCYTOGENES</i> , AND <i>LISTERIA INNOCUA</i> WITH EUKARYOTIC UNILAMELLAR IMMOBILIZED MICROEMULSIFIED LIPOSOMES.....	110
ABSTRACT.....	110
INTRODUCTION.....	111
MATERIALS AND METHODS.....	115
Immobilized Microemulsified Liposomes.....	115
Avidin Immobilization.....	116
Bacterial Strains and Growth Conditions.....	116
Liposome Capture and Sample Preparation for	
ELISAs and PCR Detection.....	117
Antibodies	117
ELISAs.....	118
Liposome Capture and PCR Analysis.....	119
Confocal Laser Scanning Microscopy.....	122
Statistical Analysis.....	123

RESULTS AND DISCUSSION.....	124
Avidin Immobilization Optimization and Liposomes Characterization.....	124
Individual Species Capture ELISAs.....	126
Liposome Capture with PCR Identification.....	128
Exact Analysis of <i>E. coli</i> O157:H7 Capture.....	131
Exact Analysis of <i>S. enteritidis</i> Capture.....	132
Exact Analysis of <i>L. monocytogenes</i> Capture.....	132
Exact Analysis of <i>L. innocua</i> Capture.....	133
Simultaneous Capture of <i>E. coli</i> O157:H7 and <i>S. enteritidis</i>	134
CONCLUSIONS.....	135
REFERENCES.....	137
V. SUMMARY AND CONCLUSIONS.....	154
NULL HYPOTHESIS.....	154
OBJECTIVES.....	155
CONCLUSIONS.....	160
FUTURE RESEARCH.....	161
APPENDICES.....	163
APPENDIX A. LIPOSOME IDENTIFICATION LEGEND.....	164
APPENDIX B. PRIMERS FOR PCR IDENTIFICATION IN CHAPTER IV.....	165
APPENDIX C. ELISA ABSORBANCE VALUES FOR CHAPTER IV STATISTICAL ANALYSIS (T-TESTS).	166
CURRICULUM VITAE.....	172

LIST OF TABLES

Table	Page
1	Percent of immobilized microemulsified biomimetic liposomes observed leaking SBR by day.....68
2	Binding interactions between surface containing immobilized microemulsified liposomes containing GM1 or laminin and soluble proteins.....69
3	Percent pixel reduction of probes labeling three types of immobilized microemulsified liposome populations during gradients over time.....104
4	Individual species and simultaneous multiple species capture verified by PCR.....141
5	Simultaneous capture of <i>E. coli</i> O157:H7 and <i>S. enteritidis</i> verified by PCR.....142
6	Exact analysis probability values for inoculation level and liposome type in both the individual and simultaneous multiple species incubation format for the capture of <i>E. coli</i> O157:H7, <i>S. enteritidis</i> , <i>L. monocytogenes</i> , and <i>L. innocua</i> in an overall test for significance ($p < 0.05$).....143
7	Exact analysis probability values for inoculation level and liposome type in both the individual and simultaneous multiple species incubation format for the capture of <i>E. coli</i> O157:H7, <i>S. enteritidis</i> , <i>L. monocytogenes</i> , and <i>L. innocua</i> in testing for significance of individual effects ($p < 0.05$).....144
8	Exact analysis probability values for inoculation level of <i>E. coli</i> O157:H7, liposome type, and inoculation level of <i>S. enteritidis</i> in the simultaneous species incubation format for the capture of <i>E. coli</i> O157:H7 or <i>S. enteritidis</i> in an overall test of significance ($p < 0.05$).....145

Table

9	Exact analysis probability values for inoculation level of <i>E. coli</i> O157:H7, liposome type, and inoculation level of <i>S. enteritidis</i> in the simultaneous species incubation format for the capture of <i>E. coli</i> O157:H7 and <i>S. enteritidis</i> in testing for significance of individual effects ($p < 0.05$).....	146
---	--	-----

LIST OF FIGURES

Figure	Page
1	Amphiphilic structure of ganglioside GM1.....37
2	Amphiphilic structure of ganglioside GM3.....38
3	Field of unilamellar microemulsified liposomes embedded in agarose matrix directly after microemulsification.....70
4	Field of immobilized unilamellar microemulsified liposomes immobilized directly after microemulsification.....71
5	Liposomes microfluidized with 0.45, 450, and 45 μ M SRB (SRB : total lipid molar ratios of 0.011 : 1, 11 : 1, and 1.1 : 1), respectfully A, B, and C.....72
6	SRB leaking from compromised membrane bound CNF-LN liposome.....73
7	SRB leaking from compromised CNF-BSA liposome.....74
8	SRB leaking from compromised GM1 liposome.....75
9	Field of CNF-BSA liposomes leaking SRB and CNF-BSA.....76
10	GM1 liposomes after interaction with CNF-CTB, CNF-BLF, CNF-BSA, and CNF-ovalbumin, respectively A, B, C, and D.....77
11	Two <i>xy</i> images collected in series of four unilamellar immobilized microemulsified liposomes scanned 0.8 μ m apart along the <i>z</i> plane (A and B).....105
12	Immobilized unilamellar immobilized microemulsified EcoMscL liposomes.....106
13	SDS-PAGE gel of EcoMscL protein fraction purification.....107
14	SDS-PAGE gel of EcoMscL protein fraction released after lysozyme treatment.....108

Figure

15	Four xy images collected of a field of unilamellar immobilized microemulsified liposomes representing a time series during the application of a 0–4 M NaCl gradient over the course of 270 s (A-D).....	109
16	Field of DiD oil labeled immobilized unilamellar microemulsified GM3 liposomes immobilized directly after microemulsification.....	147
17	Field of immobilized GM3 unilamellar microemulsified liposomes immobilized directly after microemulsification labeled with WGA conjugated Alexa-Flour® 660 (blue).....	148
18	Individual species capture of <i>E. coli</i> O157:H7 with liposomes of five GM1 concentrations verified by ELISA.....	149
19	Individual species capture of and <i>S. enteritidis</i> with liposomes of five GM1 concentrations verified by ELISA.....	150
20	Individual species capture of <i>E. coli</i> O157:H7, <i>S. enteritidis</i> , <i>L. monocytogenes</i> , <i>L. innocua</i> with GM1 liposomes verified by ELISA.....	151
21	Capture of <i>S. enteritidis</i> with laminin, GM1 or GM3 liposomes.....	152
22	Captured <i>E. coli</i> O157:H7 bacterium (orange/red) on GM1 liposomes (blue/magenta).....	153

LIST OF SYMBOLS, NOTATION, AND DEFINITIONS

Abbreviation Key

Ab	Antibody
AP	Alkaline phosphatase
Amp	Ampicillin
APTES	3-Aminopropyltriethoxysialne
B-PER	Bacterial protein extraction reagent
BAM	Bacterial analytical manual
BCA	Bicinchoninic acid
BHI	Brain heart infusion broth
Biotinyl-PE	1,2 Dioleoyl- <i>sn</i> -glycero-3-phosphoethanolamine- <i>N</i> -(Biotinyl)
BLF	Bovine lactoferrin
β -ME	Beta-mercaptoethanol
Bp	Base pairs
BSA	Bovine serum albumin
cAMP	Cyclic adenosine monophosphate
CLSM	Confocal laser scanning microscopy
CNF	5-(and-6)-carboxynaphthofluorescein
CFU	Colony forming units
cGMP	Cyclic guanosine monophosphate
Con-A	Concanavalin A
CT	Cholera toxin

CTB	Cholera toxin (beta-subunit)
DiD oil	1,1'-dioctadecyl-3,3',3',3'- tetramethylindodicarbocyanine perchlorate
DNA	Deoxyribonucleic acid
EcoMSCL	<i>Escherichia coli</i> 's mechanosensitive channel of large conductance
EcoMSCS	<i>Escherichia coli</i> 's mechanosensitive channel of small conductance
EcoMSCM	<i>Escherichia coli</i> 's mechanosensitive channel of mini conductance
EDC	1-ethyl-3-(3-dimethylaminopropyl) carbodiimide hydrochloride
EDTA	Ethylene diamine tetraacetic acid
EHEC	Enterohemorrhagic <i>Escherichia coli</i>
EIA	Enzyme immunosorbent assay
ELISA	Enzyme-linked immunosorbent assay
EPEC	Enteropathogenic <i>Escherichia coli</i>
ETEC	Enterotoxigenic <i>Escherichia coli</i>
Fluorescein-PE	1,2-dioleoyl- <i>sn</i> -glycero-3-phosphoethanolamine (Carboxyfluorescein)
GM1	Monosialoganglioside GM1
GM3	Monosialoganglioside GM3
HUS	Hemolytic uremic syndrom
kDa	Kilodaltons
LB	Luria broth
LN	Human laminin
LT	Heat-labile toxin of enterotoxigenic <i>Escherichia coli</i>
MES	2-(<i>N</i> -morpholino)-ethanesulfonic acid monohydrate

MCH-PCR	Magnetic capture hybridization polymerase chain reaction
NBD-PE	1,2-dioleoyl- <i>sn</i> -glycero-3-phosphoethanolamine- <i>N</i> -(7-nitro-2-1,3-benzoxadiazol-4-yl)
OVA	Ovalbumin
PAGE	Polyacrylamide gel electrophoresis
PC	Phosphatidylcholine
PCR	Polymerase chain reaction
PE	Phosphatidylethanolamine
PG	Phosphatidylglycerol
PLA2	Phospholipase A2
pNPP	Para-nitrophenyl phosphate
RGB	Red green blue
SDS	Sodium dodecyl sulfate
Sialic acid	<i>N</i> -acetylneuraminic acid
SLTEC	Shiga-like toxin-producing <i>Escherichia coli</i>
SPM	Sphingomyelin
SRB	Sulforhodamine B
ST	Heat-stable toxin of enterotoxigenic <i>Escherichia coli</i>
STx	Shiga toxin
Sulfo-NHS	<i>N</i> -Hydroxysulfosuccinimide
TAE	Tris HCL acetate containing EDTA
Tris	Trizma hydrochloride
WGA	Wheat germ agglutinin

CHAPTER I

INTRODUCTION AND LITERATURE REVIEW

INTRODUCTION

Scientists are now learning to produce more complex materials and machines inspired by what is seen in nature. The most remarkable and technologically attractive differences between natural and synthetic materials are the great hierarchical complexity and multifunctionality of natural materials. New materials are being synthesized, not identical to, but patterned after or analogous to those in plants, animals, and microorganisms. These biomimetic structures respond to biologic stimuli similar to their natural counterparts. Technology is advancing at an unprecedented pace and scientists see the need for more advanced materials for medically exploring and manipulating the normal and ailing human body. Deep oceanic and space exploration require new, dynamic, and complex instrumentation using advanced materials.

Biomimetics are human-made processes, substances, devices, or systems that imitate or mimic nature. The art and science of designing and building biomimetic apparatus is called biomimetics, and is of special interest to researchers in nanotechnology, robotics, artificial intelligence, and medicine. Biomimetics are changing molecular biology research and look to replace it as the most challenging and important biological science of the 21st century [1]. This revolution is the extension of the directions and achievements in the engineering design of composite materials and robotics. Molecular biology contributes to this goal. The achievement of this goal will

result from renewed vigor in basic research on the mechanisms of the function of cells, tissues, organs, organ systems, and the organisms of which they are parts.

This study focused on developing and characterizing a liposome-based system designed to mimic cell surfaces by incorporating molecules into artificial bilayers, which retained biological activity *in vitro*. Biomimetic liposomes composed of lipids and proteins imitating those found in human systems, were immobilized onto a glass surface. The physiological activity of membrane proteins and glycosphingolipids in lipid bilayers was examined using confocal laser scanning microscopy (CLSM). The information garnered from this research may lead to the development of beneficial biosensors to study molecular interactions of proteins, lipids, and microorganisms. A biosensor, based on similar technology, which captures and detects multiple medically important pathogenic agents and proteins, would reduce time requirements for presumptive positive tests to minutes rather than hours or days as are currently required. Specifically, increased understanding immobilized liposomes is necessary before liposome-based biosensors can be developed.

The liposomes and membrane bound proteins featured in this study, functioned as a dynamic system immobilized covalently on the surface of glass that responded to external chemical and physical stimulation. CLSM was used to visualize and characterize immobilized microemulsified liposomes. Surface-available receptor molecules, Monosialoganglioside GM1 (GM1) or laminin (LN), anchored in the artificial lipid bilayers of the liposomes, were exposed to solutions containing fluorescently-labeled proteins. Subsequently, interactions of proteins or bacteria and liposomes, indicated by co-localization of probes, were studied. Similarly, the interaction between

liposomes and viable bacteria in solution was studied using CLSM, enzyme-linked immunosorbant assays (ELISAs) and polymerase chain reaction (PCR) identification methods. Finally, CLSM was utilized to study the physiological response of proteins embedded in the lipid bilayer (*Escherichia coli*'s mechanosensitive channel of large conductance, denoted EcoMscL). New CLSM methodologies were developed to observe interactions between bacteria interacting with specific eukaryotic receptor molecules at the surface of liposomes. The capture and interactions of these bacteria with gangliosides (GM1 and GM3) and receptor protein LN was observed and imaged using CLSM supported by PCR identification and ELISAs. Standard t-tests and logistic regression were used to statistically analyze microbial binding of immobilized biomimetic liposomes.

Antibodies are commonly used as capture molecules in molecular biology for biosensors because they offer a high degree of specificity. The most well known commercial example of an antibody-based detection system is the home pregnancy test. The commercially available products are based on an ELISA developed for the measurement of microamounts of substances in samples, in this case, human chorionic gonadotropin in urine. The specificity of an ELISA makes these tests useful in routine analytical determinations regarding many small molecules and even bacteria such as foodborne pathogens. It is desirable to replace antibodies with other capture molecules due to their susceptibility to degradation in dynamic environmental conditions (i.e., low or high pH, low water activity, and ionic strength). Antibodies are also subject to variation among lots, leading to inconsistent binding of antigens in routine laboratory tests.

Replacement of antibodies with other capture molecules is a paradigm shift because alternative molecules may lack the required binding and specificity. Molecular mechanisms resulting in recognition and attachment to host cells are remarkably specific and exquisitely sensitive. The approach in this work exploited molecular complementarity between the signal and receptor molecules mediated by noncovalent forces that occur in enzyme-substrate and antigen-antibody interactions. The mechanism of molecular pathogenesis by bacteria and viruses occurs via specific receptors in the host cell membrane and exposed to the cell surface. Eukaryotic cell binding is a prerequisite to invasion and pathogenesis by microbes and toxins. While many types of cell surface interactions can occur, glycoproteins and glycolipids are the most common receptors for pathogens [2]. Membrane receptors of microbial pathogens include proteins, phospholipids, and glycolipids [3].

Glycosphingolipids' relative stability and binding make them attractive antibody replacement molecules. Glycosphingolipids are stable to drying, stable in organic solvents, and bind bacteria including emerging and bioengineered pathogens. These complex lipids also have protein (toxins, hormones, etc.) and bacterial association constants that are similar when compared to antibodies specific for the same antigen. The association constant between toxins and various gangliosides ranges from 10^5 to 10^8 M^{-1} [4] and dissociation constants up to 10^{10} M have been reported [5]. Therefore, these interactions are at least as strong as antibody/antigen complexes and are sufficiently strong to capture and tightly hold bacteria and proteins (toxins, hormones, etc.). As multiple bacterial species recognize and tightly bind membrane receptors, liposomes embedding gangliosides or glycoprotein molecules can be used to capture cells in a

mixed culture. In contrast, antibodies are specific for a single antigen and therefore are ineffective in capturing multiple species in mixed cultures.

The environment to which it is exposed influences the system developed and characterized during the course of the study, consisting of immobilized liposomes on glass. The modified glass surface facilitates imaging using progressive CLSM techniques. Liposomes are located a finite distance from the glass solid surface after immobilization via the avidin biotin complex. This introduces an element of spatial control resulting in the ability to view multiple liposomes in a single xy plane. Immobilization also allows unencapsulated and unincorporated materials to be physically removed via wash steps leaving the surface and liposomes, including encapsulated and embedded molecules of interest, intact. CLSM provides a means for the direct observation and characterization of microbes and proteins before, during, and after attachment [6]. It allows for direct monitoring of the liposomes during a variety of experimental conditions.

LITERATURE REVIEW

Liposomes: Current Methodologies. A liposome is a small capsule, made of phospholipids. Phospholipids are unique in that half of the molecule is soluble in water and half is not. Phospholipids form stable sheets of molecules in solution, in which the polar heads point outwards interacting with the aqueous solution and the nonpolar hydrophobic tails associate together in the middle of the sheet. A dynamic, intrinsically stable sphere vesicle is formed trapping water in the interior. This aqueous phase of the

vesicle is encapsulated by a single artificial lipid bilayer. The bilayer consists of an ordered sheet two molecules thick measuring approximately 47Å [7]. A vesicle defined by an ordered bilayer sheet of phospholipids is a unilamellar liposome. Multilamellar liposomes contain multiple bilayers of phospholipids stacked inside each other.

Liposomes have been used to deliver drugs, notably peptide drugs, because they offer protection from digestion in the stomach thereby ensuring delivery and absorption in the intestine, where they are absorbed. A specific organ can be targeted using liposomes either absorbed or injected into the blood stream. In the latter example, the organ recognizes the lipids and specifically absorbs them and the encapsulated contents.

Trapping molecules in liposomes is a form of encapsulation, and as such can be used in many other areas including biosensors. In the past liposome biosensor applications have relied on the high-electrical resistance of bilayer films or optical properties of films. Electrical sensors utilizing liposomes are based on the ability of some proteins to carry ions across a lipid membrane. Some membrane and transport proteins can be inserted into the artificial bilayer of a liposome allowing cross-membrane movement involving molecules inside or outside the liposome while maintaining the integrity of the sphere. The protein allows an amino acid, a protein, or simply ions to cross the membrane. The membrane conducts current in the presence of both charged molecules and a transport protein. In the absence of the transport protein, the membrane has a much higher resistance, because there is no path for any other charged species to cross. Thus the membrane can be used as a very sensitive detection system.

Optical sensors involving liposomes rely on the interference effects of these bilayers on reflected light. Light reflectance is critically dependent upon the thickness of

these ultra thin layers. When complexes form at the surface of the artificial bilayer (i.e. antibodies covalently bound to the bilayer binding antigens in solution) the thickness of the liposome bilayer is increased and this event can be detected optically.

The weakness of liposome based sensors stems from their mechanical and chemical instability. Many of the potentially useful proteins for liposome based biosensors are also chemically unstable or sensitive. Thus, liposome properties have been demonstrated in laboratories for some very simple, model systems. Only recently have results translated into any realistic sensor applications [8].

Liposomes are used extensively in the laboratory for diverse research, diagnostic and pharmacologic applications. The application and extension of research involving liposomes are limited by lack of technology allowing the reproducible manufacture of liposomes of predictable and uniform size. A variety of different approaches including freeze-thaw, reverse phase evaporation, sonication, and extrusion have been described for preparing liposomes [9-15]. Use of liposomes in drug delivery as target carriers of drugs and enzymes is extensively studied in pharmaceutical and cosmetic industries [12, 16, 17].

Unilamellar vesicles are more appealing than multi-lamellar vesicles (MLVs) when developing *in vitro* models of lipid bilayers. One concern with MLVs is that the interaction between different bilayers, which is absent in unilamellar vesicles and most membranes, might alter the bilayer structure. Interactions between unilamellar bilayers are too small to affect the fully hydrated bilayer structure of microemulsified liposomes because the water layer is appreciable [18]. Characterization of liposomes prepared using a microemulsifier found that using the principles of fluid dynamics, unilamellar

liposomes are created in a reproducible manner [19, 20]. Using the microfluidizing method, liposomes are prepared in amounts sufficient for pharmaceutical quality assessment, toxicological studies and multicenter clinical trials [20]. The automated high-pressure system uses a "microemulsion" process available commercially as the Microfluidizer™ (Microfluidics Corp., Newton, MA, USA). Microfluidization of lipids results in uniform lipid vesicle dispersions with the ability to encapsulate bioactive macromolecules. The encapsulation and protective effect of the liposome vesicle is only effective for a finite period of time. Compromised microemulsified liposomes leach or leak encapsulated material.

MELs, or microemulsified liposomes, generally contain phosphatidylcholine (PC), phosphatidylethanolamine (PE), phosphatidylglycerol (PG), sphingomyelin (SPM), cholesterol and triacylglycerols. Glycosphingolipids, including gangliosides, can be incorporated into liposomes during their formation since they contain a hydrophobic moiety [21]. Viruses fuse with liposomes containing PC : PE:cholesterol (1 : 1 : 1.5) and SPM [22]. Phospholipids, PE and PC can be derivatized to contain biotin or an amino functional group that can then be used to covalently link the liposomes to a glass surface. Currently, most liposomes are noncovalently adsorbed to plastic surfaces. Adsorption has many drawbacks, including establishment of an equilibrium with the liquid media, thus desorption is common. Immobilization facilitates wash steps and removal of unincorporated and weakly associated lipids, probes, and vesicles.

Glycolipids can be directly immobilized to a surface, or be incorporated into a liposome, which is then attached to a surface. Various chemistries are available for the covalent attachment to derivatized glass surfaces [23, 24]. Typically glass is silanized to

provide an active attachment site on the glass, such as derivatization with 3-aminopropyl-triethoxysilane (APTES) to generating free amino groups. APTES beads can be succinylated with succinic anhydride to generate surface carboxyl groups. For the immobilization of gangliosides, saponification generates a free amino group to conjugate the ganglioside to succinylated glass using water-soluble carbodiimide. This forms a covalent link between the ganglioside and the glass surface. Similar methods can be used to covalently attach avidin to glass via the formation of a stable amide bond [23].

Reconstituted EcoMscL and Glycolipids in Liposomes. For many years it has been assumed that the permeability of the lipid bilayer was sufficient to allow the rapid equilibration of water during dramatic changes in the osmolarity of the medium. Over the past several years it has been established that bacteria have in their cytoplasmic membranes relatively large mechanosensitive channels. In *E. coli* at least three channels of different physical dimensions and conductances have been identified by patch clamp techniques [25]. The channels display little ion or solute preference with ions moving in both directions through channels. Osmolites that migrate through channels include: K^+ , ATP, compatible solutes, glutamate. At neutral pH, *E. coli* cells recover rapidly from the transient opening of the channels, but are completely inhibited by sustained activity [25].

The proposed role of mechanosensitive channels is protection of the integrity of the cell. Two conditions generate high turgor in the cell: the accumulation of compatible solutes, or "osmotic balancing," and the transfer of the cell into media of lower osmolarity. In both cases the cell responds with the release of solutes from the cytoplasm to reduce the turgor pressure. The discovery of the genes coupled with membrane reconstitution of the three identified mechanosensitive channels of large, small, and mini

conductance (respectively termed MscL, MscS, and MscM) in *E. coli* has elucidated the roles of the Msc channels in the physiology of *E. coli* [25]. The MscL and MscS channels of *E. coli* remain active after solubilization and reconstitution into liposomes [26]. EcoMscL has the highest pressure threshold for activation and numerous reports have shown that the EcoMscL protein is probably a pentamer of 17 kDa subunits that form a 3 nS conductance [27]. The size of this channel is such that the small protein thioredoxin can exit the cell via this channel during hypoosmotic shock [25, 27, 28].

EcoMscL has been reconstituted into large, and apparently unilamellar, blisters formed on the surface of multilayer liposomes for patch-clamp experiments [28]. Other methods include: 1) disrupting bacterial membranes by French-press and reconstituting EcoMscL into patchable artificial liposomes, 2) solubilizing bacterial membranes in the detergent octylglucoside followed by reconstitution into liposomes and dialysis to remove the detergent, and 3) after detergent solubilization, EcoMscL can then be purified by affinity chromatography and reconstituted into artificial liposomes [29-34]. The protein's biological activity can be monitored after incorporation in artificial bilayers.

EcoMscL is a thermostable protein and does not undergo any unfolding of its secondary structure between 25-95°C [29]. High thermal stability is common for membrane proteins. Its structure is highly helical with roughly 111 amino acids in α -helical configuration oriented in a net transbilayer orientation. Only one-third of the protein is protected from amide H⁺/D⁺ exchange by the lipid bilayer [29, 30].

Liposome Interaction and Binding Studies. Concanavalin A (Con-A) has been studied in a liposome-based model system for the simulation of lectin-induced cell adhesion using CLSM [35]. The liposomes were extruded (Extruder, Lipex

Biomembrane, Vancouver, Canada) 6 times through a 400 nm polycarbonate membrane (Costar, Bodenheim, Germany). A head-group labeled phospholipid, 7-nitro-2-1,3-benzoxadiazol-4-yl phosphatidylethanolamine (NBD-PE), was incorporated into all preparations at a concentration of 1 mol% [35]. Con-A was coupled by covalent linkage to a hydrophobic anchor and found in large unilamellar vesicles formed through extrusion. The liposomes in the model were able to simulate the lectin-mediated adhesion of cells in a shear flow [35].

A general method for measuring interaction of liposome-protein (or potentially small molecules) without the use of CLSM was developed utilizing biotinylated liposomes to incubate with interactants [36]. Streptavidin-coated paramagnetic resins were added to the liposomes and then quickly separated using a magnetic field or slow speed centrifugation. The concentration of unbound materials in the supernatants was directly determined [36].

Bacterial and Toxin Pathogenesis Initiated by Adhesion. Bacterial and protein (toxin) pathogenesis is often initiated by the attachment of the pathogen to the surface of the host cell [37, 38]. Attachment, or adhesion, occurs by a variety of mechanisms that depend on the pathogen species or toxin and host cell type, and can result in subsequent internalization of the pathogen or toxin by phagocytosis or by endocytosis. In most cases, host and pathogen cells, or toxins, participate in this adhesion process, and activate or modify host cell signaling pathways [39, 40]. Stimulation of these signaling pathways can lead to enhancement of pathogen attachment or invasion. Signaling is mediated through a variety of cell surface receptors.

Adhesion involves components of both the pathogen and host cell, and can lead to internalization of the pathogen. Bacterial pathogens produce molecules or macromolecular structures that are generally referred to as adhesins [41-43]. Adhesins are grouped into two broad classes termed fimbrial (pili or pili-like) adhesins which are filamentous structures and afimbrial adhesins which are usually proteins and account for most other adherence molecules [44]. The adhesin molecules or structures specifically interact with host cell receptors to facilitate attachment and subsequently invasion. Examples of bacterial adhesins include invasins (*Yersinia* spp.), internalins (*Listeria* spp.), MarkD (*K. pneumoniae*), and FimH (*Salmonella* spp.) [38, 43, 45].

There are a variety of mammalian cell surface receptors that interact with bacterial adhesins. These receptors can be proteins (integrins, cadherins, LN, fibronectin, and type V collagen), glycolipids such as gangliosides, or carbohydrates such as *N*-acetylneuraminic acid (sialic acid) [35, 46-48]. They can act alone or in combination with additional receptors. Advances in cellular microbiology have revealed some of the specific molecular events that occur following attachment of adhesins to these receptors. Among the changes that often occur in the host cell after pathogen binding are modifications of multiple signal transduction pathways and remodeling of the cytoskeleton [47].

There are two identified general mechanisms by which pathogenic bacteria invade non-phagocytic host cells. Both involve significant alterations in host cell signal transduction and rearrangement of the actin filaments. Some *Salmonella* and *Shigella* species utilize a "trigger" mechanism characterized by the induction of host cell protrusions that "reach up and around" the pathogen and ultimately leads to invasion into

the host cell [3]. *Listeria monocytogenes* and *Yersinia pseudotuberculosis* utilize a “zipper” mechanism where the pathogen presumably slides or zips into the cell surface to accomplish invasion [39, 47]. Both the “trigger” and “zipper” mechanisms are initiated with modifications of host signal transduction pathways that lead to major local rearrangements of the actin cytoskeleton [39, 49, 50]. *Salmonella typhimurium*, a close relative of *E. coli*, is an enteric pathogen that is easily cultivated and genetically manipulated. As an extremely valuable tool for studying invasion and intracellular survival, this *Salmonella* species has enabled researchers to identify and characterize many of the factors involved in these processes [49, 50]. *Salmonella* species produce a number of adhesins. These include type 1 fimbriae, plasmid-encoded fimbriae, long polar fimbriae and thin aggregative fimbriae.

Glycoproteins and Glycolipids. Most of the proteins present on the surface of cells, viruses, and in the blood of animals are glycosylated. Sugars can be linked onto the proteins through the amide groups of asparagine in the short peptide sequence Asn-X-Ser/Thr, or more rarely, through the hydroxyl of serine and threonine. Therefore the extent of glycosylation can be predicted from a protein’s amino acid sequence, therefore from the sequence of its gene.

Such glycosylation is a form of co- and/or post-translational modification, meaning modification of the protein’s chemistry during or after translation. Other protein glycosylation, termed glycation, is chemical and occurs whenever a protein is exposed to sugar in solution for a considerable amount of time.

Although proteins have well-defined glycosylation sites where carbohydrate moieties are added, which carbohydrate moiety is coupled on depends on many variables.

Among these variables are the cells the proteins are made in, and the metabolic state of the cells [51]. Glyconjugates commonly act as receptors for a variety of compounds including interferon, serotonin, and glycoprotein hormones [52]. Thus proteins come in variants with different sugars linked onto the same polypeptide chain—these variants are called glycoforms. One cell can also make a mixture of different glycoforms. The different glycoforms have different functional properties in many cases, and are 'seen' as different by the immune system.

LN is a large multidomain glycoprotein important in cellular functions including induction of cell adhesion, growth promotion, and enhancement of the metastatic phenotype of tumor cells [53]. LN is a heterotrimeric glycoprotein that is found only in the basement membrane of tissues. LN is composed of α , β , and γ chains held together in an alpha-helical coiled-coil structure linked by disulfide bridges to form a characteristic asymmetric cruciform structure [54]. These classes of chains are in turn composed of subunits eight of which have been identified and characterized: A, B1, B2, S, M, K, B2t, and B1k. Normal and neoplastic cells interact with LN via a variety of different cell surface proteins including the integrins. The primary LN receptor has a molecular weight of 68-72 kDa and is found in both normal tissues and carcinomas. Expression of both LN and its receptor is regulated by TGF β 1 as is fibronectin and its receptor. LN binds to various components of the basement membrane and probably links these to one another [55]. Cell surface receptors that may play a role in LN-mediated cell adhesion have been isolated from metastatic tumor cells [56] and platelets [57]. LN, a glycoprotein known to be involved in binding and adhesion of cells, acted as a membrane receptor protein in the characterized liposome system described.

Other molecules can be glycosylated, especially cell surface lipids such as sialic acid containing gangliosides, which are the most complex class of glycosphingolipids. The resulting glycolipids act as tags to allow the body to recognize its cells, especially cells in the blood. Thus gangliosides may be important functional components of liposomes, enabling the formulation of liposomes to mimic cell surfaces in the body. These 'stealth liposomes' fool the body into thinking that they are cells. Glycolipids are especially interesting because the variety in their chemical structure is attractive for use as an anchor since the lipid is glycosylated at a single site, unlike glycoproteins. The carbohydrate moieties tend to be concentrated on the external side of the cell membrane [2]. Glycolipids can also be readily incorporated into liposomes and self-assembling monolayers to mimic cell membranes [58].

Gangliosides GM1 and GM3 consist of sialic acid containing oligosaccharides covalently attached to a ceramide lipid. The lipid portion is embedded in the host cell membrane, and the oligosaccharide is exposed on the host cell surface. Toxins, microorganisms and other biomolecules recognize the oligosaccharide moieties of these gangliosides. GM1 and GM3 are found on the surfaces of many types of cells including normal tissues of the intestinal epithelium and carcinomas and are located in the plasma membrane, where they represent a small percentage of the total lipids. The amphiphilic structures of these eukaryotic receptor molecules are shown in **Figures 1 and 2**.

Molecular Interactions Between Bacteria and Their Toxins with Host Cells.

A number of enteric pathogens invade cultured mammalian cells by triggering actin rearrangements that ultimately result in the formation of pseudopods, which engulf the bacteria. Gram-negative *Salmonella* species force host cells to engulf them, but the

process appears somewhat different from that seen in other enteric pathogens. Binding of *S. typhimurium* to cultured cells causes a change in the appearance of the surface of the host cell that resembles a liquid droplet splash on a surface. This "splash" effect, termed membrane ruffling, results in the internalization of the bacteria inside an endocytic vesicle. Ruffling and internalization of the bacteria are accompanied by extensive actin rearrangements in the vicinity of the invading bacteria. After the bacteria are engulfed in a vesicle, however, the host cell surface and the actin filaments in the region return to their native state [59].

Several cholera-like toxins and enterotoxins have been described in *Salmonella* subspecies (ssp.). Diarrheagenic enterotoxin figures prominently as a *Salmonella* ssp. virulence factor responsible for the onset of diarrheal symptoms in human cases of salmonellosis. Whereas early studies suggested a serological relationship among the *Salmonella* ssp. enterotoxin, cholera toxin (CT), and the heat-labile toxin (LT) of enterotoxigenic *E. coli*, more recent serological and nucleic acid studies indicate they are distinct entities [60]. However, the *Salmonella* ssp. enterotoxin appears to be structurally similar to CT, with a molecular mass of 90 to 100 kDa and consisting of A and B subunits that act, respectively, to stimulate host cell adenylate cyclase and produce a pore through which the former enters. Increased levels of cellular cyclic adenosine monophosphate (cAMP) lead to a net massive increase in concentration of sodium and chloride ions and a consequent accumulation of fluid in the intestinal lumen [3]. *Salmonella* ssp. strains also produce a thermolabile, membrane-bound proteinaceous cytotoxin, which is serologically and genetically distinct from Shiga toxins of *Shigella* ssp. and *E. coli*. The virulence attribute of cytotoxin stems from its inhibition of protein

synthesis and lysis of host cells, thereby promoting the dissemination of the viable salmonellae into host tissues. Host cell lysis may also result from the chelation of divalent cations by the toxin, causing disruption of the host cell membranes [61].

Yersinia, another Gram-negative organism, utilizes a very different mechanism than *Salmonella* to achieve invasion. *Yersinia* species has an outer membrane protein invasins, which mediates attachment and entry into epithelial cells [49]. Invasion specifically binds to another class of integrin receptors, B1 integrins, expressed on the surface of the host cell. *Yersinia* activates host signaling pathways that ultimately involve protein tyrosine kinases. *Yersinia* manipulation of the host cell results in zippering the host cell membrane around itself to achieve invasion [47, 49].

Listeria monocytogenes is a Gram-positive, facultative highly motile rod that causes a potentially serious type of foodborne infection. Outside host cells, *L. monocytogenes* is motile because of its flagella. As it enters a cell, these flagella are lost, but the bacteria are still motile because of their ability to polymerize actin into long actin tails that propel the bacteria through the cytoplasm. Another unusual feature of *L. monocytogenes* that contributes to its ability to cause disease is that it grows well at 37°C but also grows at refrigerator temperatures of 4°C.

L. monocytogenes attaches to and invades tissue culture cells. Adherence and the invasion process are thought to mimic what happens during a *Listeria* infection. The steps include invasion, cell-to-cell transfer, and virulence factors. Initially, the phagocytosed bacteria are contained within a vacuole that has a single membrane. They escape the vacuole by rupturing the vacuolar membrane. The bacteria then begin to polymerize actin filaments at one end, forming long actin tails that propel them through

the cytoplasm. The bacteria can move by this mechanism into adjacent cells, producing long projections, which are then pinched off in a newly invaded cell. At this point, the bacteria are encased in a vacuole surrounded by a double membrane. They eventually escape from this vacuole and enter the cytoplasm of the newly invaded cell [59].

L. monocytogenes has the potential to infect a variety of eukaryotic cells including phagocytic and nonphagocytic cells, both *in vivo* and *in vitro*. This process involves several different steps, and the virulence factors involved in each of these steps have been identified. The surface proteins internalin A (InlA) and B (InlB), encoded by *inlA* and *inlB* genes belonging to a multigene family, are required for the entry of the organism into epithelial cells. Both these proteins are members of the superfamily of leucine-rich repeats containing proteins known to be involved in protein-protein interactions. The *inlA* gene also confers invasiveness to the non-invasive species *L. innocua* [62]; hence, its product was named internalin. The release of internalin begins during the exponential phase of growth when the cell wall-associated form is most abundant.

A surface protein is utilized to bind specific host cells by *L. monocytogenes*, which invades via a zipper mechanism. The protein internalin mediates entry into mammalian cells by binding to the receptor, E-cadherin [39, 47]. Following binding of internalin with E-cadherin, a host cell signaling pathway is activated where the key enzyme is a lipid kinase called phosphatidyl inositol 3-kinase [37]. Activation of phosphatidyl inositol 3-kinase is required during infection of host cells by the bacterium [47, 49].

L. monocytogenes has been shown to preferentially target Peyer's patches, the lymphoid follicles of the gut, in some studies but its preferential site of translocation in the intestine is yet to be proven conclusively. The organisms are then internalized by resident macrophages, in which they can survive and replicate. They are subsequently transported via the blood to regional lymph nodes. Ultimately, Kupffer's cells in the liver and spleen phagocytize invasive listeriae [62]. Infection is not localized at the site of entry but involves entry and multiplication in a wide variety of cell types and tissues. The bacteria are disseminated through the bloodstream to the brain and even the placenta when present.

Little is known about adhesins of Enterohemorrhagic *E. coli* (EHEC) strains, all of which are Gram-negative, except that they mediate the same type of binding and actin reorganization seen with Enteropathogenic *E. coli* (EPEC) strains [59]. EHEC strains have an *eaeA* gene (encoding intimin) that is similar to the *eaeA* gene of EPEC strains and probably has the same function (i.e., to mediate tight binding of bacteria to the host cells).

The first stage in association of *E. coli* O157:H7, the most recognized strain of the EHEC family, with the host cell is non-intimate binding, which is mediated by pili called bundle-forming pili. In the second stage, attachment of the bacteria to the host triggers a signal transduction event, which is associated with activation of host cell tyrosine kinases and results in increased host cell intracellular Ca^{2+} levels. In the third stage, the bacteria associate more closely with the host cell (intimate binding), and extensive rearrangement of actin in the vicinity of the bacteria occurs. Histologically, the second and third stages are seen as a deformation of some of the microvilli, and elimination of others, as well as

the formation of a pedestal-like structure at locations on the host cell surface where bacteria have adhered. The pedestal-like structure is composed of a dense mat of actin fibers that causes an outpouching of the host cell membrane [59]. The genes encoding proteins involved in the attaching-effacing process are designated *eae* for *E. coli* attachment-effacement. Intimin, a 94-kDa outer membrane protein, mediates the binding of EPEC strains to host cells. This protein is essential for the actin rearrangements that lead to the formation of the pedestal-like structure in the host cell, but other proteins may also be involved in this process.

To date, the main difference found between EPEC and EHEC strains is that EHEC strains produce a toxin that is virtually identical to Shiga toxin (STx), a toxin that is probably responsible for the dysentery caused by *Shigella* species. *Shigella* species also cause Hemolytic Uremic Syndrome (HUS). There are two types of EHEC Stx-Stx1, which is most like the classical Stx from *Shigella* species, and Stx2, which is related to Stx1 but differs enough at the amino acid sequence level that there are antibodies which differentiate Stx1 from Stx2. This difference is more of an academic interest, because Stx2 is more often associated with the EHEC strains that cause HUS than Stx1 [59].

Stx is an important virulence factor in EHEC infections. Receptors for the toxin are found on kidney cells as well as intestinal cells. Thus, dissemination of Stx to the kidney after bacterial colonization of the intestinal mucosa could be responsible for the acute kidney failure and kidney hemorrhages that are hallmarks of the fatal form of EHEC infections.

Enterotoxigenic *E. coli* (ETEC) strains produce different enterotoxins known as heat-labile toxin (LT) and heat-stable toxin (ST). Heat-stable is defined as retention of

toxin activity after incubation at 100°C for 30 min, and “heat labile” means that toxin activity is lost in 30 min under the same conditions. There are two types of LT (LT-I and LT-II). LT-I shares a high degree (nearly 75%) of amino acid identity with CT [59]. Given this, it is not surprising that LT has the same structure (five B subunits, one A subunit) and the same mechanism of action as CT. The B subunits of LT-I even interact with the same host cell receptor as cholera toxin’s beta subunit (CTB), the host cell surface antigen GM1. LT appears to cause diarrhea by activating a specific intracellular mechanism. The B subunits of LT bind to host cell antigen GM1, and the A subunit ADP-ribosylates G_s, a protein which normally controls cAMP production [59]. The ensuing ion imbalance results in water loss and diarrhea.

ST is not a single toxin but is rather a family of small (~2 kDa) peptide toxins that fall into two subgroups: methanol-soluble ST (STa) and methanol-insoluble ST (STb). The small size of STs explains why they are not inactivated at high temperatures as rapidly as a full-length protein. High temperatures inactivate large proteins by unfolding them. A peptide as short as ST would not be affected to the same extent as a large protein under the same conditions. STa is excreted into the medium as a larger peptide (a 72 amino acid sequence) where it is cleaved to its final 17-19 amino acid form by a process that is not well understood. STb undergoes a similar process when excreted and activated.

STa activates host cell guanylate cyclase, the enzyme responsible for regulating levels of intracellular cyclic GMP (cGMP). STa causes an increase in the cGMP level in the host cytoplasm, which leads to the same type of fluid loss caused by an uncontrolled rise in cAMP. cGMP, like cAMP, is an important signaling molecule in eukaryotic cells,

and changes in cGMP affect a number of cellular processes, including activities of ion pumps [59].

Vibrio cholerae is a Gram-negative curved rod with a single polar flagellum. When *V. cholerae* is ingested the pH shock and temperature increase it experiences initiates gene expression resulting in the production of virulence factors. The bacterium adheres to and colonizes small-intestinal mucosa (flagella, Tcp, and others yet to be proven) and produces toxins. The bacterium and its associated toxin continue to cause much morbidity and mortality. The toxin causes extensive fluid and ion loss from tissues leading to hypertension, electrolyte imbalance, and death.

CT is an important, well-studied and understood disease virulence factor. This toxin is clearly responsible for most of the pathology seen in people with cholera. Naturally occurring strains or mutants of *V. cholera* that do not produce CT do not cause the full-blown form of the disease, either in animals or in human volunteers. CT has been intensively studied at the biochemical and genetic levels, and is currently one of the best understood of all the bacterial toxins [59].

Secreted CT attaches to the surface of a host mucosal cell by binding to GM1 gangliosides. The hydrophilic oligosaccharide head group is recognized by CTB. GM1 is found on the surfaces of many types of cells including those of the intestinal epithelium. Also found on many host cell surfaces are gangliosides with longer chains of sialic acid residues. *V. cholera* secretes a neuraminidase (also called a sialidase) that removes sialic acid residues from these more complex oligosaccharides to make them structurally more similar to GM1. It has been suggested that neuraminidase contributes

to the virulence of *V. cholera* by increasing the number of receptors available to bind cholera [59].

Once CTB is bound to GM1, the A1 subunit is released from the toxin, presumably by the reduction of the disulfide bond that links it to A2, and enters the host cell by an unknown translocation mechanism. There has been much speculation about this mechanism. One hypothesis, though still controversial, is that the five B subunits insert themselves into the host cell membrane and form a pore through which the A1 subunit passes [59].

A final example of toxins and their recognition and binding specificity for receptors, is tetanus toxin. This toxin binds at least 10 different gangliosides with varying affinity, and the specific interaction between the toxin and the ganglioside changes after treatment with a sialidase [63]. Tetanus toxin binds GT1b and GD1b more inefficiently after treatment with sialidase, while binding is unchanged for GM1. The opposite observation is true for CTB with GT1b and GD1b.

Altogether, the description of infection by the bacterial pathogens above reveals common mechanisms of divergent infection pathways. Among the common mechanisms are interactions of pathogen and host cells via receptors, modulation of host cell signaling pathways, and rearrangement of host cell cytoskeleton resulting in subsequent invasion.

Pathogen Detection: Current Methodologies. The traditional method of identifying a pathogen is to cultivate it on artificial media, isolate it in pure culture, and then identify it by means of physical and biochemical characteristics. Culture-based methods generally involve enrichment of the target bacteria to increase the cell number to a detectable level, followed by presumptive detection on selective media and

confirmation by biochemical or serological assays. Detection of *Salmonella* and *E. coli* O157:H7 may require 5 or more days to complete and may provide ambiguous results due to competing microbiota and variability in the possession or expression of biochemical immunological traits [64]. Although a presumptive identification can be made in 1 to 2 days, full identification takes 4 to 5 days for most bacteria and fungi, and longer for slow-growing or difficult-to-cultivate microbes.

Current rapid methods used to detect pathogens generally use immunological tests (EIAs) that are considered to be rapid (20 minutes to 4 hours). Limitations associated with antibody capture methods include expense and susceptibility of the immobilized antibody to degradation and environmental conditions and the need to enrich the sample via incubation.

Bacteriological Analytical Manual (BAM) is a current protocol endorsed by the Food and Drug Administration for culturing *Salmonella* in detection schemes. Shearer et al. (2001) outlined a procedure using BAM for the detection of *Salmonella*. It includes multiple overnight culturing incubations in selective media followed by plating. Plates were observed for typical *Salmonella* colonies [64]. The total time for this test is 72 h.

PCR detection schemes have been developed for a number of common foodborne pathogens using a variety of approaches for specific applications. The latest innovation of PCR detection has been real-time PCR. In real-time PCR, e.g., the 5' nuclease chemistry renders the automated and direct detection and quantification of PCR products possible. This application of 5' nuclease PCR for quantification of *L. monocytogenes* in pure cultures, water, skim milk, and unpasteurized whole milk was developed [65-67]. A detection and differentiation scheme for *Listeria* spp. by a single reaction based on

multiplex PCR has been developed [68].

BAX is a polymerase chain reaction (PCR) detection system that utilizes amplification of a specific target deoxyribonucleic acid (DNA) sequence for the detection of *S. enteritidis*, *E. coli* O157:H7, and *L. monocytogenes* on fresh produce [64]. For this test, an aliquot of an overnight culture grown in buffered peptone is added to Brain Heart Infusion (BHI) broth and incubated for 3 h at 37°C. An aliquot of the BHI culture is subjected to PCR followed by agarose gel separation [64]. It has been reported that the PCR method allowed detection of *S. enteritidis*, *E. coli* O157:H7, and *L. monocytogenes* at least 2 days earlier than the conventional culture methods (BAM) [64].

A multiplex fluorogenic PCR assay for simultaneous detection of pathogenic *Salmonella* strains and *E. coli* O157:H7 has been developed and evaluated for use in detecting very low levels of these pathogens in meat and feces [69]. Fluorogenic reporter probes were included in the PCR assay for automated and specific detection of amplified products. Detection of amplification products could be completed in ≤ 4 h after enrichment [69].

Detection of *Salmonella* in poultry using a chip-based biosensor has been investigated [70]. *S. typhimurium* was detected at levels as low as 119 colony forming units (CFU) using the Treshold[®] Immunoassay System. This system utilizes solution-based binding of the biotin and fluorescein labeled antibodies to *Salmonella*, followed by filtration-capture of the immunocomplex on a biotin-coated nitrocellulose membrane. Ultimately, an anti-fluorescein urease conjugate is bound to the immunocomplex [70]. Detection of the bound immunocomplex is made possible via the silicon chip-based light-addressable potentiometric sensor. In the presence of the urea, urease converts the

substrate to ammonia and CO₂ and this induces a pH change at the silicon surface. The resultant pH change is monitored with time and the signal output is reported [70]. The assay can be accomplished in less than 15 minutes.

Automated detection of *Salmonella* ssp. in foods was investigated and found useful [71]. Liquid eggs, shell eggs, dry eggs, skim milk, and chicken were spiked with *S. enteritidis*, *S. typhimurium*, or *S. newport*. Following pre-enrichment in universal pre-enrichment broth at 42°C for 6 h (eggs and milk) or 16 h (chicken) immunomagnetic beads coated with *Salmonella* antibody (Vicam, Watertown, MA, USA) were used to capture *Salmonella* [71]. The beads were incubated in liquid media at 42°C and positive samples were identified by black discoloration of the media during incubation. Total time for this test is estimated at 18 to 36 h.

A group of researchers at the University of Georgia, developed detection of *Salmonella* and simultaneous detection of *Salmonella* and Shiga-like toxin-producing *E. coli* (SLTEC) using the magnetic capture hybridization polymerase chain reaction (MCH-PCR) [72]. *Salmonella* was detected either individually by a single (MCH-PCR) targeting the *inv* gene or simultaneously with SLTEC by a multiplex MCH-PCR in which SLTEC were detected using primers for the *slt* genes. Both assays were found to be specific for tested pathogens and the results indicated that MCH-PCR can be used as means of detecting single or multiple bacterial pathogen(s) [72]. This complex procedure requires a minimum of 8 h.

PCR-based assays for detection of foodborne bacterial pathogens have provided increased sensitivity, allowed for more rapid processing times, and enhanced the likelihood of detecting bacterial pathogens [37]. The reliability of PCR detection

methods depends, in part, on the purity of the target template and the presence of sufficient numbers of target molecules. With complex matrices such as foods, steps must be taken to limit the effects of any potentially inhibitory compounds present that may limit PCR amplification of the intended target. Filters have been used to trap and lyse microorganisms on contact. Released DNA is sequestered and preserved intact within a membrane. Following brief washes, the filters can be used directly in PCR assays or as a solid medium to store samples for later use [73].

The development and evolution of laboratory and field techniques regarding the study and identification of foodborne pathogens has recently undergone a rapid period of change and advancement. Detection schemes each have their advantages and disadvantages but cost, speed, and reliability are at the forefront of any agenda regarding the reliance on a particular test be it for a food product for global distribution, medical diagnostics, or use for service men and women in the armed forces. Traditional plating and chemical tests are slow and labor intensive but as a method with a long history of reliability, remain the preferred methods used by food companies and medical professionals worldwide. Presumptive positive plates are often confirmed with the use of antibody-based tests in microbiology laboratories servicing the food and medical industries. Only recently have PCR methods been implicated in the detection and identification work critical to the food and medical industries. There is a distinct economic benefit and need to decrease the time a food product must be held awaiting microbiological analysis before it can be distributed to retail outlets or more importantly, served to a customer. In medicine, diagnostic efficiencies could be dramatically

improved through basic research and new techniques based on emerging technologies such as PCR detection and CLSM.

Advances in Microscopy: Confocal Laser Scanning Microscopy. Attachment of microorganisms to surfaces (food, tissues, glass, etc.) is a dynamic process, in which, cells suspended in liquid at the surface attach over time and are absorbed onto structures. CLSM provides a means for the direct observation and characterization of microbes during and after the attachment process. Although there is currently little published on the use of CLSM to study microbial attachment, the application of this technology has the potential to provide a deeper understanding of this process [6]. This tool can explore and observe captured cells, protein interactions, and characterize biological and biomimetic structures. It can be used to confirm the presence of surface receptor molecules without the need for antibodies specific for the antigen of interest. Also, CLSM can investigate and elucidate interactions between immobilized liposomes and captured cells revealed using ELISAs and PCR.

The power and advantage of CLSM lie in its potential to image fully hydrated systems in their natural state. This is accomplished by obtaining thin optical sections of the specimen using focused laser light which scans the field, and a pinhole detector to remove out-of-focus light. Since only light emanating from the focal plane is collected, the resulting image has little depth of field, but is highly focused [6, 74]. Multiple labeling techniques using specific fluorescent probes, impart flexibility in monitoring artificial and natural biological entities. Co-localization, or physical localization of two or more probes excited simultaneously, results in blending of monitor colors. Depth of image can be achieved by collecting optical sections at different sample depths and using

computer software to combine them into a 'stacked' image that projects the three-dimensional data in two-dimensions. The depth of field capability is critical. It allows examination of microbial attachment resulting from molecular recognition events in more dimensions than possible with other forms of microscopy and without the use of chemical or physical fixation.

NULL HYPOTHESIS

The reported molecular activity of biomolecules is not maintained *in vitro* when incorporated into immobilized liposomes.

RESEARCH OBJECTIVES

Objective 1. To verify biological activity of liposomes containing a mechanosensitive channel from *Escherichia coli* (EcoMscL). The artificial membrane bilayers (liposomes) were immobilized onto a glass surface and observed for channel opening with confocal microscopy.

Objective 2. To verify biological activity of liposomes containing glycosphingolipids (GM1 or GM3). The liposomes were immobilized onto a glass surface and challenged with bacteria and proteins (including cholera toxin). The *in vitro* assay used confocal microscopy, ELISA, or genetic-based detection systems to determine bacterial and toxin interactions.

Objective 3. To verify biological activity of a liposome containing LN, a eukaryotic protein receptor for bacteria. The liposomes were immobilized onto a glass

surface and challenged with bacteria and proteins (including cholera toxin). The *in vitro* assay used confocal microscopy, ELISA, or genetic-based detection systems to determine bacterial and toxin interactions.

REFERENCES

1. Wainwright S. What we can learn from soft biomaterials and structures. In: Sarikaya M, Aksay I, eds. *Biomimetics: Design and Processing of Materials*. Woodbury, New York: American Institute of Physics, 1995; 1-12.
2. Karlsson K. Microbial recognition of target cell glycoconjugates. *Curr Opin Struct Biol* 1995; 5(5):622-635.
3. Deshpande S. *Handbook of Food Toxicology*. New York: Marcel Dekkar, Inc., 2002.
4. Janshoff A, Steinem C, Sieber M, Baya A, Schmidt M, Galla H. Quartz crystal microbalance investigation of the interaction of bacterial toxins with ganglioside containing solid supported membranes. *Eur Biophys J* 1997; 26(3):261-270.
5. Mackenzie C, Hirama T, Lee K, Altman E, Young N. Quantitative analysis of bacterial toxin affinity and specificity for glycolipid receptors by surface plasmon resonance. *J Biol Chem* 1997; 272(9):5533-5539.
6. Frank J. Microbial attachment to food and food contact surfaces. *Adv Food Nutr Res* 2001; 43:319-370.
7. Machy P, Leserman L. *Research in Liposomes in Cell Biology and Pharmacology*. Vol. 2. London, England: John Libbey & Company, Ltd., 1987.
8. Park S, Durst R. Immunoliposome sandwich assay for the detection of *Escherichia coli* O157:H7. *Anal Biochem* 2000; 280:151-158.
9. Gyongyossy-Issa M, Muller W, Devine D. The covalent coupling of Arg-Gly-Asp-containing peptides to liposomes: purification and biochemical function of the liposomes. *Arch Biochem Biophys* 1998; 353(1):101-108.
10. Kawakami S, Yamashita F, Nishikawa M, Takakura Y, Hashida M. Asialoglycoprotein receptor-mediated gene transfer using novel galactosylated cationic liposomes. *Biochem Biophys Res Commun* 1998; 252:78-83.

11. Koide K, Karel M. Encapsulation and stimulated release of enzymes using lecithin vesicles. *Int J Food Sci Tech* 1987; 22:707-723.
12. Konigsberg P, Godtel R, Kissel T, Richer L. The development of IL-2 conjugated liposomes for therapeutic purposes. *Biochim Biophys Acta* 1998; 1370:243-251.
13. Lambert O, Plancon L, Rigaud J, Letellier L. Protein-mediated DNA transfer into liposomes. *Mol Microbiol* 1998; 30(4):761-765.
14. Meyer O, Kirpotin D, Hong K, Sternberg B, Park J, Woodle M, Papahadjopoulos D. Cationic liposomes coated with polyethylene glycol as carriers for oligonucleotides. *J Biol Chem* 1998; 273(25):15621-15627.
15. Stegmann T, Bartoldus I, Zumbunn J. Influenza hemagglutinin-mediated membrane fusion: Influence of receptor binding on the lag phase preceding fusion. *Biochem* 1995; 34:1825-1832.
16. Carson H. Liposomes. *Happi* 1993(March):53-54, 56, 58.
17. Gonzalez R, Sanchez J, Holmgren J, Lopez S, Arias C. Immunological characterization of a rotavirus-neutralizing epitope fused to the cholera toxin B subunit. *Gene* 1993; 133:227-232.
18. Nagle J, Tristram-Nagle S. Structure of lipid bilayers. *Biochim Biophys Acta* 2000; 1469:159-195.
19. Chang T. Artificial cells in medicine and biotechnology. *Appl Biochem Biotechnol* 1984; 10:5-24.
20. Mayhew E, Lazo R, Vail W, King J, Green A. Characterization of liposomes prepared using a microfluidizer. *Biochim Biophys Acta* 1984; 775:169-174.
21. Antes P, Schwarzmann G, Sandhoff K. Detection of protein mediated glycosphingolipid clustering by the use of resonance energy transfer between fluorescently labeled lipids: a method established by applying the system ganglioside GM1 and cholera toxin B subunit. *Chem Phys Lipids* 1992; 62:269-280.
22. Nieva J, Bron R, Corver J, Wilschut J. Membrane fusion of Semliki Forest virus requires sphingolipids in the target membrane. *EMBO J* 1994; 13(12):2797-804.
23. Hermanson G. *Bioconjugate Techniques*. New York: Academic Press, Inc., 1996.
24. Walsh M, Nam S. Rapid fractionation of bovine transferrin using immobilized gangliosides. *Prep Biochem Biotechnol* 2001; 31(2):89-102.

25. Booth I, Louis P. Managing hypoosmotic stress: Aquaporins and mechanosensitive channels in *Escherichia coli*. *Curr Opin Microbiol* 1999; 2:166-169.
26. Blount P, Moe P. Bacterial mechanosensitive channels: integrating physiology, structure, and function. *Trends Microbiol* 1999; 7(10):420-424.
27. Sukharev S, Schroeder M, McCaslin D. Stoichiometry of the large conductance bacterial mechanosensitive channel of *E. coli*. A biochemical study. *J Membr Biol* 1999; 171:183-193.
28. Sukharev S, Sigurdson W, Kung C, Sachs F. Energetic and spatial parameters for gating of the bacterial large conductance mechanosensitive channel, MscL. *J Gen Physiol* 1999; 113(4):525-540.
29. Arkin I, Sukharev S, Blount P, Kung C, Brunger A. Helicity, membrane incorporation, orientation and thermal stability of the large conductance mechanosensitive ion channel from *E. coli*. *Biochim Biophys Acta* 1998; 1369:131-140.
30. Blount P, Sukharev S, Moe P, Nagle S, Kung C. Towards an understanding of the structure and functional properties of MscL, a mechanosensitive channel in bacteria. *Biol Cell* 1996; 87:1-8.
31. Delcour A, Martinac B, Alder J, Kung C. Modified reconstitution method used in patch-clamp studies of *Escherichia coli* ion channels. *Biophys J* 1989; 56:631-636.
32. Hase C, Dain A, Martinac B. Molecular dissection of the large mechanosensitive ion channel (MscL) of *E. coli*: mutants with altered channel gating and pressure sensitivity. *J Membr Biol* 1997; 157:17-25.
33. Haumlse C, Dain A, Martinc B. Purification and functional reconstitution of the large mechanosensitive ion channel (MscL) of *Escherichia coli*. *JBC Online* 1995; 270(31):18329-18335.
34. Sukharev S, Martinac B, Arshavsky V, Kung C. Two types of mechanosensitive channels in the *Escherichia coli* cell envelope: solubilization and functional reconstitution. *Biophys J* 1993; 65:177-183.
35. Bendas G, Vogel J, Bakowski U, Krause A, Muller J, Rothe U. A liposome-based model system for the simulation of lectin-induced cell adhesion. *Biochim Biophys Acta* 1997; 1325:297-308.

36. Zhan H. A method for quick measurement of protein binding to unilamellar vesicles. *J Biochem Biophys Methods* 1999; 41(1):13-19.
37. Finlay B. Cracking *Listeria's* password. *Science* 2001; 292(5522):1665-1666.
38. Finlay B, Cossart P. Exploitation of mammalian host cell functions by bacterial pathogens. *Science* 1997; 276(5313):718-725.
39. Cossart P. Met, the HGF-SF receptor: another receptor for *Listeria monocytogenes*. *Trends Microbiol* 2001; 9(3):105-107.
40. Marcus S, Wenk M, Steele-Mortimer O, Finlay B. A synaptojanin-homologous region of *Salmonella typhimurium* SigD is essential for inositol phosphatase activity and Akt activation. *FEBS Lett* 2001; 494:201-207.
41. Hazlett L, Masinick S, Barrett R, Rosol K. Evidence for asialo GM1 as a corneal glycolipid receptor for *Pseudomonas aeruginosa* adhesion. *Infect Immun* 1993; 61(12):5164-5173.
42. Maloney M, Lingwood C. CD19 has a potential CD77 (globotriaosyl ceramide)-binding site with sequence similarity to verotoxin B-subunits: Implications of molecular mimicry for B cell adhesion and enterohemorrhagic *Escherichia coli* pathogenesis. *J Exp Med* 1994; 180:191-201.
43. Mulvey M, Huntgren S. Bacterial spelunkers. *Science* 2000; 289:732-733.
44. Huntgren S, Abraham S, Caparon M, Falk P, St Geme JW 3rd, Normark S. Pilus and nonpilus bacterial adhesions: assembly and function in cell recognition. *Cell* 1993; 73:887-901.
45. Hultgren S, Jones C. Utility of immunoglobulin-like fold of chaperones in shaping organelles of attachment in pathogenic bacteria. *ASM News* 1995; 61(9):457-64.
46. Colin M, Maurice M, Trugnan G, Kornprobst M, Harbottle R, Knight A, Cooper R, Miller A, Capeau J, Coutelle C, Brahimi-Horn M. Cell delivery, intracellular trafficking and expression of an integrin-mediated gene transfer vector in tracheal epithelial cells. *Gene Ther* 2000(7):139-152.
47. Knodler L, Celli J, Finlay B. Pathogenic trickery: deception of host cell processes. *Nat Rev Mol Cell Biol* 2001; 2(8):578-588.
48. Qiu C, Young M, Finn A, Dichek D. Cationic liposomes enhance adenovirus entry via a pathway independent of the fiber receptor and alpha_v-integrins. *Hum Gene Ther* 1998; 9:507-520.

49. Pizarro-Cerda J, Moreno E, Desjardins M, Gorvel J. When intracellular pathogens invade the frontiers of cell biology and immunology. *Histol Histopathol* 1997; 12:1027-1038.
50. Steele-Mortimer O, Meresse S, Gorvel J-P, Toh B-H, Finlay B. Biogenesis of *Salmonella typhimurium*-containing vacuoles in epithelial cells involves interactions with the early endocytic pathway. *Cell Microbiol* 1999; 1(1):33-49.
51. Matsuda K, Taki T, Hamanaka S, Kasama T, Rokukawa C, Handa S, Yamamoto N. Glycosphingolipid compositions of human T-lymphotropic virus type-I (HTLV-I) and human immunodeficiency virus (HIV)-infected cell lines. *Biochim Biophys Acta* 1993; 1168:123-129.
52. Bremer E. Glycosphingolipids as effectors of growth and differentiation. *Curr Topics Membr* 1994; 40:387-411.
53. Kleinman H, Cannon F, Laurie G, Hassell J, Aumailley M, Terranova V, Martin G, DuBois-Dalcq M. Biological activities of laminin. *J Cell Biochem* 1985; 27(4):317-325.
54. Beck K, Hunter I, Engel J. Structure and function of laminin: anatomy of a multidomain glycoprotein. *FASEB J* 1990; 4:148-160.
55. Timpl R. Structure and biological activity of basement membrane proteins. *Eur J Biochem* 1989; 180(3):487-502.
56. Rao C, Castronovo V, Schmitt M, Wewer U, Claysmith A, Liotta L, Sobel M. Evidence for a precursor of the high-affinity metastasis-associated murine laminin receptor. *Biochem* 1989; 28(18):7476-7486.
57. Sonnenberg A, Modderman P, Hogervorst F. Laminin receptor on platelets is the integrin VLA-6. *Nature* 1988; 336(6198):487-489.
58. Charych D, Cheng Q, Reichert A, Kuziemko G, Stroh M, Nagy J, Spevak W, Stevens R. A 'litmus test' for molecular recognition using artificial membranes. *Chem Biol* 1996; 3:113-120.
59. Salyers A, Whitt D. *Bacterial Pathogenesis: A Molecular Approach*. Second ed. Washington, D.C.: ASM Press, 2002.
60. Cox J. *Salmonella*: Introduction. In: Robinson R, Batt C, Patel P, eds. *Encyclopedia of Food Microbiology*. Academic Press: San Diego, 2000;1928-1937.

61. Peterson J, Niesel D. Enhancement by calcium of the invasiveness of *Salmonella* for DeLa cell monolayers. *Rev Infect Dis* 1988; 10:S319-S322.
62. Rocourt J, Cossart P. *Listeria monocytogenes*. In: Doyle M, Beuchat L, Montville T, eds. *Food Microbiology: Fundamentals and Frontiers*. Washington D.C.: ASM Press, 1997; 337-352.
63. Holmgren J, Elwing H, Fredman P, Strannegard O, Svennerholm L. Gangliosides as receptors for bacterial toxins and sendai virus. *Adv Exper Med Biol* 1980; 125:453-470.
64. Shearer A, Strapp C, Joerger R. Evaluation of a polymerase chain reaction-based system for detection of *Salmonella enteritidis*, *Escherichia coli* O157:H7, *Listeria* spp., and *Listeria monocytogenes* on fresh fruits and vegetables. *J Food Prot* 2001; 64(6):788-795.
65. Bassler H, Flood S, Livak K, Marmaro J, Knorr R, Batt C. Use of a fluorogenic probe in a PCR-based assay for the detection of *Listeria monocytogenes*. *Appl Environ Microbiol* 1995; 61(10):3724-3728.
66. Nogva H, Rudi K, Naterstad K, Holck A, Lillehaug D. Application of 5'-nuclease PCR for quantitation detection of *Listeria monocytogenes* in pure cultures, water, skim milk, and unpasteurized whole milk. *Appl Environ Microbiol* 2000; 66(10): 4266-4271.
67. Norton D-M, Batt C. Detection of viable *Listeria monocytogenes* with a 5' nuclease PCR assay. *Appl Environ Microbiol* 1999; 65(5):2122-2127.
68. Bubert A, Hein I, Rauch M, Lehner A, Yoon B, Goebel W, Wagner M. Detection and differentiation of *Listeria* spp. by a single reaction based on multiplex PCR. *Appl Environ Microbiol* 1999; 65(10):4688-4692.
69. Sharma V, Carlson S. Simultaneous detection of *Salmonella* strains and *Escherichia coli* O157:H7 with fluorogenic PCR and single-enrichment-broth culture. *Appl Environ Microbiol* 2000; 66(12):5472-5476.
70. Dill K, Stanker L, Young C. Detection of *Salmonella* in poultry using a silicon chip-based biosensor. *J Biochem Biophys Methods* 1999; 41(1):61-67.
71. Tan W, Shelef L. Automated detection of *Salmonella* ssp. in foods. *J Microbiol Methods* 1999; 37:87-91.

72. Chen J, Griffiths M. Detection of *Salmonella* and simultaneous detection of *Salmonella* and shiga-like toxin-producing *Escherichia coli* using the magnetic capture hybridization polymerase chain reaction. *Lett Appl Microbiol* 2001; 32:7-11.
73. Lampel K, Orlandi P, Kornegay L. Improved template preparation for PCR-based assays for detection of food-borne bacterial pathogens. *Appl Environ Microbiol* 2000; 66(10):4539-4542.
74. Ferrando M, Spiess W. Review: confocal scanning laser microscopy, a powerful tool in food science. *Food Sci Technol Int London* 2000; 6(4):267-284.

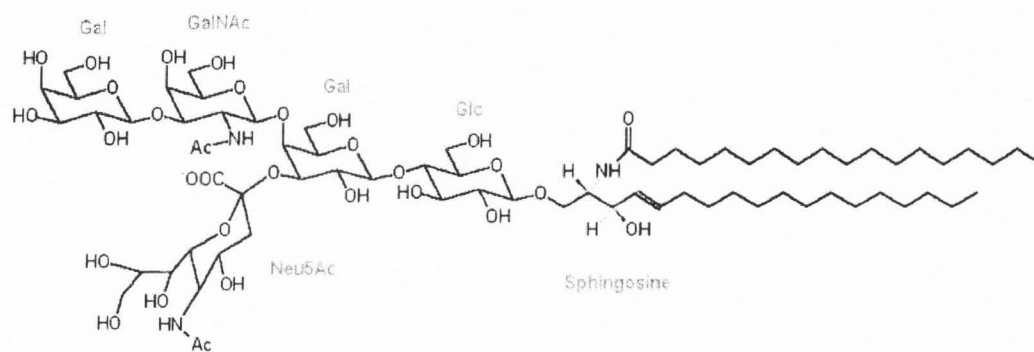


Figure 1. Amphiphilic structure of ganglioside GM1. Gal = galactose; GalNAc = *N*-acetylgalactosamine; Glc = glucose; Neu5Ac = *N*-acetylneuraminic acid

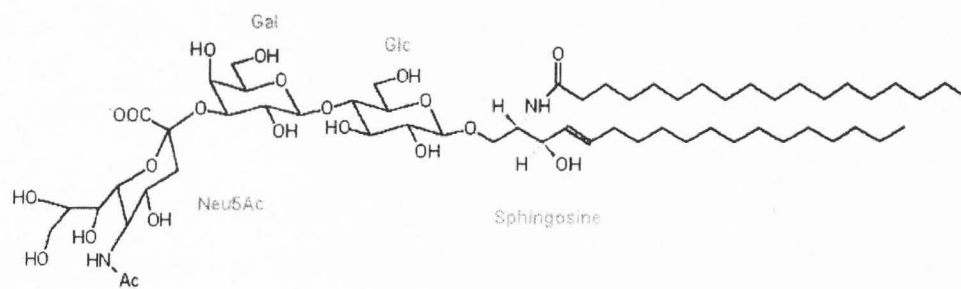


Figure 2. Amphiphilic structure of ganglioside GM3. Gal = galactose; Glc = glucose; Neu5Ac = *N*-acetylneuraminic acid

CHAPTER II

IMMOBILIZATION OF BIOMIMETIC LIPOSOMES

ABSTRACT

A stable biomimetic system consisting of liposomes containing embedded ganglioside GM1 or laminin was developed as a tool for the investigation of molecular interactions using confocal laser scanning microscopy (CLSM). In this study, microemulsified liposomes composed of phospholipids, cholesterol and *N*-biotinyl phosphatidylethanolamine were formulated, microemulsified, and immobilized to glass coverslips containing covalently immobilized avidin. The stability of immobilized microemulsified liposomes containing membrane-embedded or encapsulated biomolecules was monitored over time by following the release of sulforhodamine B. Interactions between 5-(and-6)-carboxynaphthofluorescein (CNF) labeled soluble cholera toxin β subunit (CTB), bovine lactoferrin (BLF), bovine serum albumin (BSA), or ovalbumin (OVA) and GM1 or laminin (LN) embedded liposomes were characterized by the presence of CNF. Destabilization was first observed at 59 days for CNF-BSA liposomes while destabilization of laminin liposomes were observed at 116 days. Destabilization of control liposomes, and GM1 liposomes was observed on days 146 and 131 respectively. After incubation with the labeled proteins in solution, specific interactions between liposomes containing GM1 were observed with confocal microscopy. CTB and BLF were co-localized proximate to liposomes containing GM1. CTB, BLF and OVA were not associated with control liposomes lacking GM1. These results clearly show the potential of using immobilized liposomes as biomimetics to study

molecular interactions between small and large molecules embedded in artificial bilayers and proteins.

INTRODUCTION

Liposome Production. Liposomes are used extensively in the laboratory for diverse research, diagnostic and pharmacologic applications. The applications and extension of research involving liposomes are limited by lack of technology allowing the reproducible manufacture of liposomes of predictable and uniform size. A variety of different approaches including freeze-thaw, reverse phase evaporation, sonication, and extrusion have been described for preparing liposomes [1-7]. Use of liposomes in drug delivery as target carriers of drugs and enzymes and in the cosmetics industry is a subject of great interest and is extensively studied [4, 8, 9]. Characterization of liposomes prepared using a microemulsifier found that using the principles of fluid dynamics, unilamellar liposomes can be produced in a reproducible manner [10, 11]. Using the microfluidizing method, liposomes are prepared in amounts sufficient for pharmaceutical quality assessment, toxicology studies, and multicenter clinical trials [11]. The automated high-pressure system uses a "microemulsion" process available commercially as the Microfluidizer™ (Microfluidics Corp., Newton, MA, USA). Microfluidization of lipids results in uniform lipid vesicle dispersions with the ability to encapsulate bioactive macromolecules [3, 12]. All liposomes, including microfluidized unilamellar liposomes, lose the ability to encapsulate over time. Leaky liposomes ineffectively encapsulate biomolecules [13].

Trapping molecules in the aqueous phase, or internal lumen, of liposomes is a form of encapsulation which is useful for compartmentalization in biosensors. The weakness of liposome based sensors stems from their mechanical and chemical instability. Many of the potentially useful proteins for liposome based biosensors are also chemically unstable or sensitive to the environment outside of a laboratory. Thus, liposome properties have been verified in laboratories for some very simple, model systems. Only recently have results translated into any realistic sensor applications for signal amplification [14].

Unilamellar vesicles are more appealing than multilamellar vesicles when developing *in vitro* models of lipid bilayers. In multilamellar liposomes, the interaction between different bilayers, absent in unilamellar vesicles and most membranes, is a concern. Interactions between unilamellar bilayers are too small to affect fully hydrated bilayer structure of microemulsified liposomes because the water layer is appreciable [15].

Microemulsified Liposomes. Microemulsified liposomes generally contain phosphatidylcholine (PC), phosphatidylethanolamine (PE), phosphatidylglycerol (PG), sphingomyelin (SPM), cholesterol and triacylglycerols. Phospholipids, PE and PC can be modified to contain biotin or an amino functional group that can be used to covalently link liposomes to a glass surface. Currently, liposomes are noncovalently adsorbed to plastic surfaces [14]. Adsorption has drawbacks, including establishment of an equilibrium with the liquid media leading to desorption. Immobilization is advantageous because unincorporated and weakly associated lipids, probes, and vesicles can be

removed by appropriate wash steps. Immobilized microemulsified liposomes are stable and may be useful in studying cellular interactions using emerging technologies.

Cellular Interactions. Cell interactions are observed in cancer, infection, fertilization, and immunological responses. Viruses fuse with liposomes containing PC : PE : cholesterol (1 : 1 : 1.5) and SPM [16]. A well-characterized interaction occurs between CTB and the ganglioside GM1. GM1 consists of a sialic acid-containing oligosaccharide covalently attached to a ceramide lipid. Naturally, the lipid portion is embedded in the host cell membrane, while the oligosaccharide is exposed on the host cell surface. The oligosaccharide moiety is recognized by toxins, microorganisms and other biomolecules. GM1 is found on the surfaces of many types of cells including normal tissues of the intestinal epithelium and carcinomas [17, 18].

Gangliosides are important cellular surface molecules that allow self-recognition. Thus, gangliosides might be important functional components of liposomes, enabling the formulation of liposomes to mimic cell surfaces in the body. Gangliosides are especially unique because of the variety in their chemical structure. Since the lipid is glycosylated at a single site, unlike glycoproteins, and gangliosides it tends to be concentrated on the external side of the cell membrane [19]. Glycolipids are readily incorporated into liposomes and self-assembling monolayers to mimic cell membranes [20].

Cholera toxin (CT) is an A-B ADP-ribosylating toxin, containing one A (enzymatic) subunit and five B (binding) subunits. The excreted toxin attaches to the surface of a host mucosal cell by binding to GM1. Once the CT β subunit (CTB) is bound to GM1, the A1 subunit is released from the toxin. This is presumably by the

reduction of the disulfide bond that links it to A2, entering the host cell by an unknown translocation mechanism [21].

In addition to CTB, BLF binds surface structures found on bacteria, while interacting with eukaryotic cells. Specifically, BLF has been shown to bind glycosaminoglycans, fibrinogen, collagen type I, collagen type IV, and laminin [22]. Recently, BLF has been shown to bind bovine gangliosides [23, 24].

Laminin. LN is a large multidomain glycoprotein important in cellular functions including induction of cell adhesion, growth promotion, and enhancement of the metastatic phenotype of tumor cells [25]. LN is a heterotrimeric glycoprotein that is found only in the basement membrane of tissues. LN is composed of α , β , and γ chains held together in an alpha-helical coiled-coil structure linked by disulfide bridges to form a characteristic asymmetric cruciform structure [26]. Normal and neoplastic cells interact with LN via a variety of different cell surface proteins including the integrins. The primary LN receptor protein has a molecular weight of 68-72 kDa and is found in both normal tissues and carcinomas. Membrane proteins such as LN can be uniformly incorporated in large unilamellar homogenous liposomes using microemulsification [27]. LN binds to various components of the basement membrane and likely links these to one another [28].

Confocal Microscopy. Visualization of molecular interactions between liposome-embedded receptors can be performed with CLSM. CLSM is a powerful microanalytical tool that provides a means for direct observation and characterization of dynamic processes in living structures or mimetics of these structures. The ability of CLSM to precisely image fully hydrated systems sets it apart from other forms of

microscopy [29, 30]. Sample preparation is non-invasive and permits the examination of physiologically active structures. Systems, living and artificial, can be selectively labeled and experiments including treatments that induce dynamic structural changes can be monitored during analytical processes [29].

CLSM was used to study the interaction between soluble concanavalin A-liposomes and immobilized mannose [31]. Interactions were indicated by observed patterns of fluorescently labeled phosphatidyl ethanolamine concanavalin A liposomes in a flow system. Adhered liposomes appeared as defined, resolved points whereas, free flowing liposomes in the medium were visible as trails.

In this study, microemulsified unilamellar phospholipid liposomes were designed, formulated, and immobilized to avidin-containing glass coverslips. Immobilized microemulsified liposomes were formulated to contain an encapsulated 5-(and-6) carboxynaphthofluorescein (CNF) labeled soluble protein (BSA), a CNF-labeled membrane protein (LN), or an unlabeled membrane receptor (GM1). GM1, CNF-BSA, CNF-LN, and control liposomes were characterized directly with respect to size, composition, and stability using CLSM. After establishing the stability of liposomes, a procedure and application was developed to survey interactions between soluble CNF-protein conjugates and liposomes encapsulating sulforhodamine B (SRB). GM1, LN, and control liposomes, formulated lacking CNF but encapsulating SRB, were allowed to interact with CNF-conjugate proteins (CTB, BLF, BSA, or OVA) in solution. Interactions between CNF-conjugate proteins and liposomes were determined directly by monitoring CNF co-localized with encapsulated SRB.

MATERIALS AND METHODS

Liposome Formulation Materials. Phosphatidylcholine (PC), phosphatidylglycerol (PG), NBD-phosphatidylethanolamine (NBD-PE) (1,2-Dioleoyl-*sn*-Glycero-3-Phosphoethanolamine-*N*-(7-nitro-2-1,3-benzoxadiazol-4-yl)), biotinyl-phosphatidylethanolamine (biotinyl-PE) (1,2 Dioleoyl-*sn*-glycero-3-phosphoethanolamine-*N*-(Biotinyl)), and carboxyfluorescein-phosphoethanolamine (fluorescein-PE) (1,2-Dioleoyl-*sn*-Glycero-3-phosphoethanolamine) used in formulating unilamellar microemulsified liposomes were purchased from Avanti Polar Lipids, Inc. (Alabaster, AL, USA). Cholesterol was purchased from Sigma Chemical Co. (St. Louis, MO, USA). The amine reactive probe, CNF, and the polar tracer probe SRB were purchased from Molecular Probes Inc. (Eugene, OR, USA). The ganglioside GM1, was purchased from Alexis Corporation (Lausen, Switzerland). BSA, OVA, BLF and LN were purchased from Sigma Chemical Co. (St. Louis, MO, USA). CTB was purchased from Calbiochem (La Jolla, CA, USA).

Immobilization reagents including 1-ethyl-3-(3-dimethylaminopropyl) carbodiimide hydrochloride (EDC) and *N*-Hydroxysulfosuccinimide (Sulfo-NHS) were purchased from Pierce Chemical Co. (Rockford, IL, USA). Buffer salts, acetic anhydride, glass cover slips, and 3-aminopropyl-triethoxysilane were purchased from Fisher Scientific (Pittsburgh, PA, USA). Avidin and succinic anhydride were purchased from Sigma Chemical Co.

Unilamellar Microemulsified Liposome Formulations. The base lipid composition for the formulation of unilamellar microemulsified liposomes consisted of

PC, cholesterol, PG, PE, and biotinyl-PE. Lipids, purchased dry and suspended in chloroform to facilitate formulation, were added to 50 mM Tris-Cl (pH 7.2) at lipid molar ratios of 73 : 15 : 10 : 2 : 0.15, respectively. Head-labeled lipid probes NBD-PE and fluorescein-PE were substituted for PE at concentrations of 0.15 lipid molar percent to probe the artificial bilayers of liposomes. Polar tracing SRB was encapsulated during microfluidization to label the lumen of the liposomes. While holding the lipid component of the formulation constant, a dilution series was designed to determine the appropriate SRB concentration generating liposome lumens that could be viewed and imaged using the CLSM system. The range of the dilution series was 0.45 μM – 4.5 mM SRB as expressed as a concentration of the polar tracer applied prior to processing the buffered lipid containing solution in the Microfluidizer™ 110S (Microfluidics International Corp. Newton, MA, USA). The concentrations used in the series can also be expressed as SRB : total lipid molar ratios. These included 0.011, 0.110, 1.10, 11.0, and 101 moles SRB to every 1 mole of the total lipid in a specific formulation.

The base lipid composition was used to formulate liposomes encapsulating a soluble protein conjugate (CNF-BSA), a membrane protein conjugate (CNF-LN), or glycosphingolipid, ganglioside (GM1). Control liposomes consisted of the identical lipid composition with encapsulated SRB (ganglioside and laminin absent). The lipids were suspended in 10 mL 50 mM Tris-Cl (pH 7.2) and microemulsified in the presence of CNF-protein conjugates (lipid : protein molar ratios of 5844 : 1.0) or ganglioside (ganglioside : lipid molar ratios of 0.089 : 1.0). The SRB : total lipid molar ratio of 1.1 : 1.0 was constant in these formulations.

Liposomes were formed using a Microfluidizer™ equipped with a 10 ml sample hold volume and a cooling loop submerged in an ice bath. The lipid solution was microemulsified for 270 s at maximum pressure (10,000 psi). Immediately following microemulsification, the microemulsified liposome solutions were suspended in agarose or immobilized onto glass coverslips via biotin-avidin interactions. The total volume of solution applied to the Microfluidizer™ was constant in all preparations at 10 ml.

Avidin and Microemulsified Liposome Immobilization. Avidin containing coverslips were prepared by derivatizing the entire surface area of glass coverslips 22 x 22 mm² (484 mm² x 2 = 968 mm²) using 3-aminopropyl-triethoxysilane followed by succinylation with succinic anhydride and acetylation with acetic anhydride [24]. Avidin, 6.0 ng (1.0 x 10⁻¹³ moles) per coverslip, was presented to the derivatized coverslips for immobilization via EDC and Sulfo-NHS using 10 ml 0.1 M MES (2-(*N*-morpholino)ethanesulfonic acid) and 0.5 M NaCl (pH 6.0, adjusted with NaOH) [32]. The coverslips were incubated with avidin for 45 min at room temperature on a platform shaker (150 rpm) followed by 3, 10 ml washes using 50 mM Tris-Cl containing 1 M NaCl (pH 7.2) to eliminate nonspecifically bound avidin. Avidin bound coverslips were stored at 4°C in 50 mM Tris-Cl (pH 7.2). The lipid solutions were formulated, microfluidized, and reacted with avidin containing coverslips to immobilize the biotinylated liposomes via the avidin-biotin interaction.

Prepared liposome suspensions were distributed to beakers containing 5 immobilized avidin coverslips (1.12 x 10⁻⁶ moles total lipid assuming 100% recovery / 4840 mm² total glass surface area) in 10 ml 50 mM Tris-Cl (pH 7.2). The liposome suspensions were allowed to react with coverslips at room temperature for 30 min while

shaking at 150 rpm followed by 3, 10 mL washes of 50 mM Tris-Cl (pH 7.2) containing 1 M NaCl (pH 7.2) to eliminate non-specifically bound liposomes.

Immobilized Liposome Stability Determination. The stability of liposomes was followed during storage. Each liposome formulation contained SRB at the same concentration. The release of encapsulated SRB was used to as an indicator of bilayer integrity. A stable liposome was defined as a liposome characterized by internal encapsulation of SRB surrounded by a lipid bilayer that exhibited no leakage of SRB. A destabilized, or compromised liposome, was defined as a liposome characterized by SRB localized external of the artificial lipid bilayer. Three coverslips of each liposome type (CNF-BSA, CNF-LN, GM1, and control liposomes lacking CNF-conjugates or GM1) were stored dry at 4°C and monitored at 2-week intervals to observe the integrity of the liposomes over a six month period. Three representative fields containing 15+ liposomes were used to determine the percent destabilized liposomes (estimated to the nearest 10).

Fluorescent Labeling of Proteins. Proteins (BSA, BLF, CTB, LN, and OVA) were labeled with CNF. Proteins (0.8 μM) in 0.1 M MES and 0.5 M NaCl (pH 6.0, adjusted with NaOH) were reacted for 45 min with EDC (4.8 μM) and Sulfo-NHS (13 μM). CNF (1.5 μM) was added to the solutions and the reactions allowed to proceed for 2 h at room temperature. The reactions were quenched upon addition of hydroxylamine hydrochloride to a final concentration of 10 mM. The labeled proteins were dialyzed in a Slide-A-Lyzer[®] 10K cassette (Pierce) for 72 hr against 50 mM Tris-Cl (pH 7.2) at 4°C to remove excess CNF.

ELISAs for GM1 and LN Liposomes. ELISA used antibodies (Abs) to confirm the presence of GM1 embedded in liposome bilayers and confirm the presence of

biologically active recognition sites. The Ab was specific for the carbohydrate moiety of GM1. Immobilized GM1 liposomes were formulated containing GM1 at a concentration of 8.9 (molar percent of total lipid). Each ELISA utilized rabbit anti-ganglioside GM1 IgG Ab (Calbiochem). The tests were performed in triplicate; liposomes lacking GM1 were tested identically and acted as the negative control. Anti-ganglioside GM1 Abs, 10 μ l of a 100 μ g/ml stock, was diluted 1 : 500 and 1 ml was used to bind and label the GM1 embedded in the liposome membranes. This was followed by a wash step (30 min, 30 ml of 50 mM Tris-Cl, pH 7.2). Samples were then transferred to a new sterile tube and exposed to goat anti-rabbit IgG alkaline phosphatase conjugates (Sigma). Anti-rabbit IgG alkaline phosphatase conjugate, 1 μ l of a 1.0 mg/ml stock, was diluted 1 : 33,000 and 33 ml added to samples followed by another wash (30 min, 30 ml of 50 mM Tris-Cl (pH 7.2) in 50 ml tube).

Individual coverslips were placed in individual wells of six-well ELISA plates (Costar, VWR, Brisbane, CA, USA) and submerged in 3 ml glycine buffer (pH 10). The alkaline phosphatase substrate, para-nitrophenyl phosphate (pNPP) (Sigma), 3 ml, of a 0.25 mg/ml solution in glycine buffer was added to each well. Presence of the product was followed measuring absorbance with a detection wavelength fixed at 405 nm using a HTS 7000 Bio Assay Reader (Perkin Elmer, Wellesley, MA, USA). After 35 min of product formation, the absorbance measurement for each treatment, in triplicate, were averaged resulting in a single value per treatment. Liposomes prepared in the absence of GM1 acted as negative controls. A signal-to-noise ratio value was calculated for each treatment by subtracting the average absorbance of negative controls from the average absorbance of the treatment.

Abs were used to confirm the presence of the membrane protein LN embedded in artificial lipid bilayers of liposomes by ELISA. The Ab was specific for LN. Immobilized liposomes containing LN at a ratio of 59 : 1 (w/w) lipid to protein (5844 : 1 mole lipid to protein) were immobilized on a glass solid support. Rabbit anti-laminin IgG Ab (Sigma) was used in the ELISA and the assays were performed in triplicate. Anti-laminin Ab, 1 μ l of a 100 μ g/ml stock, was diluted 1 : 25,000 and 25 ml was used to bind and label the GM1 embedded in the liposome membranes. This was followed by a wash step (30 min, 30 ml of 50 mM Tris-Cl, pH 7.2). Samples were then transferred to a new sterile tube and exposed to goat anti-rabbit IgG alkaline phosphatase conjugates (Sigma). Anti-rabbit IgG alkaline phosphatase conjugate, 1 μ l of a 1.0 mg/ml stock, was diluted 1 : 33,000 and 33 ml added to samples followed by another wash (30 min, 30 ml of 50 mM Tris-Cl (pH 7.2) in 50 ml tube).

Individual coverslips were treated as described in the GM1 ELISA procedure. A signal to noise ratio value was calculated for each treatment by subtracting the average absorbance of negative controls, liposomes lacking LN, from the average absorbance of the treatment.

Soluble Protein Binding Studies. GM1 and LN liposomes were separately incubated with CNF-CTB, CNF-BSA, CNF-BLF, or CNF-ovalbumin at 6.7×10^{-9} moles protein in 10 mL 50 mM Tris-Cl (pH 7.2) for 1 h at room temperature. The total surface area containing GM1 or LN liposomes was 3872 mm². Liposomes formulated in the absence of ganglioside and protein and immobilized on the same amount of surface area acted as controls. The incubation was performed on a shaking platform (100 rpm) in triplicate. Coverslips were washed with 50 mM Tris-Cl (pH 7.2) followed by 0.5 M

NaCl, 50 mM Tris-Cl (pH 7.2) and finally 1 M NaCl, 50 mM Tris-Cl (pH 7.2) washes of 30 ml each.

Immediately following the incubation, CLSM was used to observe the localization of CNF-protein conjugates. Three coverslips were monitored for the presence of CNF using the blue monitor channel (668 nm) during a progressive scan. GM1 and LN liposomes encapsulating SRB, monitored using the red monitor channel (598 nm) were labeled blue or magenta in the presence of an interaction between the CNF-labeled proteins and immobilized liposomes. GM1 and LN liposomes exhibiting co-localization were compared against control liposomes formulated in the absence of receptor molecules subjected to the same CNF-protein conjugate under the same conditions. Evidence of an interaction by comparison with the appropriate control was noted as absent (liposomes simply red), possible (some co-localization), strong (strong co-localization), or definite (intense co-localization).

Confocal Laser Scanning Microscopy. Confocal laser scanning microscopy images were generated using a Keller type MRC 1024 krypton/argon laser scanning confocal system (Bio-Rad, Hercules, CA, USA) interfaced with an inverted microscope (Diaphot TE300, Nikon, Tokyo, Japan). The pinhole diameters were 2.5, 2.5 and 4.0 mm respectively for the 488, 598, and 668 nm laser lines and the objective lens was a Nikon 100X, plan apo, oil immersion with a numerical aperture of 1.40. The 488 nm line excited the fluorescein-PE and NBD-PE encaged as components of the liposome bilayers. The 647 nm laser line was used for liposomes containing CNF-protein conjugates. The 568 nm laser line was used to excite the encapsulated SRB. Dual and triple labeling of

microemulsified liposomes afforded flexibility and specificity in monitoring the artificial structures.

Images (512 x 512 pixels and 226.50, 1,415.64, or 22,650.25 μm^2) were taken consecutively with the dichroic beam splitters and filters to minimize cross talk between channels. The photomultiplier gain/sensitivity/contrast was adjusted to give a slightly over-modulated signaling in the normal scan mode. Holding all other factors constant, the photobleaching, or quenching, of probes was investigated by continuously scanning fields of liposomes at increased magnification for 60 s. The resulting RGB images were overlaid using LaserSharp® version 3.2 (Bio-Rad).

RESULTS AND DISCUSSION

Composition of Liposomes. Liposomes produced using the Microfluidizer™ were immediately embedded in agarose and CLSM was used to characterize the liposomes. The 488 nm laser line was used to excite the probe labeled lipid bilayer components (fluorescein-PE and NBD-PE) while the encapsulated SRB was excited using the 568 nm laser line. The 488 nm line was processed to the green channel while the 568 was monitored by the red channel. A population of agarose matrix embedded NBD-PE, fluorescein-PE, SRB probed liposomes is shown in **Figure 3**. The size and shape of a representative liposome with a 2.3 μm diameter is shown inset (**Figure 3**). The yellow appearance results from the combined green and red probes imaged simultaneously. This phenomenon is known as co-localization. The average diameters of agarose entrapped liposome was 1.8 μm . The diameters ranged $\pm 1.5 \mu\text{m}$ ($n=10$) in the

population but did not exceed 3.5 μm . Liposomes were clearly observed as distinct entities. The probe molecules, NBD-PE and fluorescein-PE used to illuminate the membrane structures, were localized in the bilayer of the liposomes resulting in a green coloration. SRB was localized in the aqueous void space, or lumen. The liposomes were unilamellar and similar to one another in all measures and observations. No clumping, aggregation or agglutination was observed. There was no evidence of interactions between individual liposomes.

The distribution of liposomes embedded in agarose was random. **Figure 3** shows fluorescent artifacts of liposomes located directly above and below the xy scan plane. Artifacts appear as dull, unclear, out of focus blotches of green/yellow fluorescence contrasting with distinct cross-section of spheres located centrally in the scan plane. Such artifacts result because fluorescently labeled three-dimensional subjects are imaged two-dimensions.

Immobilized Liposome Formulations. The liposome formulations consisted of lipids and various combinations of fluorescent probes. The probes were selected for their ability to label and identify liposomes. A legend of the microemulsified liposome type, probed component(s), fluorescent probes and monitor channel is attached as Appendix A. For example, the lipid head-group labeled probes used to illuminate the lipid bilayers of liposomes embedded in agarose also labeled immobilized liposomes. The fluorophores of these probes were located physically on both the internal and external membrane surface, thus marking bilayers of agarose embedded and immobilized liposomes. Similarly useful in both liposome formulations, SRB was found to specifically label the lumen after encapsulation during processing in the Microfluidizer™. After

immobilization and washes of immobilized liposomes with the buffers described, the only visible SRB fluores were encapsulated inside the liposomes. Therefore, SRB specifically labeled the liposomal lumen of individual immobilized liposomes.

The fluorescent artifacts observed using the agarose matrix were successfully eliminated using the avidin-biotin immobilization procedure (**Figure 4**). Use of head-group labeled phospholipids and encapsulated SRB probes allowed for direct visualization of co-localized fluorophores (yellow). The composition of immobilized liposomes and liposomes embedded in agarose were identical. The average diameters of immobilized liposomes was $1.5 \mu\text{m}$ (mean $\pm 1.2 \mu\text{m}$, $n=10$). Physical comparison of immobilized liposomes to the liposomes embedded in agarose (**Figure 3**) found no observable differences other than the physical location resulting from avidin-biotin immobilization. An immobilized liposome viewed at increased magnification (diameter of this liposome was estimated at $1.3 \mu\text{m}$), is shown in the inset (**Figure 4**).

The advantage of immobilization lies in facilitating the removal of unincorporated and weakly associated lipids, probes, and vesicles without affecting the liposomal surface or lumen. A liposome must contain at least one biotinylated phospholipid to potentially be immobilized on the glass surface containing avidin as these two molecules constitute the necessary link relied on in the immobilization strategy described. Liposomes were designed to contain biotinyl-PE at an appropriate concentration that would result in effective immobilization. The biotinyl-PE was used at a molar ratio of 0.015 : 1.0 (biotinyl-PE : total lipid). This ratio is equivalent to 1.5 biotinylated phospholipids for every 100 lipids in the formulations processed using the Microfluidizer™. Theoretically,

each liposome was composed of at least 67 lipids contains a potential binding site, a biotinyl-PE molecule, for immobilization using the methods and formulations described.

Another advantage of the described unique immobilization protocol is the ability to control the spatial location of liposomes. The confocal advantage of highly focused light in optical sections allowed the vertical scanning of individual fields of liposomes at close range near the limits of the microscope and vertical scans of individual liposomes in detail. This specificity of location, especially at high powers of magnification, necessitates the liposomes be located in the same xy plane in order to view multiple liposomes and image similar cross sections of multiple liposomes. Examination of populations of liposomes proved that these vesicles were immobilized in relatively the same plane. In other words, they were equidistant from the surface of the coverslips to which they were bound. This was not the case of the randomly distributed liposomes embedded in the agarose matrix. The shape of liposomes was consistent before and after immobilization, indicating no evidence of a non-specific interaction between the liposomes and the glass support (other than the intended, specific immobilization).

Probes indicating the location of the artificial membrane bilayers (NBD-PE and fluorescein-PE) were subject to photobleaching, or quenching, more profoundly than the SRB or CNF-conjugates. This was easily observed during continuous scanning representative fields of liposomes at increased magnification. While scanning using the continuous mode, the originally brilliantly green and yellow liposomes would fade to red holding all other factors constant over a 60 s period. The red signal, indicating the presence of SRB, was observed to be less susceptible to photobleaching over the same time period. CNF-protein conjugates, monitored using the blue channel was also less

susceptible to photobleaching when compared to the head-group labeled phospholipid probes. Due to the observed photobleaching effect on NBD-PE and fluorescein-PE, subsequent experiments were designed to rely on the encapsulated SRB as an indicator of liposome stability rather than the head-group labeled lipids. It was also noted that SRB, when used at an appropriate encapsulation concentration is a better illuminator of liposomes. NBD-PE and fluorescein-PE were effective when characterizing liposomes imbedded in agarose. Many of the liposomes were labeled simply red by SRB. Green probes, NBD-PE and fluorescein-PE, were absent in many of the smaller liposomes (diameters $> 1.0 \mu\text{m}$).

Optimizing SRB Concentration. Unencapsulated fluore, when present above a specific concentration, cause increased background fluorescence. To increase the encapsulation of SRB and optimize CLSM visualization of liposomes using this polar tracing probe, various concentrations of SRB ranging from $0.45 \mu\text{M}$ – 4.5 mM or (SRB : total lipid molar ratio of $0.011 : 1$ to $110 : 1$) were included in the soluble phase prior to microfluidization. It was desirable to include SRB at increased concentrations to facilitate identification of the maximum number of liposomes located in specific surface area. As shown in **Figure 5A**, lumens of liposomes microfluidized with $0.45 \mu\text{M}$ SRB (SRB : total lipid molar ratio of $0.011 : 1$) encapsulated little SRB. The SRB concentration was too high when liposomes were microfluidized with $450 \mu\text{M}$ SRB (SRB : total lipid molar ratio of $11 : 1$). SRB bound the glass and therefore the immobilization surface was labeled red (**Figure 5B**). It was not possible to distinguish liposome lumens from the background using the red monitor channel.

The optimum concentration of SRB in the soluble phase prior to microemulsification was determined to be 45 μM (SRB : total lipid ratio of 1.1 : 1) (**Figure 5C**). Liposomes lumens were labeled red while glass surface background fluorescence was minimized. This concentration was held constant for the liposomes formulations used to estimate the time required to observe destabilization and leakage of encapsulated SRB.

Again, SRB was a more effective probe in identifying liposomes because it specifically labeled each individual liposome found throughout the population distribution. Liposomes encapsulating SRB are labeled red in the absence of other probes. A distribution of red liposomes and are found interdispersed among the yellow/green liposomes at the concentrations tested (**Figures 5A-C**).

Characterization and Stability of Liposomes. Liposomes containing GM1, CNF-BSA, or CNF-LN were homogenous distributions of individual liposomes. No complexes of liposomes interacting with other liposomes in any of the described formulations were observed. All liposome, irrespective of incorporated biomolecule were successfully immobilized and viewed using the parameters described. The size, shape and distributions were nearly identical to liposomes formulated in the absence of protein and ganglioside. ELISAs confirmed the presence of GM1 associated with GM1 liposomes, and LN with LN liposomes. The stabilities of GM1, CNF-BSA, CNF-LN, and control liposomes were determined directly by monitoring leakage of encapsulated SRB.

CNF-BSA and CNF-LN liposomes were easily distinguished from control liposomes. Immediately after immobilization, the co-localization of blue and red probes

resulted in a distinct magenta color of the liposome spheres. This co-localization was used for identification of membrane bound CNF-LN and CNF-BSA liposomes containing encapsulated SRB (insets **Figures 6 and 7**, respectively). This coloration contrasted with liposomes identified by SRB (red) or yellow co-localization of SRB (red) and head-group labeled phospholipids (green).

After liposomes were stored dry at 4°C for a period of days, indications of compromised bilayer integrity was observed. SRB was observed diffusing in a symmetrical ring extending beyond the artificial bilayers. **Figure 6** inset shows SRB located only in the liposomal lumen after immobilization. The aqueous lumen is red and the bilayer contains CNF-LN (blue) while the local area around the liposome is clearly void of fluorescence. **Figure 6** shows a different, single destabilized liposome containing CNF-LN leaking SRB. Some SRB remained centrally located in the liposomal lumen; But, the characteristic red ring of diffused SRB is evident external of the blue liposome bilayer. The area immediately local to the liposome is unlabeled because the SRB has migrated evenly away from the centrally located bilayer.

Figure 7 inset shows an liposome encapsulating CNF-BSA and SRB prior to destabilization. CNF-BSA (blue) and SRB (red) are co-localized in the aqueous lumen while the local area around the liposome is clearly void of fluorescence. **Figure 7** shows a different, single destabilized liposome that initially encapsulated CNF-BSA and SRB. SRB is shown leaking in a uniform manner external of the bilayer as was noted from CNF-LN liposomes. The lumen is void of SRB and CNF-BSA; but, the red ring of SRB is clearly external of the magenta bilayer. Co-localization of CNF and SRB at the

artificial membrane indicates that the CNF-BSA remains internally encapsulated but associated with the permeable bilayer that has released SRB.

In time, similar SRB leakage was evident in GM1 liposomes. **Figure 8** inset shows a GM1 liposome prior to destabilization. This GM1 liposome did not exhibit colocalization. GM1 liposomes were probed using NBD-PE, fluorescein-PE, and encapsulated SRB. After destabilization, little SRB remained located in the lumen, but a distinct ring of SRB was located externally of the bilayers (**Figure 8**). The concentrations of NBD-PE and fluorescein-PE were less effective as probes indicating bilayer integrity. Therefore, SRB was solely used as an indicator of bilayer permeability and destabilization.

A field of destabilized CNF-BSA liposomes is shown in **Figure 9**. The SRB rings are evident in red emerging from central points of origin. Central to each ring are the liposomes formerly encapsulating CNF-BSA and SRB, while the yellow liposomes (CNF-BSA absent) show no evidence of SRB leakage. It was noted that CNF-BSA liposomes ultimately released some of the CNF-protein conjugate. As shown inset, a field of destabilized CNF-BSA encapsulating liposomes, CNF-BSA was primarily localized along the membrane. It was also found externally forming a second ring (blue) similar to the SRB ring (red). The inset of **Figure 9** shows leakage of SRB and CNF-BSA from another field of CNF-BSA liposomes.

The permeation of SRB was non-uniform with respect to liposome type, but a linear, time dependent trend was evident (**Table 1**). The earliest evidence of SRB leaking from any liposome was found after at 59 days. Ten percent of the CNF-BSA liposomes had lost their initial ability to encapsulate SRB after this period. Whereas, 50 percent of

the CNF-BSA liposomes had destabilized after 103 days and finally at 146 days, 80 percent of the CNF-BSA liposomes were destabilized. CNF-BSA was also observed external of the membrane at 146 days. This contrasted with the observed destabilization of CNF-LN liposomes over the same period. Ten percent of the CNF-LN liposomes had lost the initial ability to encapsulate the polar tracing probe after 116 days. At 146 days, 20 percent of the CNF-LN liposomes had destabilized and finally at 188 days, 50 percent of the CNF-LN liposomes were destabilized. CNF-LN was not observed external of the membrane, even after 188 days. The earlier release of SRB by CNF-BSA liposomes appears to be related to the encapsulation of the probed protein in the aqueous lumen when compared to CNF-LN liposomes. The hydrophobic probe, bound to soluble BSA encapsulated in the lumen, may have contributed to an earlier onset of SRB leakage when compared to the membrane bound CNF-LN conjugate.

The control SRB encapsulating liposomes, composed of only of lipids, destabilized at slower rate than both the CNF-BSA and CNF-LN liposomes. Only 20 percent of the control liposomes had destabilized at 188 days. The destabilization of the GM1 liposomes was similar to the control liposomes with only 30% of the liposomes destabilized at 188 days. The percent destabilized as a function of time, listed in **Table 1**, of the 4 liposome types is shown as percent calculated by determining the number of immobilized liposomes destabilized in 3 to 5 representative fields (estimated to the nearest 10).

As noted in previous reports using CLSM, quantitative comparison of fluorescence intensities is not trivial for a variety of reasons, because of photo-bleaching and quenching [33]. The immobilized liposomes characterized in this study, labeled with

appropriate fluorophores, have the advantage of direct monitoring over a long period of time. Stabilities of GM1, CNF-BSA, CNF-LN, and control liposomes were compared over weeks and months rather than a period of minutes or hours as done previously with soluble liposomes [13, 34].

Binding of Soluble Proteins. Interactions between soluble proteins and immobilized liposomes were determined directly using the blue and red monitor channels. GM1, LN, and control liposomes encapsulating SRB were exclusively red in the absence of soluble CNF-conjugate proteins, while magenta color indicated binding of soluble CNF-conjugates.

CNF-CTB bound GM1 liposomes. GM1 liposomes were subjected to treatment with the CNF-CTB conjugate and subsequently labeled magenta due to co-localization of the SRB and CNF probes. This strong co-localization indicated a definite interaction between CNF-CTB and the GM1 liposomes. CNF was absent in proximity to identically treated control liposomes. Therefore, no co-localization of the two probes was observed. CNF-LN liposomes interacted with CNF-CTB conjugate also exhibited magenta coloration indicating the presence of recognition and interaction of CNF-CTB with LN liposomes. The co-localization was not as pronounced as what was observed between CNF-CTB and GM1 liposomes indicating the interaction is not as strong. **Figures 10A, 10B, 10C and 10D** show GM1 liposomes after reaction with CNF-CTB, CNF-BLF, CNF-BSA, and CNF-OVA, respectively. The inset images show liposome groupings at similar or increased magnification.

Co-localization, indicated by magenta coloration, of CNF-BLF and SRB was observed with GM1 but not LN or control liposomes. The co-localization was similar in

fields of CNF-BLF (**Fig 10B**) and CNF-CTB (**Fig. 10A**). This indicates CNF-BLF recognizes and binds ganglioside GM1 embedded in liposomes as does CNF-CTB. CNF-CTB and CNF-BLF did not interact with liposomes. CNF-BSA did not bind to LN liposomes and only showed evidence of possible interaction with GM1 and control liposomes. This interaction has not been characterized and appears to be non-specific. The presence of CNF-OVA was not observed after incubation with GM1, LN, and control liposomes. CNF-OVA therefore constituted a negative control in the protein binding studies. Representative GM1 liposomes are shown after interaction with the respective CNF-protein conjugates. The binding interaction characterization of the CNF-conjugate protein with GM1, LN, and control liposomes is summarized in **Table 2**.

Interactions of soluble proteins and liposomes were characterized by the observance of co-localized probes. The channel mixing and resultant coloration schemes were easy to identify and interpret. In our system, images were captured in a static environment rather than a flow system, which identifies interactions, or lack thereof, based on fluorescent trails compared to points [31]. Selection and optimization of probes, in particular SRB, afforded specificity in labeling liposome components and minimal non-specific labeling of the immobilization surface. SRB release, measured spectrophotometrically, has been used in other studies to indicate unilamellar liposome destabilization and membrane permeability [34]. Our system was designed to benefit from the capabilities of a confocal system to characterize and use immobilized microemulsified liposomes to study a well-characterized interaction between CTB and bilayer embedded GM1. The findings complement recent reports of nitrocellulose

membrane supported ganglioside-liposome immunoassays designed to detect cholera [35] and botulinum toxins [36].

CONCLUSIONS

A stable biomimetic system consisting of immobilized microemulsified liposomes containing embedded GM1 or laminin on a solid glass support was developed. The immobilization procedure did not alter the composition or dimensions of the liposomes but presented several advantages to alternative strategies. Immobilization affords an important element of spatial control. Confocal microscopy revealed that all liposomes irrespective of incorporated biomolecule were located in relatively the same *xy* plane equidistant from the glass surface as compared to liposomes embedded in an agarose matrix. Therefore using the described methods, multiple immobilized liposomes can be observed in a single field under a number of treatments. Avidin-biotin immobilization is advantageous because nonspecifically bound molecules can be removed by washing the immobilized surface with buffer. After a wash, destabilization can be monitored directly over time by the observance of SRB located external of the bilayer.

Confocal microscopy was used to analyze immobilized artificial structures formulated specifically for determining the stability and interactions of immobilized liposomes with proteins in solution. A stable liposome was defined as a liposome characterized by internal encapsulation of SRB surrounded by a lipid bilayer with no leakage of SRB. All liposome preparations were stable for a period of at least 46 days, and some up to 188 days.

Molecular interactions between molecules in solution can be identified using multiple labeling techniques. The molecular interactions between soluble CNF-protein conjugates (BSA, BLF, CTB, and OVA) and SRB encapsulating liposomes containing GM1 and LN were investigated. CNF conjugated CTB and BLF co-localized with GM1 liposomes. LN liposomes and CNF-CTB, but not CNF-BLF. CNF-CTB and CNF-BLF did not bind liposomes containing only lipid and SRB. No interaction between CNF-OVA was observed with any of the liposomes tested.

To our knowledge we are the first group to successfully develop immobilization methodology of unilamellar GM1 and LN liposomes on glass and observe bilayer encapsulation and interactions using CLSM.

REFERENCES

1. Gyongyossy-Issa M, Muller W, Devine D. The covalent coupling of Arg-Gly-Asp-containing peptides to liposomes: purification and biochemical function of the liposomes. *Arch Biochem Biophys* 1998; 353(1):101-108.
2. Kawakami S, Yamashita F, Nishikawa M, Takakura Y, Hashida M. Asialoglycoprotein receptor-mediated gene transfer using novel galactosylated cationic liposomes. *Biochem Biophys Res Commun* 1998; 252:78-83.
3. Koide K, Karel M. Encapsulation and stimulated release of enzymes using lecithin vesicles. *Int J Food Sci Tech* 1987; 22:707-723.
4. Konigsberg P, Godtel R, Kissel T, Richer L. The development of IL-2 conjugated liposomes for therapeutic purposes. *Biochim Biophys Acta* 1998; 1370:243-251.
5. Lambert O, Plancon L, Rigaud J, Letellier L. Protein-mediated DNA transfer into liposomes. *Mol Microbiol* 1998; 30(4):761-765.
6. Meyer O, Kirpotin D, Hong K, Sternberg B, Park J, Woodle M, Papahadjopoulos D. Cationic liposomes coated with polyethylene glycol as carriers for oligonucleotides. *J Biol Chem* 1998; 273(25):15621-15627.

7. Stegmann T, Bartoldus I, Zumbunn J. Influenza hemagglutinin-mediated membrane fusion: Influence of receptor binding on the lag phase preceding fusion. *Biochem* 1995; 34:1825-1832.
8. Carson H. Liposomes. *Happi* 1993(March):53-54, 56, 58.
9. Gonzalez R, Sanchez J, Holmgren J, Lopez S, Arias C. Immunological characterization of a rotavirus-neutralizing epitope fused to the cholera toxin B subunit. *Gene* 1993; 133:227-232.
10. Chang T. Artificial cells in medicine and biotechnology. *Appl Biochem Biotechnol* 1984; 10:5-24.
11. Mayhew E, Lazo R, Vail W, King J, Green A. Characterization of liposomes prepared using a microfluidizer. *Biochim Biophys Acta* 1984; 775:169-174.
12. Rodriguez R, Xamani M. Liposomes prepared by high-pressure homogenizers. In: Duzgunes N, ed. *Methods in Enzymology*. San Francisco, California: Elsevier Inc., 2003; 28-46.
13. Fabani M, Gargini R, Taira M, Iacono R, Alonso-Romanowski S. Study of *in vitro* stability of liposomes and *in vivo* antibody response to antigen associated with liposomes containing GM1 after oral and subcutaneous immunization. *J Liposome Res* 2002; 12(1-2):13-27.
14. Park S, Durst R. Immunoliposome sandwich assay for the detection of *Escherichia coli* O157:H7. *Anal Biochem* 2000; 280:151-158.
15. Nagle J, Tristam-Nagle S. Structure of lipid bilayers. *Biochim Biophys Acta* 2000; 1469:159-195.
16. Nieva J, Bron R, Corver J, Wilschut J. Membrane fusion of Semliki Forest virus requires sphingolipids in the target membrane. *EMBO J* 1994; 13(12):2797-804.
17. Kishida E, Goldstein L. Characterization of gangliosides from Ehrlich ascites tumour cells and their variants. *Glycoconj J* 1996; 13(2):127-134.
18. Steck T, Dawson G. Topographical distribution of complex carbohydrates in the erythrocyte membrane. *J Biol Chem* 1974; 249(7):2135-2142.
19. Karlsson K. Microbial recognition of target cell glycoconjugates. *Curr Opin Struct Biol* 1995; 5(5): 622-635.

20. Charych D, Cheng Q, Reichert A, Kuziemko G, Stroh M, Nagy J, Spevak W, Stevens R. A 'litmus test' for molecular recognition using artificial membranes. *Chem Biol* 1996; 3:113-120.
21. Salyers A, Whitt D. *Bacterial Pathogenesis: A Molecular Approach*. Second ed. Washington, D.C.: ASM Press, 2002.
22. Dionysius D, Milne J. Antibacterial peptides of bovine lactoferrin: purification and characterization. *J Dairy Sci* 1997; 80:667-647.
23. Walsh M, Nam S. Rapid fractionation of bovine transferrin using immobilized gangliosides. *Prep Biochem Biotechnol* 2001; 31(2):89-102.
24. Walsh M, Nam S. Affinity enrichment of bovine lactoferrin in whey. *Prep Biochem Biotechnol* 2001; 31(3):229-240.
25. Kleinman H, Cannon F, Laurie G, Hassell J, Aumailley M, Terranova V, Martin G, DuBois-Dalcq M. Biological activities of laminin. *J Cell Biochem* 1985; 27(4):317-325.
26. Beck K, Hunter I, Engel J. Structure and function of laminin: anatomy of a multidomain glycoprotein. *FASEB J* 1990; 4:148-160.
27. Rigaud J-L, Levy D. Reconstitution of membrane proteins into liposomes. In: Duzgunes N, ed. *Methods in Enzymology*. San Francisco, California: Elsevier Inc., 2003; 65-86.
28. Timpl R. Structure and biological activity of basement membrane proteins. *Eur J Biochem* 1989; 180(3):487-502.
29. Ferrando M, Spiess W. Review: confocal scanning laser microscopy, a powerful tool in food science. *Food Sci Technol Int London* 2000; 6(4):267-284.
30. Frank J. Microbial attachment to food and food contact surfaces. *Adv Food Nutr Res* 2001; 43:319-370.
31. Bendas G, Vogel J, Bakowski U, Krause A, Muller J, Rothe U. A liposome-based model system for the simulation of lectin-induced cell adhesion. *Biochim Biophys Acta* 1997; 1325:297-308.
32. Hermanson G. *Bioconjugate Techniques*. New York: Academic Press, Inc., 1996.

33. Cevc G, Schatzlein A, Richardsen H. Ultradeformable lipid vesicles can penetrate the skin and other semi-permeable barriers unfragmented. Evidence from double label CLSM experiments and direct size measurements. *Biochim Biophys Acta* 2002; 1564:21-30.
34. Agafonov A, Gritsenko E, Belosludtsev K, Kovalev A, Gateau-Roesch O, Saris N-E, Mironova G. A permeability transition in liposomes induced by the formation of Ca²⁺/palmitic acid complexes. *Biochim Biophys Acta* 2003; 1609:153-160.
35. Ahn-Yoon S, DeCory T, Baeumner A, Durst R, Ganglioside-liposome immunoassay for the ultrasensitive detection of cholera toxin. *Anal Chem* 2003; 75(10):2256-2261.
36. Ahn-Yoon S, DeCory T, Durst R, Ganglioside-liposome immunoassay for the detection of botulinum toxin. *Anal Bioanal Chem* 2004; 378(1):68-75.

Table 1. Percent of Immobilized Microemulsified Biomimetic Liposomes Observed Leaking SRB by Day.¹

	DAY											
	32	46	59	73	88	103	116	131	146	160	175	188
Control Liposomes	0	0	0	0	0	0	0	0	10	10	20	30
LN Liposomes	0	0	0	0	0	0	10	10	20	20	30	50
GM1 Liposomes	0	0	0	0	0	0	0	10	10	20	20	30
BSA Liposomes	0	0	10	20	20	50	60	70	80	80	80	80

¹ Percent liposomes, rounded to the tenth, leaking SRB after surveying 5 representative fields for a total count of 45-65 liposomes

GM1 = monosialoganglioside

BSA = bovine serum albumin

LN = laminin

SRB = sulforhodamine B

Table 2. Binding Interactions Between Surface Containing Immobilized Microemulsified Liposomes Containing GM1 or Laminin and Soluble Proteins.¹

CNF-Protein Conjugate	Biomimetic Liposomes		
	Control	GM1	LN
CTB	-	+++	++
BLF	+	+++	-
BSA	-	+	-
OVA	-	-	-

¹ Presence of CNF-protein co-localized on biomimetic liposomes observed with confocal microscopy

(+++)
(++)

(+++)
(++) indicates highest degree of co-localization, a definite interaction between CNF-protein in solution and liposomes

(+) indicates high degree of co-localization, strong evidence of interaction between CNF-protein in solution and liposomes

(+) indicates some co-localization, evidence of possible interaction between CNF-protein in solution and liposomes

(-) indicates no co-localization, no evidence of interaction between CNF-protein in solution and liposomes

BLF = bovine lactoferrin

BSA = bovine serum albumin

CTB = cholera toxin (beta subunit)

GM1 = monosialoganglioside

LN = laminin

OVA = ovalbumin

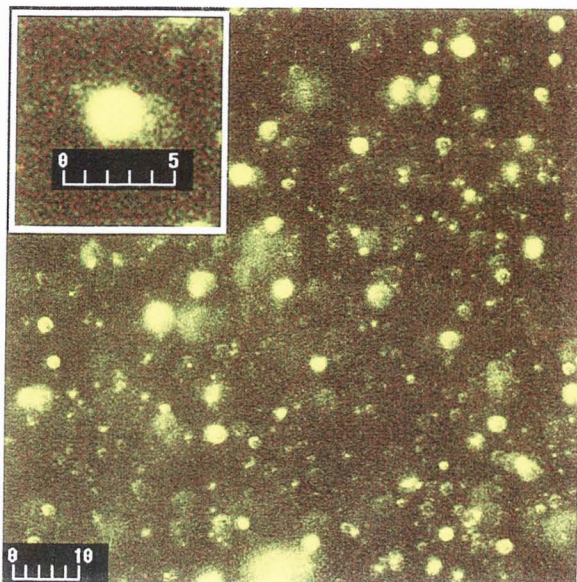


Figure 3. Field of unilamellar microemulsified liposomes embedded in agarose matrix directly after microemulsification. Liposomes contain NBD-phosphatidylethanolamine (green) and carboxyfluorescein-phosphatidylethanolamine (green) localized in the artificial bilayer. Encapsulated sulforhodamine B (red) was localized in the liposomal lumen. Co-localized green and red probes appear yellow. Single representative liposome shown in inset. Scale values represent μm .

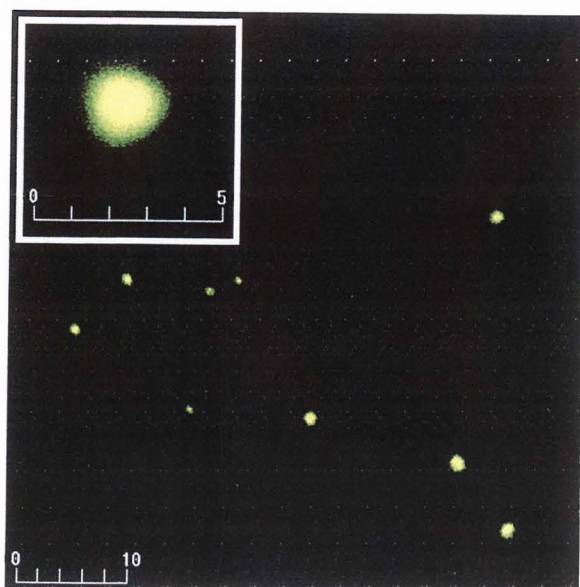


Figure 4. Field of immobilized unilamellar microemulsified liposomes immobilized directly after microemulsification. Liposomes immobilized via biotinylated phospholipids on coverslips containing covalently bound avidin. Liposomes contain NBD-phosphatidylethanolamine (green) and carboxyfluorescein-phosphatidylethanolamine (green) localized in the artificial bilayer. Encapsulated sulforhodamine B (red) was localized in the liposomal lumen. A representative liposome is shown at increased magnification in inset. Scale values represent μm .

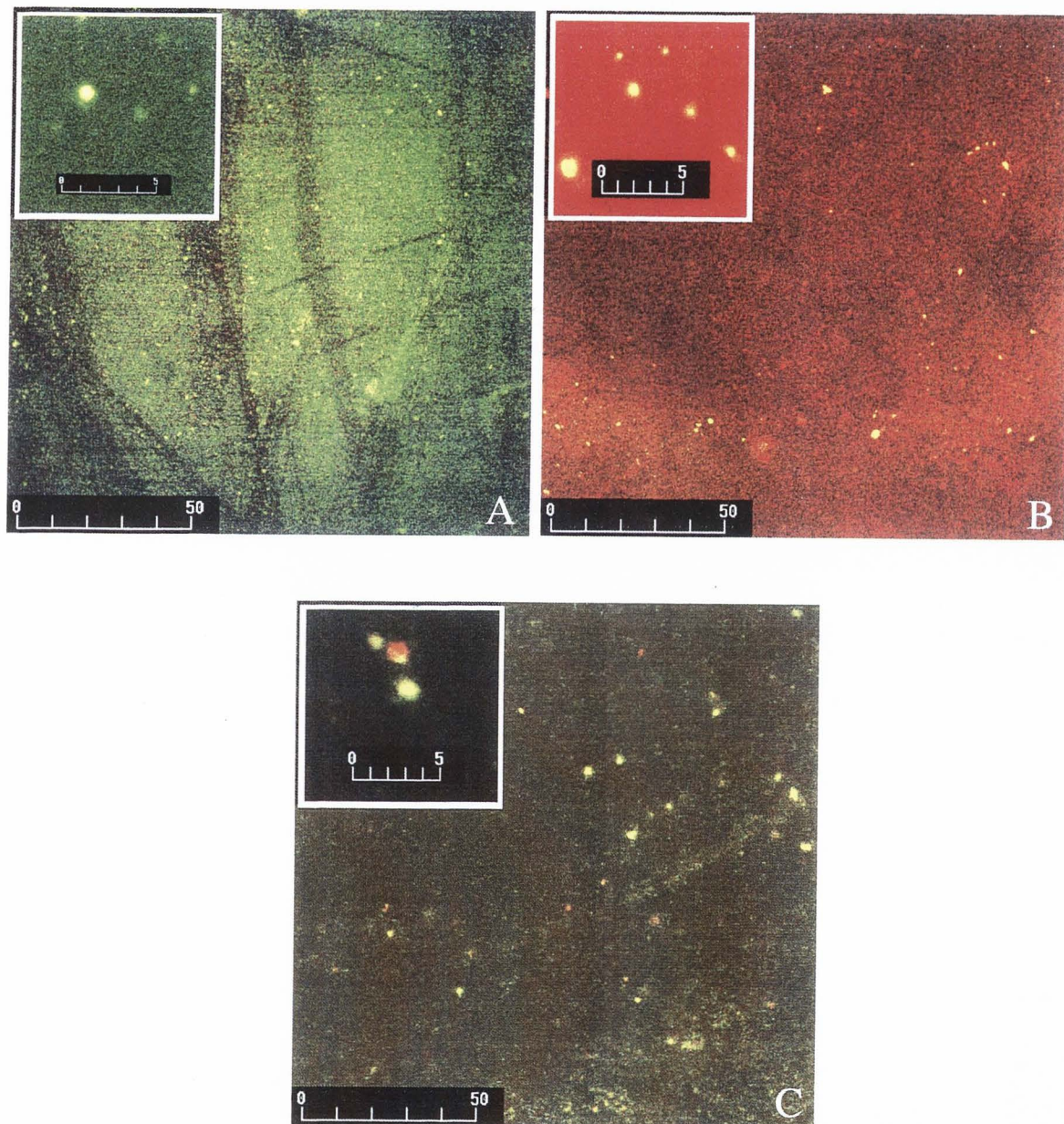


Figure 5. Liposomes microfluidized with 0.45, 450, and 45 μM SRB (SRB : total lipid molar ratios of 0.011 : 1, 11 : 1, and 1.1 : 1), respectively A, B, and C. A representative liposome grouping is shown at increased magnification in inset. Scales in μm .

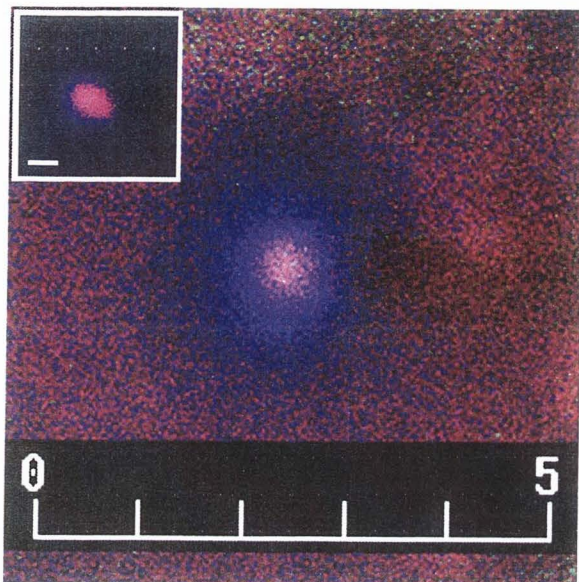


Figure 6. SRB leaking from compromised membrane bound CNF-LN liposome. Scale values represent μm . Inset: Membrane bound CNF-LN (blue) in artificial bilayer and encapsulating SRB (red) prior to destabilization. Bar = $1 \mu\text{m}$. Co-localization results in magenta coloration.

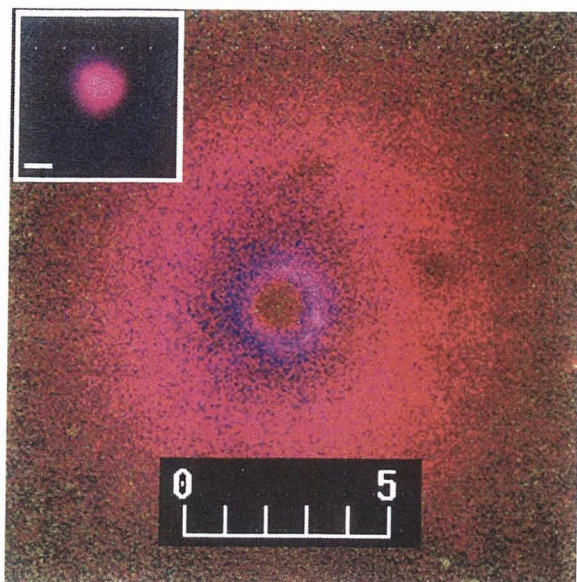


Figure 7. SRB leaking from compromised CNF-BSA encapsulating liposome. Scale values represent μm . Inset: Liposome encapsulating CNF-BSA (blue) and SRB (red) prior to destabilization. Bar = $1 \mu\text{m}$. Co-localization results in magenta coloration.

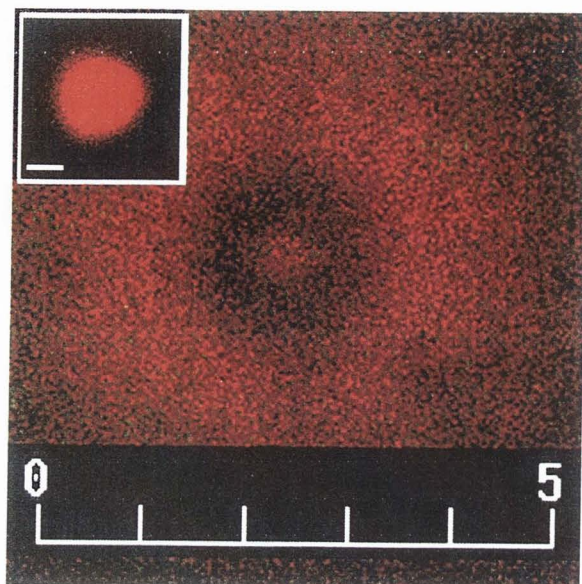


Figure 8. SRB leaking from compromised GM1 liposome. Scale values represent μm . Inset: GM1 liposome containing GM1 in artificial bilayer and encapsulating SRB (red). Bar = 1 μm .

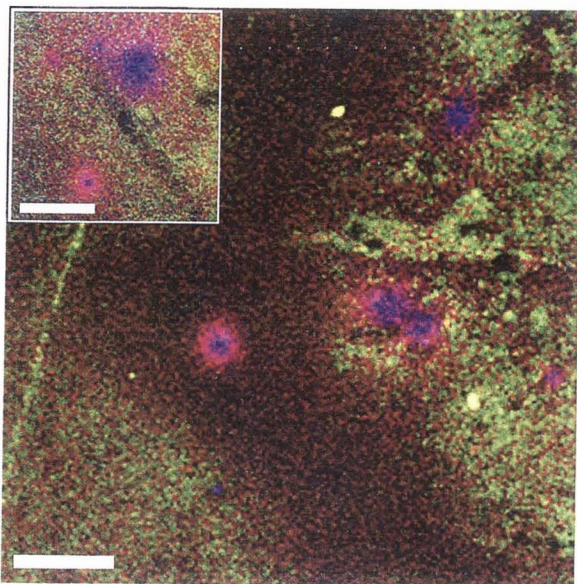


Figure 9. Field of CNF-BSA encapsulating liposomes leaking SRB and CNF-BSA. Inset: Group of CNF-BSA encapsulating liposomes leaking SRB (red) and CNF-BSA (blue). Bars = 10 μm .

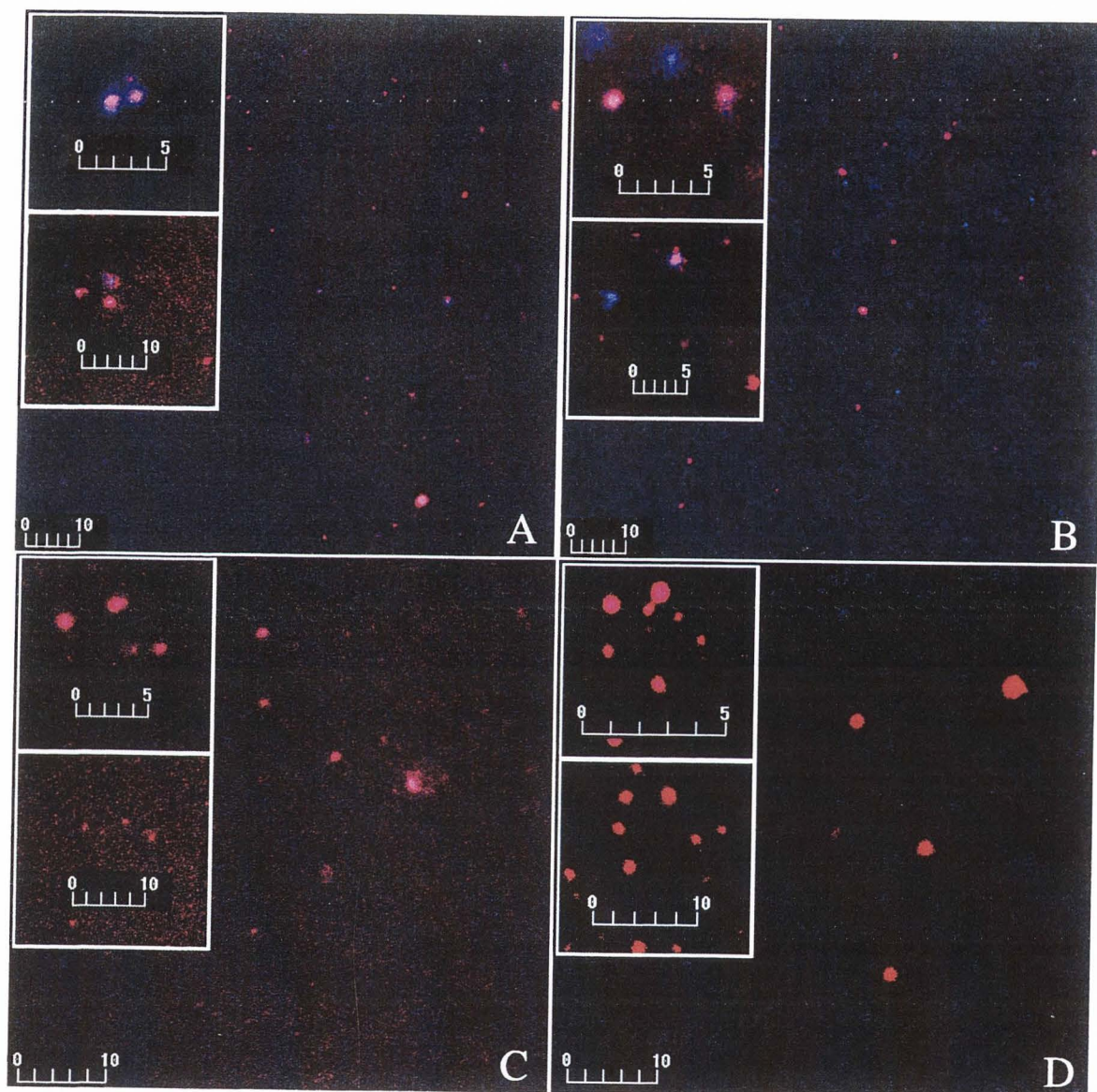


Figure 10. GM1 liposomes after interaction with CNF-CTB, CNF-BLF, CNF-BSA, and CNF-ovalbumin, respectively A, B, C, and D. Co-localization of encapsulated SRB and CNF-protein conjugate results in magenta coloration. No co-localization of encapsulated SRB and CNF-protein conjugate results in red coloration. The inset images show GM1 liposome groupings at similar or increased magnification. Scale values represent μm .

CHAPTER III

CHARACTERIZATION OF IMMOBILIZED MICROEMULSIFIED
LIPOSOMES CONTAINING ESCHERICHIA COLI'S
MECHANOSENSITIVE CHANNEL OF LARGE
CONDUCTANCE (MscL) USING CONFOCAL
LASER SCANNING MICROSCOPY

ABSTRACT

Microemulsified liposomes composed of phospholipids, cholesterol, proteins and *N*-biotinyl phosphatidylethanolamine were immobilized on glass coverslips containing covalently immobilized avidin. *Escherichia coli*'s mechanosensitive channel of large conductance (EcoMscL) was cloned, expressed, labeled with carboxynaphthofluorescein (CNF), and incorporated as a membrane protein. CLSM was employed to visualize the diffusion and release of an encapsulated polar-tracing probe, sulforhodamine B (SRB), during osmotic stress (0-4 M NaCl). The recombinantly produced CNF-EcoMscL localized in the artificial bilayers of liposomes decreased in fluorescence when compared to CNF-bovine serum albumin (BSA) liposomes encapsulating SRB and control liposomes, containing only lipids, encapsulating SRB under identical 0-4 M NaCl gradient environments. SRB was released in response to the osmotic stress indicating the large membrane protein channel was functionally reconstituted in immobilized liposomes. SRB was not released during application of gradients of 0-200 mM EDTA or 0-300 mM NaCl.

INTRODUCTION

Phospholipid vesicle suspensions (liposomes) have been used in diverse research approaches as mimics or models to study various cellular interactions, penetrations, and permeations of the lipid bilayer. Confocal laser scanning microscopy (CLSM) provides a means for direct observation and characterization of dynamic processes in living structures. The ability of CLSM to precisely image fully hydrated systems in their natural state and during external stress situations sets it apart from other forms of microscopy [1, 2]. Sample preparation is non-invasive and permits the examination of physiologically active structures. Living systems can be selectively labeled and dynamic experiments including structural changes can be monitored during analytical processes [1]. In this study, a liposome system composed of immobilized unilamellar phospholipid vesicles was directly monitored using CLSM to visualize the *in vitro* activity of a membrane bound mechanosensitive channel protein.

Recently, a consortium of scientists used a liposome system to study the permeability transition of liposomes induced by the formation of calcium ion/palmitic acid complexes [3]. The study was designed to mimic the permeability transition in mitochondria, which is currently thought to be involved in the palmitic-acid induced apoptosis of cardiomyocytes. Sulforhodamine B (SRB) was encapsulated in liposomes with palmitic-acid encaged in the bilayer. Calcium ion complexing palmitic acid containing liposomes resulted in an instant release of SRB from the interior aqueous phase of the liposomes. This release was hypothesized to occur through lipid pores [3]. We encapsulated SRB in immobilized unilamellar liposomes containing a

mechanosensitive channel protein and simulated environmental stresses using osmotic gradients at constant pH. Our study was designed to determine whether bioactivity of a large mechanosensitive channel could be directly observed using CLSM during osmotic events similar to what a bacterium experiences during environmental osmotic variation. This would confirm the reported functional reconstitution of EcoMscL utilizing a novel approach.

To take advantage of CLSM's ability to highly focus light in hydrated systems, we developed techniques for capturing liposomes onto a surface via the incorporation of biotinylated phospholipids and the use of immobilized avidin slides. Similarly, CLSM has been used to study concanavalin A in a liposome-based model system for the simulation of lectin-induced cell adhesion using CLSM [4]. Interactions of liposome-protein (or potentially small molecules) were measured utilizing biotinylated liposomes. In another study, streptavidin-coated paramagnetic resins were added to the liposomes and then separated using a magnetic field or centrifugation. The concentration of unbound materials in the supernatants was directly determined [5]. Immobilized liposomes impart flexibility to experimental approaches regarding artificial bilayers and their constituents.

Before the discovery of aquaporins in *Escherichia coli* (*aqpz*) and other organisms, the permeability of the bacterial lipid bilayer was assumed sufficient to allow the rapid equilibration of water during rapid changes in environmental osmolarity [6]. It has been established that many Gram-positive and Gram-negative bacteria have in their cytoplasmic membranes relatively large mechanosensitive channels. In *E. coli*, discrete

channels with conductances ranging from 0.1 to 3 nS have been identified by patch clamp techniques [7].

The proposed role of mechanosensitive channels is to protect of the integrity of the cell. Two conditions generate high turgor in the cell: the accumulation of compatible solutes, or "osmotic balancing," and the transfer of the cell into media of lower osmolarity [8, 9]. In both cases the cell responds with the release of solutes from the cytoplasm to reduce the turgor pressure. The discovery of the respective genes coupled with membrane reconstitution of the three identified mechanosensitive channels (MscL, MscS, and MscM) in *E. coli* has elucidated the roles of the Msc channels in the physiology of *E. coli* [10].

The *E. coli mscL* gene encodes a protein of 136 amino acids and proteins of similar size are strongly conserved across Gram-negative and Gram-positive bacteria [11]. EcoMscL has the highest pressure threshold for activation and is probably a pentamer of 17 kDa subunits that form a 3 nS conductance [12]. Membrane tension is the governing factor in the opening of EcoMscL reconstituted in liposomes [13, 14]. The size of this channel is sufficiently large to allow the small protein thioredoxin passage via this channel during hypoosmotic shock [12].

EcoMscL is a thermostable protein that does not undergo unfolding of its secondary structure between 25-95°C [15]. Its structure is highly helical with roughly 111 amino acids in α -helical configuration oriented in a net transbilayer orientation. Only one-third of the protein is protected from amide H⁺/D⁺ exchange by the lipid bilayer [15, 16]. EcoMscL displays little ion or solute preference and transient opening of the channel perturbs the normal ion gradients of the cell including K⁺, ATP, and glutamate

[10]. These channels can be reconstituted in liposomes while maintaining their biological activity and likely represent the simplest example of a membrane-based mechanosensory response [17-19].

The overall objective of this research was to develop and characterize a novel immobilized liposome system containing EcoMscL. The *in vitro* biological activity of MscL in a liposome was investigated in response to osmotic challenges using a buffered immersing solution. The first objective included the formulation, microemulsification and immobilization of liposomes, which could be directly immobilized on glass and submerged in buffered solution using CLSM. The second objective involved the expression of an osmotic sensitive protein (EcoMscL) and the incorporation of this protein into immobilized artificial liposome bilayers. The stability of immobilized EcoMscL liposomes was then estimated over a six-month period. Finally, the EcoMscL liposomes were monitored using CLSM for changes in fluorescence during changes in osmotic conditions. We designed methods to allow active monitoring of membrane channels imbedded in artificial membranes of liposomes during osmotic events *in vitro* using CLSM as a new approach to compliment and confirm reports of functional reconstitution using patch clamp techniques with the protein in its native location, the plasma membrane of microbial cells [20].

MATERIALS AND METHODS

Unilamellar Microemulsified Liposome Composition and Preparation. The phospholipids used in formulating unilamellar microemulsified liposomes were purchased from Avanti Polar Lipids, Inc. (Alabaster, AL, USA) and cholesterol was

purchased from Sigma Chemical Co. (St. Louis, MO, USA). The amine reactive probe, 5-(and-6) carboxynaphthofluorescein (CNF), used to label proteins, and polar tracer probe, sulforhodamine B (SRB), were purchased from Molecular Probes Inc. (Eugene, OR, USA).

Unilamellar microemulsified liposomes were formulated using phosphatidylcholine, cholesterol, phosphatidylglycerol, NBD-phosphatidylethanolamine (1,2-Dioleoyl-*sn*-Glycerol-3-Phosphoethanolamine-*N*-(7-nitro-2-1,3-benzoxadiazol-4-yl)), biotinyl- phosphatidylethanolamine (1,2 Dioleoyl-*sn*-glycerol-3-Phosphoethanolamine-*N*-(Biotinyl)), and carboxyfluorescein-phosphoethanolamine (1,2-Dioleoyl-*sn*-Glycerol-3-Phosphoethanolamine) at concentrations of 30, 6, 4, 0.060, 0.060, and 0.002 μM , respectively. All liposome preparations were cast in 50 mM Tris-Cl (pH 7.2). Lipid formulations, dissolved in chloroform, were applied to a Microfluidizer™ 110S (Microfluidics International Corp. Newton, MA, USA) and homogenized in the casting buffer. Polar tracing SRB probe molecules were encapsulated and used to label the lumen of the artificial bilayers. CNF-labeled proteins and SRB were microemulsified at concentrations of 0.002 and 45 μM , respectively. The total volume of solution applied to the Microfluidizer™ was 10 ml.

The Microfluidizer™ 110S was equipped with a 10 ml sample hold volume and a cooling loop. SRB dispersed in 50 mM Tris-Cl (pH 7.2) and lipids dispersed in chloroform were microemulsified for 270 s. Immediately following microemulsification, the liposomes containing solution was immobilized on glass via biotin-avidin interactions. Please refer to Chapter II for more information on the methods used to produce and immobilize the liposomes.

Immobilization and Stability of Liposomes. Avidin containing slides were prepared by derivatizing glass cover slips using 3-aminopropyl-triethoxysilane (Fisher Scientific, Pittsburgh, PA, USA) followed by succinylation with succinic anhydride (Sigma) and acetylation with acetic anhydride (Mallinckrodt, Paris, KY, USA) [21]. The concentration of avidin (Sigma) available for immobilization was 0.6 ng avidin per 22 x 22 mm cover slip. This protein was covalently immobilized to the cover slips via EDC and Sulfo-NHS (Pierce Biotechnology, Inc., IL, USA) in activation buffer 0.1 M MES [2-(*N*-morpholino)ethanesulfonic acid] and 0.5 M NaCl (pH 6.0, adjusted with NaOH) [22]. The cover slips were incubated with avidin for 45 min at room temperature on a platform shaker (150 rpm) followed by washing of the slides using the same buffer (3x) to eliminate non-specifically bound avidin. Freshly prepared liposomes were incubated with avidin containing cover slips for 30 min followed by 3x washes of 50 mM Tris-Cl (pH 7.2).

The stability of liposomes was determined by storing the cover slips dry at 4°C for six months. Monitoring release of encapsulated SRB using CLSM was used to estimate bilayer stability and integrity. Samples were imaged at 2-week intervals to observe the integrity of the liposomes over time during the course of six months.

PCR, Cloning, and Sequencing of EcoMscL. The two primers used in PCR were designed from published *E. coli* MscL sequences namely EmsclFor and EmsclRev [23]. The primer sequences were ATGAGCATTATTAAAGAATTTTCG and CCAGTGGCAAGAAAGTAAATC for EmsclFor and EmsclRev, respectively. The forward primer EmsclFor begins at the start codon (ATG) at the 5' end of EcoMscL to

ensure the correct reading frame and translation process. The reverse primer EmsclRev includes a stop codon and terminator sequence to ensure sequence termination.

A PCR kit (Read-To-Go PCR, Amersham Biosciences Corp., Piscataway, NJ) was used for all PCR experiments. The PCR sample consisted of 1 μ M of each primer, 1 μ l of 1 nM *E. coli* genomic DNA as the template, 1 μ l of Taq polymerase, and of sterile water for a final volume of 25 μ l. The cycling conditions for PCR included: 94°C/1 min, 52°C/1 min, and 72°C/1 min with a final 10 min extension at 72°C.

The cloning vector and host used were purchased from Invitrogen (Carlsbad, CA, USA). The vector, pBAD/Thio, included an ampicillin resistance gene and the cloning site was surrounded by HP-thioredoxin, and 6xHis tag at the target protein's N-terminus and C-terminus. The *E. coli* host cell, TOP10 has a genotype of F⁻ *mcrA* Δ (*mrr-hsdRMS-mcrBC*) ϕ 80*lacZ* Δ M15 Δ *lacX74* *recA1* *deoR* *araD139* Δ (*ara-leu*)7697 *galU* *galK* *rpsL* (Str^R) *endA1* *nupG*. The cloning reaction was transformed into competent TOP10 and plated onto agar plates containing ampicillin. Ten colonies were picked the following day and assayed for plasmid DNA size. Colonies containing the correct insert size were purified and sequenced. The forward and reverse primers were supplied by Invitrogen and Utah State University's Biotechnology and Genomics Research Center (Logan, UT, USA) performed the sequencing.

***E. coli* Cell Growth and EcoMscL Induction.** Recombinant *E. coli* was grown in 2 ml Luria broth (LB) containing 100 μ g/ml ampicillin overnight at 37°C while shaking (225 rpm). The overnight growth was subcultured into five tubes each containing 10 ml of LB with 100 μ g/ml ampicillin. Samples were grown at 37°C with

shaking (250 rpm) to mid-log phase ($OD_{600} = 0.5$). A 1 ml aliquot of each sample was removed, pelleted and stored at -80°C as the zero induction point.

For induction of the EcoMscL-thioredoxin fusion protein, arabinose was added to each of the five tubes at final concentrations of 0.00002%, 0.0002%, 0.002%, 0.02% and 0.2%. Samples were grown at 37°C with shaking for 4 hr. Aliquots, 1 ml, from each tube were collected and the cells pelleted. The cell pellets were resuspended in 100 μl of 1X SDS-PAGE sample buffer along with zero time point samples collected as described above. Samples were heated for 5 min at 70°C and 10 μl of each sample analyzed on a 10% SDS-PAGE gel.

EcoMscL Fusion Protein Purification. Recombinant cells were grown in 500 ml of LB/Amp to mid log phase and induced with arabinose. Cells were pelleted and resuspended in 5 ml B-PER, bacterial protein extraction reagent (Pierce) containing 0.65 μl of 0.1 M phenyl methyl sulphonyl fluoride. The sample was centrifuged and after careful removal of the supernatant, 5 ml of B-PER reagent was added again and the pellet was resuspended. Lysozyme (100 μl of 10 mg/ml stock solution) was added to the suspension for a final concentration of 200 $\mu\text{g/ml}$. After incubation for 5 min at room temperature, the soluble fraction was separated from the insoluble fraction by centrifugation at 10,000 rpm for 20 min.

The 2 ml ThioBond resin (Invitrogen) was equilibrated according to the manufacturers directions and the lysate was applied and incubated for 30 min at room temperature. The resin was drained and washed with 4 bed volumes (8 ml) of wash buffer containing 1 mM β -mercaptoethanol (β -ME). The fusion protein was eluted with

3 bed volumes (6 ml) of running buffer with increasing β -ME concentrations of 5, 10, 50, 100, 200, and 500 mM β -ME. Elutants were collected and analyzed by SDS-PAGE.

Fluorescent Protein Labeling. Recombinant EcoMscL-thioredoxin protein fractions were labeled with 5-(and-6)-carboxynaphthofluorescein (CNF). Recombinant EcoMscL-thioredoxin fractions (0.8 μ M) were reacted for 45 min with EDC (4.8 μ M) and Sulfo-NHS (13 μ M). The activation buffer contained 0.1M MES [2-(*N*-morpholino)ethanesulfonic acid] (Merck, Darmstadt, Germany) and 0.5 M NaCl (pH 6.0, adjusted with NaOH). CNF (1.5 μ M) was added to the solution and the reaction allowed to proceed for 2 h. The reaction was quenched upon addition of excess hydroxylamine hydrochloride (Mallinckrodt). The labeled protein was dialyzed in a Slide-A-Lyzer[®] 10K cassette (Pierce) overnight against 50 mM Tris-Cl, pH 7.2 at 4°C to remove excess CNF. Bovine serum albumin (BSA) was labeled with CNF as described above for EcoMscL.

Liposome Formulations Containing EcoMscL. Lipids listed previously were dissolved in 1 ml chloroform and microemulsified in the presence of 0.2 nM thioredoxin-EcoMscL-CNF (hereafter CNF-EcoMscL) and 1.8 μ M SRB. The total volume of the solution applied to the Microfluidizer[™] 110S containing 50 mM Tris-Cl (pH 7.2) and lipid components in chloroform was 10 ml. Liposome formulations were microemulsified at 10,000 psi for 270 s. Liposome suspensions were distributed to beakers containing 5 immobilized avidin cover slips in 10 ml 50 mM Tris-Cl (pH 7.2). The liposome suspensions were allowed to react with coverslips at room temperature for 30 min followed by 3x washes of 50 mM Tris-Cl (pH 7.2).

EcoMscL liposomes were observed using CLSM before, during, and after modulation of the microenvironment by addition of pH buffered gradients of various

concentrations to the immersing solution. Each cover slip containing immobilized liposomes was secured onto a 22 x 22 mm² hole in a petri dish. For all treatments, the liposomes were immersed in 1 ml 50 mM Tris-Cl (pH 7.2) followed by the addition of 24 ml salt containing 50 mM Tris-Cl (pH 7.2) buffers until the immersing solution (25 ml total volume) was 200 mM EDTA, 300 mM NaCl, or 4 M NaCl. Scanning and image collection was performed at 30 s intervals during a 270 s time period during each treatment.

Identical lipid profiles were used for formulation of control liposomes consisting of liposomes produced encapsulating SRB in the absence of protein and CNF-BSA liposomes produced encapsulating and SRB. The control liposomes were produced, immobilized, and imaged using the same procedure as for EcoMscL liposomes.

Confocal Laser Scanning Microscopy. Each series of confocal laser scanning microscopy images was generated using a Keller type MRC 1024 krypton/argon laser scanning confocal system (Bio-Rad, Hercules, CA, USA) interfaced with an inverted microscope (Diaphot TE300, Nikon, Tokyo, Japan). The pinhole diameters were 2.5, 2.5 and 4.0 mm respectively for the 488, 598, and 668 nm laser lines and the objective lens was a Nikon 100X, plan apo, oil immersion with a numerical aperture of 1.40. The 488 nm laser line was used for the liposome formulation and immobilization studies. The 488 nm line excited the fluorescein and NBD labeled phosphatidylethanolamine engaged as a component of the artificial bilayers of the liposomes. The 647 nm laser line was used for liposomes containing CNF labeled proteins. The 568 nm laser line was used to excite the encapsulated SRB.

The 647 nm line from the Kr/Ar laser was used to excite the amine reactive probe (CNF). CNF was used to label the membrane protein and exhibits an excitation and emission of 598 and 668 nm, respectively. The aqueous probe, SRB, was used to monitor the water-phase encapsulated by the liposome bilayer during the microemulsification of the lipid solutions. SRB exhibits an excitation and emission of 565 and 586 nm, respectively. It was excited using the 568 nm line. SRB fluorescent emissions were detected and directed to the red channel while the 647 nm line from CNF were directed to the blue channel. The resulting red and blue images were overlaid using LaserSharp® version 3.2 (Bio-Rad) and analyzed using Adobe® Photoshop® 5.0 (Adobe Systems, Inc., San Jose, CA, USA).

Images ($82 \times 82 \mu\text{m}^2$) were taken consecutively with the dichroic beam splitters and filters to minimize cross talk between channels. All images were acquired with identical settings. The photomultiplier gain/sensitivity/contrast was adjusted to give a slightly over-modulated signaling in the normal scan mode. The consecutive images represented time points 0, 60, 120, 180, and 270 s. Ten normal scans were performed on the time zero field to reduce photo-bleaching in subsequent scans as a comparison was made between time points 0 and 270 s. The time zero image, representing the starting point of the treatment gradient, was converted to a posterized (Adobe® Photoshop®) image with 2 levels. This resulted in images with one tonal level for each channel. The mapped pixels of each channel were tabulated using Adobe® Photoshop®'s histogram tool from this simplified image and compared to an identically treated posterized image collected at the termination, time = 270 s, of the osmotic treatment time series for a given field. This conversion, tabulation, and comparison allowed the images to be analyzed

quantitatively by comparing the pixels of images before and after the treatment. The change in fluorescence was expressed as a percent reduction of pixels for each treatment along each channel, red and blue, respectively. Each treatment was performed in triplicate and replicated at least once. Average pixel reductions generated from individual treatments were used to determine an approximate average pixel reduction for each gradient and liposome composition.

RESULTS

Unilamellar Microemulsified Liposome Composition and Preparation. The composition of the solution containing lipids and labeled proteins subjected to microemulsification met the goals of our experimental design in that when subjected to the Microfluidizer™, unilamellar liposomes were formed and dispersed in solution. The produced liposomes immobilized on coverslips and imaged. The selected probes specifically and consistently labeled liposome components (i.e. lipid bilayer monitored using the green channel, proteo-lipid bilayer monitored using the blue channel, and lumen monitored using the red channel). See detailed methods in Chapter II.

Immobilization and Stability of Liposomes. Figures 11A-B were obtained using a series of scans (0.8 μm apart in the vertical or z plane) showing immobilized liposomes formulated in the absence of protein. SRB was encapsulated, labeling the lumen of the liposomes. The images of the dorsal (**Figure 11A**) portion of the liposomes resulted in predominantly green images whereas, the central section (**Figure 11B**) show strong co-localization of probes labeling both the bilayer and the lumen. Here bilayer

embedded probes (green) and lumen encapsulated probes (red) undergo simultaneous excitation in the same location in space resulting in a pronounced yellow appearance in the image.

CNF-EcoMscL liposomes were produced, immobilized and imaged. As with both the liposomes embedded in agarose or immobilized directly after microemulsification, the immobilized CNF-EcoMscL liposomes were uniformly unilamellar. Please refer to Composition of liposomes in the Results and Discussion section of Chapter II and **Figures 3 and 4**. The diameters ranged from 0.2 - 2.1 μm and no clumping, aggregation or agglutination was observed. The encapsulation of SRB observed in immobilized CNF-EcoMscL liposomes was similar to liposomes immobilized on glass previously in the absence of CNF-protein conjugates. Co-localization of SRB and CNF imaged without exciting the head-group labeled phospholipids resulted in a vivid magenta (**Figure 12A**). The inset shows a grouping of immobilized CNF-EcoMscL liposomes in greater detail (**Figure 12A, inset**).

After immobilized CNF-EcoMscL liposomes were stored dry at 4°C for 4 months, indications of compromised bilayer integrity was observed. SRB was observed diffusing in a symmetrical ring extending beyond the artificial bilayers. A field of destabilized liposomes is shown in **Figure 12B**. The insets show representative CNF-EcoMscL liposomes at the one and 6-month intervals (**Figure 12B** inset above and below, respectively). After 4 months, 1 in 10 liposomes had lost its initial ability to encapsulate probe. After 5 months, 5 in 10 artificial bilayers had destabilized and finally at 6 months, 8 in 10 liposomes were destabilized. This rate of destabilization was similar to that determined for CNF-LN liposomes as described in Chapter II.

PCR, Cloning, and Sequencing of EcoMscL. PCR with an annealing temperature of 52°C generated a specific PCR product at the expected 481 base pair product size. The PCR product was cloned into the TOPO vector and two positive clones were identified, MscL2 and MscL6. Although MscL6 contained a PCR insert, sequencing confirmed the presence of multiple errors in the base-pair sequence. MscL2 contained one base-pair error, which changed amino acid 65 in the target MscL protein sequence from valine to alanine. We assumed this change would not affect EcoMscL protein functionality, as these two amino acids share similar chemical properties.

***E. coli* Cell Growth and EcoMscL Induction.** The pBAD/TOPO vector was selected because the TOPO vector is advantageously easier and faster than traditional PCR cloning vectors and this vector contains the araBAD promoter, which is tightly controlled by the arabinose concentration in medium. Use of the tightly controlled arabinose promoter ensured that a potential lethal effect of the expressed protein would not occur during the cell growth phase. In addition, the fusion protein containing a thioredoxin tag has the advantage of increased solubility in cell plasma when compared to other affinity tags. This theoretically improves the nickel column affinity purification. The thioredoxin tag is linked to the N-terminal of target protein via an enterokinase (EK) site, which can be used for cleavage to remove the thioredoxin tag. The molecular weight of the EcoMscL fusion protein was calculated to be 28 kDa based on amino acid sequence.

Protein Fraction Purification. The expression of the EcoMscL fusion protein was maximum at 0.2% arabinose in the medium as determined by SDS-PAGE analysis (Figure 13). Higher arabinose concentrations resulted in less protein expressed which

may be due to the lethality of this protein to the host at the high expression rate. The initial effort to lyse the induced cells with B-PER failed to release recombinant EcoMscL protein into the soluble lysate. Since EcoMscL is a membrane protein, we added an additional lysozyme treatment after treating with B-PER to degrade the cell wall. As expected, recombinant EcoMscL was released into supernatant. Use of the ThioBond resin for affinity purification did not result in purified recombinant fusion protein. The recombinant protein did bind to the resin, but could not be released with any of the concentrations of β -ME tested. To confirm the fusion protein had bound to the affinity resin, the resin was boiled in SDS-PAGE loading buffer. The released protein was analyzed by SDS-PAGE and showed a protein band at 28 kDa, but this purified protein could not be used in the liposome experiments. We concluded that the almost irreversible binding of the recombinant protein to the resin was due to the specific binding properties of EcoMscL, not the thioredoxin.

Since the recombinant fusion protein could not be purified using the nickel resin, the protein fraction released after lysozyme treatment was used in further experiments. SDS-PAGE analysis of this protein fraction followed by scanning densitometry showed that 40% of the total protein resulted in a 28 kDa band (**Figure 14**). We assumed this band to be the EcoMscL-thioredoxin fusion protein. This sample was labeled with CNF using a concentration ratio of 1.8 moles CNF: 1 mole recombinant protein.

Fluorescent Labeling and Liposome Formulations of EcoMscL. The cloning of recombinant EcoMscL into an *E. coli* expression system yielded an EcoMscL-thioredoxin fusion protein that was subsequently labeled with a blue fluorescent probe, CNF, and incorporated into the membrane of liposomes. These EcoMscL enriched

membrane proteins as well as CNF-BSA were directly observed using the blue channel of the confocal system.

The protein fraction was predictably labeled with the amine reactive probe, CNF. The labeling procedure resulted in the formation of an amide bond between the carboxyl group of the probe molecules and the reactive amine groups of the protein. This CNF probe allowed visualization of liposomes containing CNF-EcoMscL which appeared blue. Liposomes formed in the absence of this probe holding all other variables constant could be easily distinguished because they appeared red due to the encapsulation of the SRB probe found in the liposomal lumen. Magenta liposomes resulted when CNF-labeled protein containing liposomes encapsulated SRB (**Figure 12A** and inset). Again, magenta coloration in the image represents co-localization of both red and blue channels.

Immobilized liposomes containing CNF conjugated proteins were visualized with confocal microscopy. The composition of the solution subjected to microemulsification consisted of lipids, CNF labeled proteins, and SRB labeled buffer. These CNF-EcoMscL liposomes were observed to be in all respects similar to CNF-BSA liposomes and liposomes produced in the absence of protein using identical methodologies and lipid profiles (**Figure 12A** and inset).

Confocal Laser Scanning Microscopy. Modulations in fluorescent intensity of SRB was used to indicate biological activity in protein containing liposomes. This probe is impermeable to cells and consistently and predictably labeled the internal aqueous phase of the liposomes used in the study. The diameter of this probe is estimated at 1.5 nm [3]. The probes CNF and SRB showed consistent, minimal photo-bleaching under experimental conditions. This allowed for their use as qualitative indicators and in the

case of SRB, allowed us to monitor its diffusion through the large mechanosensitive membrane channel and/or quenching due to exposure to the immersing solution using the available confocal system.

The functionality of the CNF-EcoMscL incorporated into artificial bilayers was tested by increasing the osmolyte concentration of the buffered immersing solution. Native and reconstituted EcoMscL form a large open channel in response to membrane pressure. The immobilized CNF-EcoMscL liposomes contained internalized, water soluble SRB which could be released to the immersing solution upon the opening of the pore or quenched due to exposure to the osmolytes in solution. Although the orientation of the membrane protein can not be determined using microscopy, we found that upon the addition of osmolytes, namely Na^+ and Cl^- , to the immersing solution, the internalized SRB was released (or quenched internally), yet the liposome integrity of CNF-EcoMscL liposomes remained unchanged. **Figures 15A-D** show a time series of CNF-EcoMscL liposomes with encapsulated SRB (magenta due to co-localization of blue and red channels) along with liposomes containing only SRB (red) during osmotic shock.

These images were captured after initial prolonged exposure from progressive scanning as control for and to reduce photo-bleaching. The field was located in the absence of any solution. Buffer, 50 mM Tris-Cl (pH 7.2), was used to immerse the surface of the cover slip followed by 10 progressive scans of the field at the normal speed setting (constant for all treatments). Finally, after the photo-bleaching effect of the initial scans was accounted for, images were collected before, during, and after the addition of 4 M NaCl in 50 mM Tris-Cl (pH 7.2). These images exhibit an observable decrease in the intensity of the red channel, labeling the external aqueous phase during the course of the

treatment while the red channel intensity of the liposomes not containing protein was apparently unaffected.

The insets of **Figures 15A-D** show a representative immobilized CNF-EcoMscL liposome containing fluorescently labeled phospholipids and encapsulated SRB observed in a time series during an osmotic treatment identical to those in the greater fields (**Figures 15A-D**). The individual liposome reacted similarly to the liposome population observed in **Figures 15A-D**. Again, these images represent a time series after the addition of 4 M NaCl.

Controls included liposomes which did not contain CNF-EcoMscL and liposomes formulated with CNF-BSA. A time series identical to those used in the CNF-EcoMscL liposomes studies was used for the control treatments. The encapsulated SRB in control liposomes was observed to be relatively unaffected regardless of the osmolyte concentration. The polar tracer remained encapsulated in the interior of the liposomes under the conditions tested. Low salt concentration gradient treatments (0-300 mM NaCl and 0-200 mM EDTA) applied to the immersing solution of CNF-EcoMscL, CNF-BSA, and non-protein control liposomes resulted in little observable effects in the fields tested.

Quantitative data was generated from time series images tabulating total pixels in individual channels using Adobe® Photoshop®'s posterize function and histogram tool. This technique offers a quantitative measure of what is observed subjectively at the microscope. Average pixel count reductions for each treatment quantitatively expressed what was empirically observed. During a time series, images were collected of a field of CNF-MscL liposomes while a NaCl gradient of 0-4 M was applied. The red channel intensity was reduced on average by 50.4% where as the blue channel intensity was

reduced on average by 15.5% (**Table 3**). Identically imaged fields of CNF-BSA liposomes had average channel intensity reductions of 2.76% and 7.61% for red and blue channels respectively when the same gradient was applied. The reductions of red pixels for treatment groups were found similar in magnitude when comparisons were made between the different liposome compositions exposed to 0-200 EDTA and 0-300 NaCl treatments. The blue channel intensity, as measured by pixel reductions during the course of time series, was similar for all tested treatments except the EcoMscL liposomes where the reduction was larger than CNF-BSA liposome fields (15.49% for EcoMscL vs. 7.61% for CNF-BSA liposomes). The orientation of MscL in the membrane and the presence of the thioredoxin tag did not appear to interfere with the release of SRB under high salt conditions.

DISCUSSION AND CONCLUSIONS

The aim of this study was to investigate the influence of osmotic stress on immobilized unilamellar liposomes containing a membrane bound mechanosensitive channel protein (EcoMscL). Liposomes were designed to mimic analogous larger cells known to rely on mechanosensitive channels for survival during osmotic shock. It was hypothesized that if the protein retained its biological activity when labeled and incorporated into liposomes, it would open during an osmotic treatment and this opening would be observable as a change in fluorescence. The methods described allowed active monitoring of liposomes during osmotic events *in vitro* using CLSM as a new approach to compliment and confirm reports of functional reconstitution of mechanosensitive proteins in liposomes. The results show the mechanosensitive channel protein pentamer

to be biologically active as evidenced by the reduction in pixels of the red channel when liposomes containing MscL were exposed to 0–4 M NaCl at pH 7.2 as compared to identically treated CNF-BSA liposomes and control liposomes absent of protein.

As noted in previous reports using CLSM, quantitative comparison of fluorescence intensities is not trivial for a variety of reasons, such as photo-bleaching and quenching [24]. Scanning the time zero field to reduce the photo-bleaching effect of image collection during a time series was an effective method of reducing variation among individual fields subjected to the same treatment. The rate of pixel loss over the course of a time series in a given treatment was highly variable before time point 180 s but did not exhibit comparable variability after 180 s up to 540 s. Thus, preliminary scanning of the hydrated time zero liposome field before the onset of treatments minimized the photo-bleaching effect that would have confounded the data.

Quenching can reflect variations in the microenvironment of the fluorescent probe; changes in the local salt or oxygen concentration; pH differences, to which the particular probe is sensitive, etc. [24]. In our experimental design, we used the quenching of probes as our indicating outcome. As this fixed condition is inherent to CLSM studies, we decided to exploit it as our indicator of channel activity. The indicator probe, SRB was encapsulated in artificial immobilized liposome bilayers at time zero for all osmotic treatments.

In order to determine SRB's independent ability to permeate lipid bilayers, SRB was encapsulated in control liposomes of identical lipid compositions. These purely red liposomes were incubated in solutions composed of 50 mM Tris-Cl (pH 7.2) and increasing NaCl concentrations and monitored over time. The fluorescent intensity of

SRB did not vary appreciably because the microenvironment of the probe was unaltered at time zero for all treatments and 10 *xy* scans were performed to preempt any photo-bleaching effect before the application of the salt treatment. This was also confirmed by imaging representative fields of liposomes during a time series in the absence of a NaCl or EDTA gradient. As before, immersing solution, in this case, 25 ml of 50 mM Tris-Cl (pH 7.2), was applied to the petri dish during imaging of the time series but a treatment gradient was absent. Images were generated and pixel reductions were calculated. Channel intensities reductions, or pixel reductions expressed as a percent, were similar to those tabulated in the EDTA gradient (ranging from 0.6 to 1.7%). The effect of the altered microenvironment on the encapsulated SRB was observed only in EcoMscL liposomes.

Significant quenching of the probe was only observed when the probe was subjected to the 0–4 M NaCl gradient due to the opening of the EcoMscL channel allowed the release of internalized SRB. Controls consisting of fields of CNF-BSA liposomes or liposomes without proteins experienced a dramatically smaller decrease of red channel intensity in the same gradient (0–4 M NaCl). Other gradient treatments (0–300 mM NaCl and 0–200 mM EDTA) resulted in no difference in red channel reduction for each of the three immobilized liposome variations.

The percent blue pixel reduction calculated individually for the CNF-EcoMscL and CNF-BSA liposomes for all three treatments was largest during the 0–4 M NaCl treatment of CNF-EcoMscL liposome fields. All other percent blue pixel reductions calculated for the treatments and controls tested were similar in magnitude with respect to one another. The increased average loss of blue pixels calculated with respect to CNF-

EcoMscL liposomes as compared to CNF-BSA liposomes indicates the treatment resulted in a physical modification and release of SRB. This observed difference confirms previous work regarding EcoMscL which has estimated that approximately 66% of the protein is exposed to the microenvironment of the immersing solution [15, 16] and is able to respond to an osmotic change in the environment. Although the orientation of EcoMscL in the lipid bilayer was not determined and the protein contained a thioredoxin tag, it appeared to function with a change in osmotic conditions.

The stability of liposomes containing membrane proteins and recombinant EcoMscL from *E. coli* was estimated with respect to the liposomes' relative ability to encapsulate SRB in a dry-state. The immobilized liposome system was stable for approximately four months stored dry at refrigeration temperatures. The liposomes' composition and dimensions are suitable for monitoring and imaging using CLSM. EcoMscL has physical dimensions large enough that when opened allows encapsulated water soluble SRB to be released from the liposomal lumen to the immersing solution. The modulation in fluorescence resulting from the change of the microenvironment was monitored using CLSM and channel intensities were tabulated using Adobe® Photoshop®.

Immobilized liposomes of various compositions were monitored using CLSM and maintained their integrity while the osmotics of the immersing solution were modified to simulate hypo- and hyperosmotic shock. The quenching or diffusion of the red encapsulated probe indicated the biological activity of EcoMscL was maintained when reconstituted in immobilized liposomes using CLSM. To our knowledge we are the first

group to successfully immobilize unilamellar liposomes on glass and study reconstituted EcoMscL liposome bioactivity and bilayer encapsulation and integrity using CLSM.

REFERENCES

1. Ferrando M, Spiess W. Review: Confocal scanning laser microscopy. A powerful tool in food science. *Food Sci Technol Int London* 2000; 6(4):267-284.
2. Frank J. Microbial attachment to food and food contact surfaces. *Adv Food Nutr Res* 2001; 43:319-370.
3. Agafonov A, Gritsenko E, Belosludtsev K, Kovalev A, Gateau-Roesch O, Saris N-E, Mironova D. A permeability transition in liposomes induced by the formation of Ca²⁺/palmitic acid complexes. *Biochim Biophys Acta* 2003; 1609:153-160.
4. Bendas G, Vogel J, Bakowski U, Krause A, Muller J, Rothe U. A liposome-based model system for the simulation of lectin-induced cell adhesion. *Biochim Biophys Acta* 1997; 1325(2):297-308.
5. Zhan H. A method for quick measurement of protein binding to unilamellar vesicles. *J Biochem Biophys Meth* 1999; 41(1):13-19.
6. Calamita G, Bishai W, Preston G, Guggino W, Agre P. Molecular cloning and characterization of *Aqpz*, a water channel from *Escherichia coli*. *J Biol Chem* 1995; 270:29063-29066.
7. Blount P, Sukharev S, Moe P, Nagle S, Kung C. Towards an understanding of the structure and functional properties of MscL, a mechanosensitive channel in bacteria. *Biol Cell* 1996; 87:1-8.
8. Poolman B, Glaasker E. Regulation of compatible solute accumulation in bacteria. *Mol Microbiol* 1998; 29:397-407.
9. Schleyer M, Schmid R, Bakker E. Transient, specific, and extremely rapid release of osmolytes from growing cells of *Escherichia coli* K-12 exposed to hypoosmotic shock. *Arch Microbiol* 1993; 160:424-431.

10. Booth I, Louis P. Managing hypoosmotic stress: Aquaporins and mechanosensitive channels in *Escherichia coli*. *Curr Opin Microbiol* 1999; 2:166-169.
11. Moe P, Blount P, Kung C. Functional and structural conservation in the mechanosensitive channel MscL implicates elements crucial for mechanosensation. *Mol Microbiol* 1998; 28:583-592.
12. Sukharev S, Schroeder M, McCaslin D. Stoichiometry of the large conductance bacterial mechanosensitive channel of *E. coli*. A biochemical study. *J Membr Biol* 1999; 171:183-193.
13. Berrier C, Garrigues A, Richarme G, Ghazi A. Elongation factor Tu and DnaK are transferred from the cytoplasm to the periplasm of *Escherichia coli* during osmotic downshock presumably via the mechanosensitive channel MscL. *J Bacteriol* 2000; 182(1):248-251.
14. Betanzos M, Chiang C-S, Guy H, Sukharev S. A large iris-like expansion of a mechanosensitive channel protein induced by membrane tension. *Nature Struct Biol* 2002; 9(9):704-710.
15. Arkin, I, Sukharev S, Blount P, Kung C, Brunger A. Helicity, membrane incorporation, orientation and thermal stability of the large conductance mechanosensitive ion channel from *E. coli*. *Biochim Biophys Acta* 1998; 1369:131-140.
16. Blount P, Sukharev S, Moe P, Schroeder M, Guy H, Kung C. Membrane topology and multimeric structure of a mechanosensitive channel protein of *Escherichia coli*. *EMBO J* 1996; 2(18):4798-4805.
17. Blount P, Moe P. Bacterial mechanosensitive channels: Integrating physiology, structure, and function. *Trends Microbiol* 1999; 7(10):420-424.
18. Sukharev S. Purification of the small mechanosensitive channel of *Escherichia coli* (MscS): the subunit structure, conduction, and gating characteristics in liposomes. *Biophys J* 2002; 83(1):290-298.
19. Sukharev S, Martinac B, Arshavsky V, Kung C. Two types of mechanosensitive channels in the *Escherichia coli* cell envelope: solubilization and functional reconstitution. *Biophys J* 1993; 65:177-183.
20. Sukharev S, Sigurdson W, Kung C, Sachs F. Energetic and spatial parameters for gating of the bacterial large conductance mechanosensitive channel, MscL. *J Gen Physiol* 1999; 113(4):525-540.

21. Walsh M, Nam S. Affinity enrichment of bovine lactoferrin in whey. *Prep Biochem Biotech* 2001; 31(3):229-240.
22. Hermanson G. *Bioconjugate Techniques*. New York: Academic Press, Inc. 1996.
23. Blattner F, Plunkett G, Bloch C, Perna N, Burland V, Riley M, Collado-Vides J, Glasner J, Rode C, Mayhew G, Gregor J, Davis N, Kirkpatrick H, Goeden M, Rose D, Mao B, Shao Y. The complete genome sequence of *Escherichia coli* K-12. *Science* 1997; 277(5331):1453-1474.
24. Cevc G, Schatzlein A, Richardsen H. Ultradeformable lipid vesicles can penetrate the skin and other semi-permeable barriers unfragmented. Evidence from double label CLSM experiments and direct size measurements. *Biochim Biophys Acta* 2002; 1564:21-30.

Table 3. Percent pixel reduction of probes labeling three types of immobilized microemulsified liposome populations during gradients over time. Reduction of pixels indicates release or quenching of internalized SRB (red pixels) and CNF (blue pixels).

Gradient	Immobilized Microemulsified Liposome Type				
	Embedded CNF-EcoMscL and Encapsulated SRB		Embedded CNF-BSA and Encapsulated SRB		Encapsulated SRB (Control)
	Red Pixels	Blue Pixels	Red Pixels	Blue Pixels	Red Pixels
0–200 mM EDTA	0.84%	6.36%	0.68%	5.34%	2.12%
0–300 mM NaCl	3.99%	7.85%	3.50%	6.46%	5.15%
0–4 M NaCl	50.45%	15.49%	2.76%	7.61%	7.53%

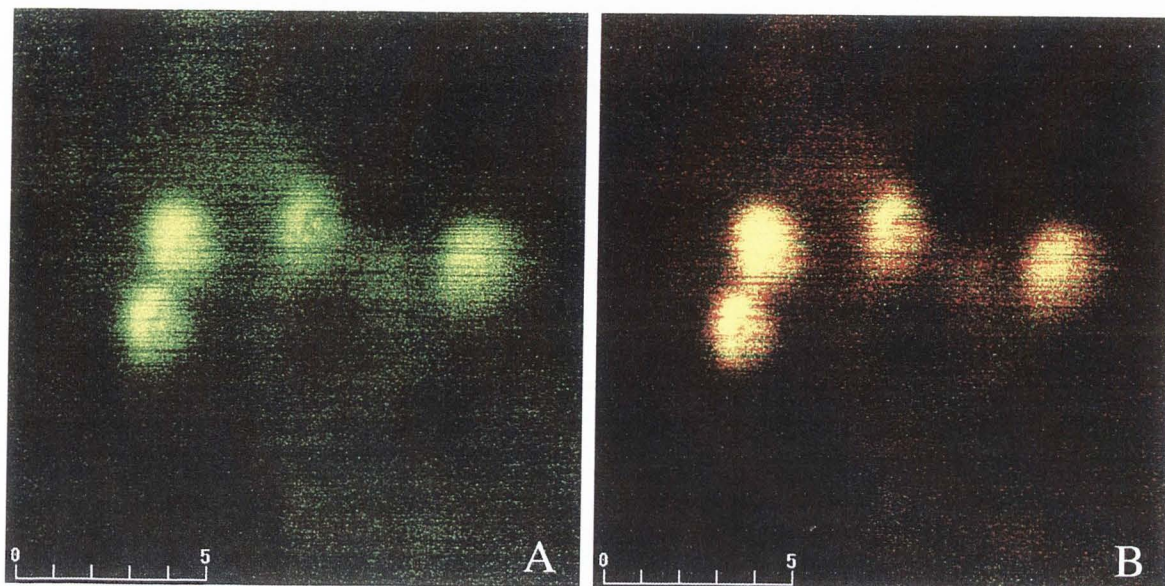


Figure 11. Two xy images collected in series of four unilamellar immobilized microemulsified liposomes scanned $0.8 \mu\text{m}$ apart along the z plane (A and B). Liposomes immobilized via biotinylated phospholipids on slides containing covalently bound avidin. Artificial lipid bilayer contained NBD-phosphatidylethanolamine (green) and carboxyfluorescein-phosphatidylethanolamine (green) and sulforhodamine B (red) was encapsulated in the liposomal lumen. Co-localized green and red probes appear yellow. Scale values represent μm . (A) Dorsal scan. (B) Central scan.

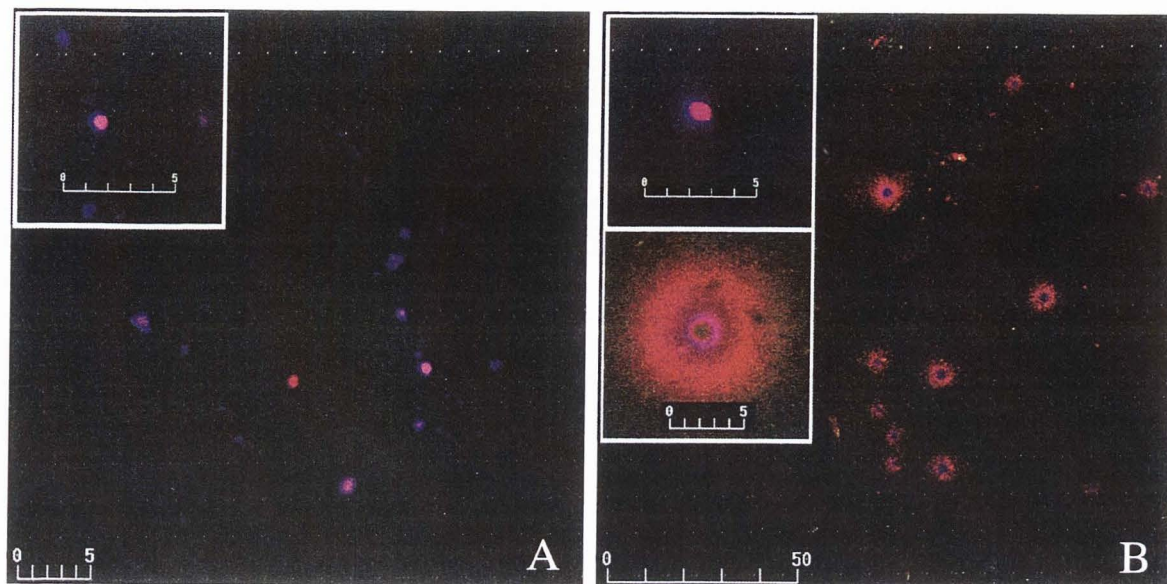


Figure 12. Immobilized unilamellar immobilized microemulsified EcoMscL liposomes. Liposomes immobilized via biotinylated phospholipids on slides containing covalently bound avidin. Artificial lipid bilayers contained CNF-labeled proteins including EcoMscL (blue). Sulforhodamine B (red) was encapsulated in the liposomal lumen. Co-localized blue and red probes appear magenta. Scale values represent μm . (A) Field of immobilized EcoMscL liposomes ranging in color from blue to magenta. A liposome absent of CNF labeled protein is centrally located (red). (Inset A) Increased magnification of immobilized EcoMscL liposomes in A. (B) Field of destabilized immobilized unilamellar EcoMscL liposomes after six months dry storage at 4°C . (Inset B above) EcoMscL liposome encapsulating SRB imaged at one month. (Inset B below) EcoMscL liposome imaged at six months. SRB was no longer encapsulated in the liposomal lumen but has diffused along the surface of the glass.

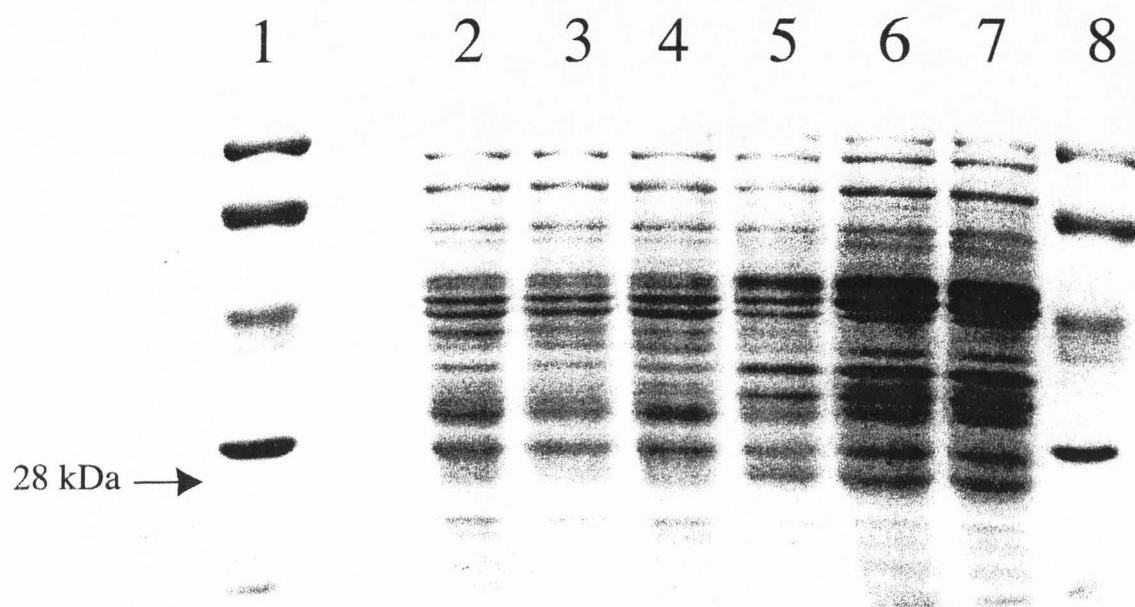


Figure 13. SDS-PAGE gel of EcoMscL protein fraction purification. Lanes: 1) molecular weight marker, 2) 0.00002 % arabinose treatment, 3) 0.0002 % arabinose treatment, 4) 0.002 % arabinose treatment, 5) 0.02 % arabinose treatment, 6) 0.2 % arabinose treatment, 7) 0.2 % arabinose treatment, 8) molecular weight marker.

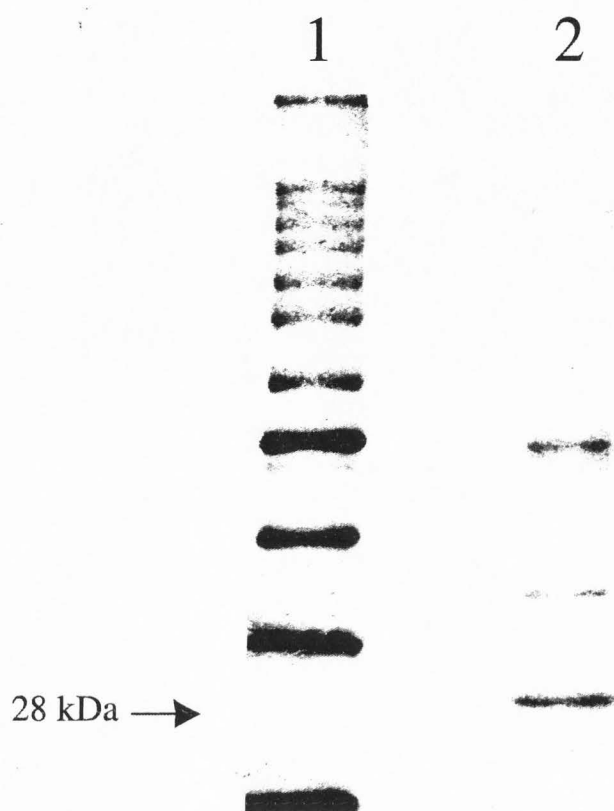


Figure 14. SDS-PAGE gel of EcoMscL protein fraction purification released after lysozyme treatment. Lanes: 1) molecular weight marker, 2) protein released after lysozyme treatment.

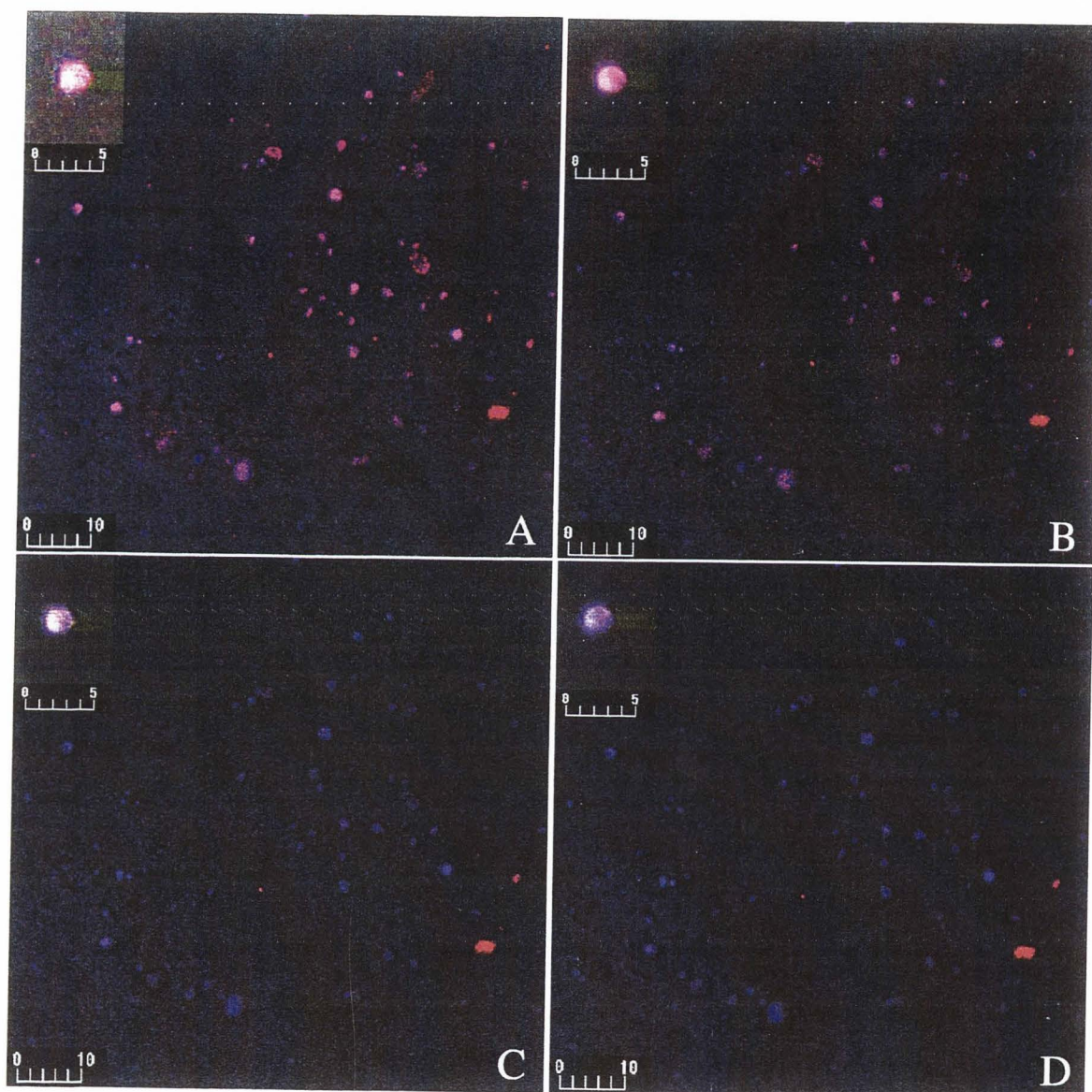


Figure 15. Four *xy* images collected of a field of unilamellar immobilized microemulsified liposomes representing a time series during the application of a 0–4 M NaCl gradient over the course of 270 s (A–D). Liposomes immobilized via biotinylated phospholipids on slides containing covalently bound avidin. Artificial lipid bilayers contained CNF-labeled proteins including EcoMscL (blue). Sulforhodamine B (red) was encapsulated in the liposomal lumen. Co-localized blue and red probes appear magenta. Red liposomes are absent of EcoMscL. Inset images show a single EcoMscL liposome during gradient. Scale values represent μm . (A and A') Time = 0. (B and Inset B) Time = 120 s. (C and Inset C) Time = 180 s (D and Inset D) Time = 270 s.

CHAPTER IV

BIOMIMETIC BINDING OF *ESCHERICHIA COLI* O157:H7,
SALMONELLA ENTERITIDIS, *LISTERIA MONOCYTOGENES*, AND
LISTERIA INNOCUA WITH EUKARYOTIC UNILAMELLAR
IMMOBILIZED MICROEMULSIFIED LIPOSOMES

ABSTRACT

Microemulsified liposomes are effective biomembrane models for studying cellular interactions. Eukaryotic receptor biomolecules gangliosides (GM1 and GM3) and laminin (LN), a glycoprotein, were incorporated into unilamellar immobilized microfluidized liposomes. Liposomes were immobilized to an avidin containing solid support. *In vitro* capture of *Escherichia coli* O157:H7, *Salmonella enteritidis*, *Listeria monocytogenes*, and *Listeria innocua* with liposomes containing GM1, GM3, or LN was investigated using ELISAs and confirmed by PCR analysis. Capture of individual bacterial species with GM1, GM3, and LN liposomes was determined in the absence and presence of other species at the same inoculation level. Simultaneous capture of *E. coli* O157:H7 and *S. enteritidis* was determined with GM1, GM3, and LN liposomes at six combinations of cell concentrations 2×10^3 , 2×10^5 , and 2×10^7 CFU/ml. Adhesion and capture of *E. coli* O157:H7 and the *Listeria* species was evidenced on GM1 and LN liposomes, respectively.

INTRODUCTION

Biomembranes and Model Membranes. Biomembranes contain a large number of different lipids and proteins. Experiments on lipid (or glycolipid)-protein interactions with biomembranes are very complex to analyze, due to the multiple variables. As an alternative, well-defined model systems can be utilized to elucidate basic, specific interactions between biomolecules and host receptors masked in the complexity of a biological membrane. For example, the dependence of phospholipase A2 (PLA2) activity on membrane lateral heterogeneity is well established in model membranes [1-3]. The same membrane properties were shown to determine the PLA2 activity also in biological membranes (erythrocytes), indicating that mechanisms obtained from simple model membranes also apply to complex biological systems [4].

Biomimetic Liposomes. Glycosphingolipids are assumed to serve as recognition markers at the cell surface and can be involved in the various forms of cell response. Increasing evidence implies that gangliosides serve as binding sites in the membrane-mediated transfer of information. Their highly differentiated oligosaccharide chains provide a variety of sites for specific binding that is translated through intramembrane events, and results in the activation of adenylyl cyclase and other systems controlling protein phosphorylation and dephosphorylation in cellular recognition mechanisms.

Liposomes are spherical lipid vesicles formed by a single (unilamellar) or multiple (multilamellar) bilayers, enclosing small volumes of aqueous solution inside the vesicle [5]. The diameter of liposomes ranges from ~30 nm to several μm and depends on the preparation technique. The curvature of liposomes and the lipid composition of a

single liposome cannot be precisely controlled. Liposomes can be visualized directly by phase contrast, fluorescence, and confocal microscopy [6].

Bilayer curvature depends on the liposome diameter, with small unilamellar vesicles (diameters < 50 nm) having the highest curvature. For large unilamellar liposomes (diameters > 1 μm) the average bilayer curvature is similar to planar membranes when considering curvature at the molecular level. These liposomes are excellent candidates for *in vitro* model systems.

Gangliosides. Gangliosides are normal components of the plasma membrane of vertebrate cells and are particularly abundant in the nervous system. Gangliosides are asymmetrically located in the outer lipid layer of the membrane and exhibit strong amphiphilic properties. Gangliosides are glycosphingolipids constituted by a hydrophilic sialic acid-containing oligosaccharide and a hydrophobic ceramide portion, connected by a glycosidic linkage. The concentration of sialic acid containing gangliosides of the cortex gray matter is approximately one-tenth that of total phospholipids [7]. The gastric mucosa also contains a similar proportion of GM3 with respect to total phospholipid content [8]. The oligosaccharide portion protrudes from the outer membrane surface, and the ceramide moiety is inserted into the lipid core of the membrane.

Cellular Recognition and Interactions. Bacterial pathogenesis *in vivo* is often initiated by the attachment of the pathogen to the surface of the host cell [9, 10]. Attachment, or adhesion to host cells, occurs by a variety of mechanisms that depend on the host cell surface, type, and the specific pathogen or toxin. Attachment can result in subsequent internalization of the pathogen or toxin by phagocytosis or by endocytosis. In most cases of internalization, host and pathogen cells participate in this adhesion process,

and activation or modification of host cell signaling pathways is common [11-13].

Stimulation of these signaling pathways leads to enhancement of pathogen attachment or invasion, and signaling is activated through a variety of cell surface receptors [14].

Modulations in signaling pathways ultimately are manifest in common foodborne illness symptoms such as cramping and diarrhea.

Adhesion involves components of both the pathogen and host cell, and can lead to internalization of the pathogen. Bacterial pathogens produce molecules or macromolecular structures that are generally referred to as adhesins [15-17]. The adhesin molecules or structures specifically interact with host cell receptors to facilitate attachment and subsequently invasion. Examples of bacterial adhesins include invasins (*Yersinia* spp.), internalin (*Listeria* spp.), MarkD (*K. pneumoniae*), and FimH (*Salmonella* spp.) [10, 17, 18]. A variety of mammalian cell surface receptors that interact with bacterial adhesions including proteins such as integrins, cadherins, laminin, fibronectin, type V collagen, glycolipids such as gangliosides, or carbohydrates such as sialic acid [19-22].

Two general mechanisms by which pathogenic bacteria invade non-phagocytic host cells have been identified. Both involve significant alterations in host cell signal transduction and rearrangement of the actin filaments. Some *Salmonella* species utilize a "trigger" mechanism characterized by the induction of host cell protrusions that "reach up and around" the pathogen and ultimately leads to invasion into the host cell [23]. *Listeria monocytogenes* utilizes a "zipper" mechanism where the pathogen presumably slides or zips into the cell surface to accomplish invasion [12, 21]. Both the "trigger" and "zipper" mechanisms are initiated with modifications of host signal transduction pathways that

lead to major local rearrangements of the actin cytoskeleton [12, 24, 25]. *Salmonella typhimurium*, a close relative of *Escherichia coli*, is an enteric pathogen that is easily cultivated and genetically manipulated. As an extremely valuable tool for studying invasion and intracellular survival, this *Salmonella* species, which produces a number of adhesins, has enabled researchers to identify and characterize many of the factors involved in these processes [24, 25].

Confocal Microscopy. Molecular interactions between liposome-embedded receptors indicated by presence and proximity of fluorescent probes labeling specific molecules or structures can be observed with confocal laser scanning microscopy (CLSM). CLSM is a powerful microanalytical tool that provides a means for direct observation and characterization of dynamic processes in living structures or mimetics of these structures. The ability of CLSM to precisely image fully hydrated systems sets it apart from other forms of microscopy [26, 27]. Sample preparation is non-invasive and permits the examination of physiologically active structures. Systems, living and artificial can be selectively labeled and monitored during analytical processes including microbial detection [6].

In this study, unilamellar microemulsified liposomes were produced, and immobilized to avidin-containing glass coverslips. Immobilized microemulsified liposomes were formulated to contain the membrane glycolipid receptors (GM1 or GM3) or an embedded membrane glycoprotein laminin (LN). The capture of *E. coli* O157:H7, *S. enteritidis*, *L. monocytogenes*, and *L. innocua* after incubation and wash was assessed using ELISAs and PCR techniques. *E. coli* O157:H7 cells were captured on GM1 and imaged using CLSM.

MATERIALS AND METHODS

Immobilized Microemulsified Liposomes. Unilamellar immobilized microemulsified liposomes were prepared encapsulating the polar tracer, sulforhodamine B (SRB), and embedding ganglioside GM1, GM3, or laminin as described in Chapter II. In brief, the lipid composition for the formulation of liposomes consisted of phosphatidylcholine, cholesterol, phosphatidylglycerol, phosphatidylethanolamine, and biotinyl-phosphatidylethanolamine. Lipids, purchased dry and suspended in chloroform to facilitate formulation, were added to 50 mM Tris-Cl (pH 7.2) at lipid molar ratios of 73 : 15 : 10 : 2 : 0.15, respectively. Human laminin (LN), or bovine ganglioside (GM1) was added to solutions processed in the Microfluidizer™ 110S (Microfluidics International Corp. Newton, MA, USA). The lipids were suspended in 10 mL 50 mM Tris-Cl (pH 7.2) and microemulsified in the presence of LN (lipid : protein molar ratios of 5844 : 1.0) or ganglioside (ganglioside : lipid molar ratios of 0.089 : 1.0). A SRB : total lipid molar ratio of 1.1 : 1.0 was constant in all formulations. LN was purchased from Sigma Chemical Co. (St. Louis, MO, USA), GM1 and GM3 from Alexis Corporation (Lausen, Switzerland), and fluorophores from Molecular Probes Inc. (Eugene, OR, USA).

Control liposomes containing no gangliosides or laminin consisted of the identical lipid composition. The lipid solution was microemulsified for 270 s at maximum pressure (10,000 psi). Immediately following microemulsification, the liposome solutions were immobilized onto glass coverslips via biotin-avidin interactions.

For GM1 liposomes used in the initial ELISA capture study, the GM1 concentration was serially diluted resulting in molar percent concentrations of 0.0, 0.0089, 0.089, 0.89, and 8.9. All other ELISA and PCR capture studies compared GM1 molar percent concentrations of 0.0 and 8.9.

Avidin Immobilization. Avidin was immobilized on salinized glass coverslips as described in Chapter II. Avidin concentrations used for immobilization were increased logarithmically in a series from the concentration used in previous liposome studies (6.0 ng, or 1.0×10^{-13} moles per 968 mm^2) to determine the maximum amount of avidin that could be immobilized. Coverslips were prepared by increasing the amount of avidin in the immobilization reaction step-wise by a power of 10 in a range from 1.0×10^{-14} to 1.0×10^{-9} moles (or 0.9 ng to 90 μg) per 968 mm^2 .

Bacterial Strains and Growth Conditions. *E. coli* O157:H7 (American Type Culture Collection, ATCC 35150), *S. enteritidis* (ATCC 8326), *L. innocua* (ATCC 33090), and *L. monocytogenes* (ATCC 43251), were obtained from the Department of Nutrition and Food Sciences at Utah State University. Stock cultures of each bacterium were prepared from single colony isolates after growth as described by the ATCC instruction sheet. Each culture was inoculated (1%) into 10% non-fat dry milk powder containing 33% sterile glycerol and stored frozen in liquid nitrogen (-196°C). All strains were kept overnight at -20°C prior to a rapid thaw and inoculation into 10 ml sterile broth. *E. coli* O157:H7 was grown in tryptic soy broth containing 0.05% agar (Difco, Detroit, MI, USA). *S. enteritidis* were grown in nutrient broth (Difco). The *Listeria* species were grown in brain, heart, infusion broth (Difco). Cells were incubated overnight (12-14 h) in a 37°C in an Environ-Shaker incubator (Lab-Line, Melrose Park,

II) shaking at 160 rpm to allow for confluent growth (population densities of $\sim 10^9$ CFU/ml).

Before adding cells to a sample, the pure culture was washed twice (1 ml cell pellet resuspended twice in 1 ml of 50 mM Tris-Cl, pH 7.2). Cells were harvested by centrifugation (model CR3i-V1, Jouan S.A., Saint-Herblain, France) at 4,000 rpm for 5 min and the cell pellet resuspended into 1 ml volumes for use as working stocks.

Liposome Capture and Sample Preparation for ELISAs and PCR Detection.

E. coli O157:H7, *L. innocua*, *L. monocytogenes*, and *S. enteritidis* were grown as stated previously and a stock solution was prepared in 50 mM Tris-Cl (pH 7.2). An ELISA for each organism was performed to evaluate binding of microorganisms on GM1 liposomes. Liposomes lacking GM1 were used as the control and established a baseline. The capture protocol for ELISAs was identical for the samples evaluated by PCR as described below.

The samples evaluated by PCR used coverslips containing GM1, GM3, LN or control liposomes, washed with 250 ml of 50 mM Tris-Cl (pH 7.2). Three coverslips of each type were placed in 50 ml 50 mM Tris-Cl (pH 7.2) and inoculated at 2×10^3 , 2×10^5 , or 2×10^7 CFU/ml with resuspended prepared cells. The coverslips were incubated for 30 min at room temperature on an orbital shaker (150 rpm). Coverslips were transferred into individual sterile 50 ml tubes and washed. A wash step included the addition of 30 ml of 50 mM Tris-Cl (pH 7.2) while shaking at 150 rpm for 30 min.

Antibodies. All antibodies (Abs) used were IgG. The polyclonal Abs, rabbit anti-*E. coli* and rabbit anti-*Salmonella*, with concentrations of 4.5 mg protein/ml were obtained from OEM Concepts (Toms River, NJ, USA, products R4-V102 and R4-V61, respectively). The rabbit polyclonal Anti-*Listeria* Ab, also 4.5 mg protein/ml, was from

Biodesign International Inc. (Saco, ME, USA, product DB65420R). The enzyme-linked Ab, anti-rabbit IgG conjugated to alkaline phosphatase (AP) with a concentration of 1.2 mg protein/ml, was obtained from Sigma (St. Louis, MO, USA, product A3687). All Abs were stored at 4°C.

The optimum Ab concentration of each Ab solution was determined by performing an ELISA based on the method published previously [28]. Each Abs was tested against cells at concentrations ranging from 3.0×10^{-6} to 3.0×10^{-15} M for each respective Ab as described by [29] and [30].

ELISAs. For the *E. coli* ELISA, 1.1 μ l of the purchased stock (4.5 mg/ml) anti-*E. coli* IgG Abs, used at a 1:20,000 dilution, was incubated with the coverslip capture surface for 20 min with samples after a wash step. All antibody incubations were preceded with a wash step, which consisted of a sterile transfer coverslips to a tube containing 30 ml of 50 mM Tris-Cl (pH 7.2) and shaking at 150 rpm for 30 min. Anti-rabbit IgG alkaline phosphatase conjugate, 1 μ l of a 1.0 mg/ml stock, resulting in a 1:33,000 dilution, was incubated 20 min with samples followed by another wash step. Individual coverslips were placed in individual wells of six-well ELISA plates (Costar, VWR, Brisbane, CA) and submerged in 3 ml glycine buffer (pH 10.4).

ELISAs for detection of other organisms followed the same protocol described for *E. coli* O157:H7, but the primary Abs used in a given assay were specific for the *Listeria* species or *S. enteritidis*. For the *Listeria* species ELISA, anti-*Listeria* IgG Abs, 4 μ l of the purchased stock (4.5 mg/ml) used at a 1:5,000 dilution, was incubated with a coverslip for 20 min with samples. For the *S. enteritidis* species ELISA, anti-*Salmonella*

IgG Abs, 1.1 μ l of the purchased stock (4.5 mg/ml) resulting in a 1:30,000 dilution, was incubated 20 min to label captured bacteria after a wash step.

The substrate *p*-nitrophenyl phosphate (pNPP), at a concentration of 0.25 mg per ml in 0.1 M glycine buffer (pH 10.4) containing 1 mM MgCl₂ and 1 mM ZnCl₂, was the substrate for the AP conjugated Ab. Color development of the product was followed using a HTS 7000 Bio Assay Reader (Perkin Elmer, Wellesley, MA, USA) with a detection wavelength fixed at 405 nm. Aluminum foil was used to minimize the substrate's exposure to light during the 30 min incubation and evaluation. The ELISAs were each performed at room temperature.

Cells were diluted in series and controls void of cells were treated identically to the treatment groups. Each treatment was compared to identically treated controls on the same six-well plate prepared in the absence of *E. coli* O157:H7, *L. innocua*, *L. monocytogenes*, and *S. enteritidis*.

Liposome Capture and PCR Analysis. PCR was used to identify the presence of *E. coli* O157:H7, *L. innocua*, *L. monocytogenes*, and *S. enteritidis* after incubation at the same inoculation levels used in the ELISAs. Individual species liposome capture was performed with a single species at three cell concentrations (2×10^3 , 2×10^5 , or 2×10^7 CFU/ml) for four liposome types (GM1, GM3, LN, or control liposomes) and replicated a total of four times. Simultaneous species liposome capture was performed with all four species at cell concentrations of 2×10^3 , 2×10^5 , or 2×10^7 CFU/ml for the four liposome types and replicated a total of three times with new samples. Finally, a simultaneous capture of *E. coli* O157:H7 and *S. enteritidis* was performed with all possible

permutations of the three concentrations tested and each of the four types of immobilized biomimetic liposomes.

For PCR analysis in all formats, the cells were incubated 30 min with three coverslips per 50 ml volume for each treatment. Coverslips were washed in a new 50 ml tube by adding 30 ml of 50 mM Tris-Cl (pH 7.2) and shaking at 150 rpm for 30 min. The coverslips were then fractured with sterile forceps and transferred to a 15 ml tube. Sterile ddH₂O, 1 ml, was added and the fractured coverslips were submerged. The samples were vortexed for 2 s.

Pure cultures of *E. coli* O157:H7, *L. innocua*, *L. monocytogenes*, or *S. enteritidis* were used as a positive control along with the liposome capture samples. For PCR, both pure culture and fractured coverslips were boiled at 96°C for 10 min to lyse the cells. After, lysis, the solutions were kept on ice and the DNA precipitated with ethanol. The precipitated DNA was resuspended in 100 µl sterile ddH₂O. Amplification was carried out in 0.5 ml microcentrifuge tubes containing one puReTaq™ Ready-To-Go Polymerase Chain Reaction Beads obtained from Amersham Biosciences (Buckinghamshire, England). Each tube contained 0.018 ml of sterile ddH₂O, 0.001 ml each primer, 0.005 ml of the ethanol precipitated DNA cell lysis solution as template DNA for a final reaction volume of 0.025 ml. The primer concentration in the final reaction volume was 20 pmol.

Each organism was specifically detected using a published primer set. The primer sets were purchased from Qiagen Operon (Alameda, CA, USA). For *E. coli* O157:H7, the *rfb O157* gene fragment was targeted and produced a replicon of 420 base pairs (bp) as described by [31]. The PCR procedure was adapted from [32]. For the *Listeria*

species, the *iap* gene fragment was targeted and produced replicons of 870 and 660 bp for *L. innocua* and *L. monocytogenes* respectively, as described by [33]. The PCR procedure was adapted from [33] and used by [29]. For *S. enteritidis*, the *invA* gene was targeted and produced a replicon of 284 bp as described in [34, 35]. The PCR procedure was used by [30, 36]. Primer sets used in the study are included as Appendix B.

The PCR took place in an automated temperature control PTC-200 Peltier Thermal Cycler (MJ Research, Watertown, MA, USA). For *E. coli* O157:H7, initial denaturation was set at 94°C for 5 min, followed by 30 amplification cycles each consisting of denaturation at 94°C for 1 min, annealing of the primers to the target DNA at 53°C for 1 min, and extension at 72°C for 1 min. The final extension was at 72°C for 5 min. For *L. innocua* and *L. monocytogenes*, initial denaturation was set at 95°C for 1 min, followed by 40 amplification cycles each consisting of denaturation at 94°C for 15 s, annealing of the primers to the target DNA at 58°C for 30 s, and extension at 72°C for 45 s. The final extension was at 72°C for 4 min. For *S. enteritidis*, initial denaturation was set at 95°C for 5 min, followed by 35 amplification cycles each consisting of denaturation at 95°C for 30 s, annealing of the primers to the target DNA at 64°C for 30 s, and extension at 72°C for 30 s. The final extension was at 72°C for 7 min. After completion of PCR, the samples were held at 4°C until proceeding to the next step (or -20°C if held overnight).

PCR products were separated and analyzed on 1.8% agarose gels. The PCR product solution, 10 µl, was combined with 1.5 µl gel-loading dye (BlueJuice, Gibco BRL, CA), mixed, and loaded into 1.8% agarose gels (FMC Bioproducts, Rockland, ME, USA). Electrophoresis was performed for 90-110 min at 4°C using a voltage of 80 V/cm

in 1x TAE buffer (40 mM Tris base, 40 mM acetic acid, and 1 mM EDTA). The gel was stained with ethidium bromide (1 $\mu\text{g/l}$) for 20 min and the bands were detected on a transilluminator (UVP, Upland, CA). Photographs of the gel were obtained using a Polaroid Land Camera MP4. A 100 bp DNA ladder (Pierce, Madison, WI, USA) was included in each gel.

Confocal Laser Scanning Microscopy. Confocal laser scanning microscopy images were generated using a Keller type MRC 1024 krypton/argon laser scanning confocal system (Bio-Rad, Hercules, CA, USA) interfaced with an inverted microscope (Diaphot TE300, Nikon, Tokyo, Japan). The pinhole diameters were 2.5, 2.5 and 3.0 mm, respectively, for the 488, 598, and 668 nm laser lines and the objective lens was a Nikon 100X, plan apo, oil immersion with a numerical aperture of 1.40. The 488 and 598 nm lines excited the SYTOX[®] Orange (Molecular Probes, Eugene, OR, USA), which labeled bacterial cells. The 647 nm laser line was used to excite 1,1'-dioctadecyl-3,3,3',3'-tetramethylindodicarbocyanine perchlorate (DiD oil) (Molecular Probes), which labeled liposomes. This line also was used to excite wheat germ agglutinin (WGA) conjugated Alexa Fluor[®] 660 used to label GM1 and GM3 liposomes embedded in the artificial bilayers. The 568 nm laser line was used to excite the encapsulated SRB. Dual and triple labeling of microemulsified liposomes afforded flexibility and specificity in monitoring the artificial structures and viable cells.

After incubation and wash, coverslips were fixed on plastic petri dishes using epoxy resin and hardener (Loctite[®], Henkel Loctite, Auburn Hills, MI, USA) in preparation for microscopy. The product was used as directed by the manufacturer. Before fixation of coverslips, a 20 x 20 mm² section was removed in the petri dishes

using a flamed knife. Individual coverslips, epoxied to a petri dish over the cut holes, formed a watertight seal and allowed buffer and probes in solution to be applied to the samples during active scanning at the inverted microscope.

At the microscope, lipophilic tracing probe DiD oil, was suspended in ethanol and applied to coverslips immersed in 2 ml 50 mM Tris-Cl (pH 7.2). The final concentration of DiD oil in the immersing solution was 0.51 mM for each concentration of avidin tested. Avidin immobilization was indirectly determined using CLSM to monitor increases in population densities of immobilized microemulsified liposomes containing *N*-biotinyl phosphatidylethanolamine.

GM1, GM3, and control liposome containing coverslips were incubated for 30 min with WGA conjugated Alexa Fluor® 660 (10 $\mu\text{g/ml}$) in 50 mM Tris-Cl, (pH 7.2). The coverslips were subsequently washed with 500 ml 50 mM Tris-Cl, (pH 7.2). WGA conjugate labeling of GM1, GM3, and control liposome containing coverslips was determined directly using CLSM.

Images (512 x 512 pixels and 226.50, 1415.64, or 22650.25 μm^2) were taken consecutively with the dichroic beam splitters and filters to minimize cross talk between channels. The photomultiplier gain/sensitivity/contrast was adjusted to give a slightly over-modulated signaling in the normal scan mode. The resulting RGB images were overlaid using LaserSharp® version 3.2 (Bio-Rad).

Statistical Analysis. The Descriptive Statistics and t-Test for Correlated Samples procedures of Statistica (Statsoft, Tulsa, OK, USA) were used to analyze triplicate absorbance measurements from ELISAs. The mean absorbance of three coverslips for each biomimetic liposome type and inoculation level was compared by difference to the

mean absorbance of three identically treated, uninoculated coverslips containing liposomes of the same type. The t-test used the raw absorbance values and statistical significance was determined at $p < 0.05$. Values approaching significance were also noted.

Exact analysis was used to fit a logistical regression model to statistically analyze the PCR data from each of the three captures (individual and simultaneous multiple species for all four species; and simultaneous capture of *E. coli* O157:H7 and *S. enteritidis*). The individual species capture was repeated four times. The simultaneous multiple species capture was performed in triplicate. The simultaneous capture of *E. coli* O157:H7 and *S. enteritidis* was also performed in triplicate. For each analysis, the outcome variable was the presence or absence of the species-specific PCR product. An overall test for significance was performed treating ordinally the two covariates inoculation level and biomimetic liposome type. Finally, a test for individual effects was performed treating the covariates categorically. Statistical Analysis Software 9.0[®] (SAS Institute Inc., Cary, NC, USA) was used to perform the required algorithms. Again, significance was determined at $p < 0.05$ and values approaching significance were noted.

RESULTS AND DISCUSSION

Avidin Immobilization Optimization and Liposome Characterization. DiD oil molecules consist of fatty hydrocarbon tails, 18 carbons in length, which intercalate into the artificial membranes, thus specifically labeling the liposomes and differentiating them from the unlabeled solid support. This lipid tracing probe is used to identify lipid

bilayers and fatty surfaces of cells. Glass slides coated with avidin at $6 \mu\text{g}$ or 1.0×10^{-10} moles avidin / 968 mm^2 (**Figure 16**), promoted uniform binding of liposomes without problematic background. The inset shows an image of cross-sectioned immobilized liposomes. Clearly the liposomes were located in closer proximity to one another and the population density is greater on the immobilized surface than at lower levels of immobilized avidin as compared to **Figure 5** (Chapter II). DiD oil's background labeling was not problematic at this, or increased DiD concentrations as was noted with increased levels of the polar-tracing probe, SRB (see Chapter II, **Figure 5**).

DiD oil predictably labeled each of the individual liposome types (GM1, GM3, LN, and control liposomes). Distributions and characteristics of GM1, GM3, LN, and control liposomes illuminated using DiD oil were observed to be similar in uniformity and dimension when compared to previously characterized liposomes identified using encapsulated probes and head-group labeled phospholipids (see Chapter II, Insets of **Figures 4-8**). This increase in avidin concentration was effective in increasing the number of immobilized liposomes and therefore potential bacterial binding sites reducing the probability of liposomes limiting microbial capture and detection.

WGA conjugated Alexa-Flour® 660 (blue), labeled liposomes formulated and processed in the presence of GM3 (**Figure 17**). LN and control liposomes were not labeled under the same conditions as this probe specifically labels *N*-acetylneuraminic acid (sialic acid) residues [37]. The binding of WGA conjugated Alexa-Flour® 660 to GM1 and GM3 liposomes indicating these molecules were embedded in the artificial bilayers of GM1 and GM3 liposomes, respectively. Previously, an ELISA utilizing an anti-GM1 Ab was used to confirm the presence of embedded GM1 molecules as

described in Chapter II. An Anti-GM3 Ab was not available, and thus the sialic acid specific probe was used to indicate the presence or absence of GM3 in GM3 and control liposomes, respectively. A representative GM3 liposome labeled using the sialic acid specific WGA conjugated probe is clearly shown (inset **Figure 17**).

Individual Species Capture ELISAs. Absorbance values were compared between GM1 liposomes incubated with cells at inoculation levels of 2×10^3 , 2×10^5 , and 2×10^7 CFU/ml (treatments) and samples treated identically without cells (controls). A Student's t-test for each inoculation and GM1 level was performed comparing the absorbance values for each treatment and GM1 level compared to the appropriate control on the same six-well plate. The normalized difference in mean absorbance values is plotted for *E. coli* O157:H7 and *S. enteritidis*, respectively shown in **Figures 18 and 19**, indicates that cells were captured on the 8.9% GM1 (molar percent of total lipid) liposomes when compared to the control liposomes lacking GM1 for each of the lower molar percent GM1 concentrations and inoculation levels. Subtracting the mean of the liposomes lacking GM1 from the treatment mean normalized the differences in absorbance values.

For *E. coli* O157:H7, at the 2×10^3 CFU/ml inoculation level and 8.9% GM1 liposomes, the normalized mean absorbance difference was 0.037 ($p = 0.0099$). At the 2×10^5 and 2×10^7 CFU/ml levels, the normalized differences between means was 0.042 ($p = 0.0323$) and 0.036 ($p = 0.0085$), respectively. Nonspecific binding caused some variability of the assay resulting in false positives but after normalization, no significant differences were indicated at GM1 levels less than 8.9%.

Similarly, for *S. enteritidis*, the normalized differences in the absorbance means was again found significant at each of the inoculation levels tested for the 8.9% GM1 liposomes. The normalized difference in mean absorbance for 8.9% GM1 liposomes inoculated at 2×10^3 CFU/ml was 0.033 ($p = 0.0168$). At the 2×10^5 and 2×10^7 CFU/ml inoculation levels, the difference in mean absorbance for inoculated 8.9% GM1 liposomes and uninoculated control was 0.040 ($p = 0.0388$) and 0.031 ($p = 0.0491$), respectively. Again, false positives were observed. This illustrates the susceptibility of the ELISA to result in false positives when attempting to differentiate between the lowest molar percent concentrations of GM1 in GM1 liposomes and lowest inoculation level. The normalization of the data accounted for this variability and set nonsensical negative values equal to zero. The ELISAs did however indicate that both enterobacteriaceae (*E. coli* O157:H7 and *S. enteritidis*) biologically recognize and bind 8.9 molar percent GM1 liposomes. Therefore, the GM1 concentration of 8.9 molar percent of total lipid was constant for further capture studies.

ELISAs were again performed to determine the capture of *E. coli* O157:H7 and *S. enteritidis* on GM1 liposomes (GM1 at 8.9 molar percent) and control liposomes, lacking GM1, with comparable results (**Figure 20**). Normalized differences in absorbance means for each inoculation level were significant and comparable to those reported in **Figures 18 and 19**, indicating adhesion and capture of *E. coli* O157:H7 and *S. enteritidis* with GM1 liposomes. This allowed us to conclude presumptively that GM1, embedded in the artificial bilayers of liposomes, is recognized by *S. enteritidis* and *E. coli* O157:H7. *L. monocytogenes* and *L. innocua* did not bind with GM1 liposomes or control liposomes lacking GM1 (**Figure 20**). The ELISA absorbance values are attached as Appendix C.

The ELISAs were developed using Abs screened for detection of the particular microorganisms tested in similar capture formats using Abs immobilized on glass beads [29, 30]. The same Abs were able to detect captured cells at concentrations as low as 4×10^1 CFU/ml [29, 30]. The ELISAs described in this study were modified to suit biomimetic liposome capture. Specifically, liposomes were incubated with viable cells in solution on a platform orbital shaker rather than in a flow system or fluidized bed. *E. coli* O157:H7 and *S. enteritidis* recognize and specifically bind to biomimetic GM1 liposomes. For this and other reasons, including the need to differentiate between *Listeria* species in future evaluations, it was decided that this preliminary method of determining microbial capture on liposomes could be improved by using PCR methods which can also determine binding and capture of multiple microorganisms after incubation. The samples evaluated by PCR were treated identically to those subjected to the ELISAs.

Liposome Capture with PCR Identification. Capture and detection using an ELISA assay depends on the specificity of the Abs used. PCR identification after liposome capture was performed to definitively establish the presence of the microorganism of interest using primers specific for that species (Appendix B). This approach allowed specific identification of microorganisms, even distinguishing between the *Listeria* species [38]. In an ELISA format, cross-reactivity of Abs would have made this impossible unless species specific Abs were available.

The detection limit of the PCR protocols using the species-specific primers was determined by diluting cell concentrations in solution and lysing by boiling. After the prescribed PCR protocol was followed, the presence of the species-specific PCR products

indicated the ability to detect the particular microorganism at a given inoculation level. *E. coli* O157:H7, *L. innocua*, and *S. enteritidis* were detectable at 2×10^2 CFU/ml. *L. monocytogenes* was detectable at 2×10^1 CFU/ml.

Individual species at inoculation levels of 2×10^3 , 2×10^5 , and 2×10^7 CFU/ml were separately incubated with GM1, GM3, and LN liposomes. Liposomes lacking GM1, GM3 and LN were treated identically and acted as controls. Cell capture with liposome types was evidenced by the presence of the specific PCR product. The results of the individual species capture and simultaneous multiple species capture are found in **Table 4**. The results of the simultaneous capture of *E. coli* O157:H7 and *S. enteritidis* are listed in **Table 5**. An example gel containing PCR products after capture of *S. enteritidis* with LN, GM1, or GM3 liposomes is shown in **Figure 21**.

General trends are observed in the individual species capture data presented in **Table 4A**. Capture was more likely at inoculation levels of 2×10^5 and 2×10^7 CFU/ml when compared to 2×10^3 CFU/ml. *E. coli* O157:H7 and *S. enteritidis* were more likely to be captured on GM1 and GM3 liposomes when compared to control and LN liposomes. Both of the *Listeria* species were more likely to be captured on LN than control, GM1, or GM3 liposomes.

In the simultaneous multiple species capture, presented in **Table 4B**, general trends are similar but less apparent. The *Listeria* species were captured on GM1 liposomes at 2×10^5 and at 2×10^7 CFU/ml whereas no capture was reported in the individual species capture at the same inoculation levels.

In the simultaneous capture of *E. coli* O157:H7 and *S. enteritidis* presented in **Table 5**, the species inoculated at the highest cell concentration in a given treatment was

found captured for each of the four combinations of 2×10^7 and 2×10^5 CFU/ml inoculations regardless of the liposome type. Such a trend was not evident in the two 2×10^5 and 2×10^3 CFU/ml inoculation treatments.

Logistic regression was used to analyze the data presented in **Tables 4 and 5**.

This form of regression is a powerful statistical analysis for categorical data. As in other forms of statistical analysis, logistic regression requires that sample size must be sufficiently large for parameter estimates to be normally distributed. Given the size of the data set, mathematical assumptions that suit large samples are clearly not justified. However, recent improvements in computational methods afford logistic regression models to be fit when sample sizes are small. This new field of logistic regression is known as the exact method [39].

The central theory of exact methods for logistic regression is to construct a statistical distribution that can, with efficient algorithms, be completely enumerated. This distribution can be constructed from extremely small data sets. Exact methods are recommended for fitting models to small sample size data, such as those presented in this study, or unbalanced data that result in zero frequency calls [39]. Exact analysis was performed using an overall test for significance for the inoculation level and biomimetic liposome type, similar to analysis of variance. A test for individual effects used a pairwise comparison to differentiate the inoculation levels (2×10^3 , 2×10^5 , and 2×10^7 CFU/ml) and four biomimetic liposome types (GM1, GM3, LN, or control liposomes).

For the inoculation levels, the capture of the bacteria at the 2×10^7 CFU/ml level was independently compared to capture of bacteria at the 2×10^3 CFU/ml or 2×10^5 CFU/ml levels. For the liposomes types, the capture of the bacteria on control liposomes

lacking GM1, GM3, and LN was independently compared to capture of bacteria on GM1, GM3, or LN liposomes. The exact analysis overall test for significance probability values of the individual and simultaneous multiple species capture are given in **Table 6**. The exact analysis probability values of the individual and simultaneous multiple species capture analyzed to determine individual effects are given in **Table 7**. The exact analysis overall test probability values of the simultaneous *E. coli* O157:H7 and *S. enteritidis* capture are given in **Table 8** and the probabilities from the individual effects given in **Table 9**.

Exact Analysis of *E. coli* O157:H7 Capture. In the individual species capture format, the overall test found *E. coli* O157:H7 inoculation level to be highly significant ($p < 0.0001$) (**Table 6A**). A pair-wise comparison was used to determine that treatments of 2.0×10^3 CFU/ml were significantly different than treatments of 2.0×10^7 CFU/ml ($p = 0.0009$) (**Table 7A**). Capture of the bacterium was significantly more likely to occur at the higher inoculation level. Binding to GM1 liposomes was more frequent than control liposomes ($p = 0.0209$) (**Table 7A**), though liposome type was not found to be significant in the overall test (**Table 6A**). Capture on other liposome types, GM3 and LN liposomes, respectively, was not found statistically different when compared to capture on control liposomes. CLSM confirmed the specific adhesion of *E. coli* O157:H7 cells to GM1 liposomes. A bacterium (orange/red) adhering to a GM1 liposome (blue/magenta) is shown in **Figure 22**. No evidence of specific capture on control, GM3, or LN liposomes was found using CLSM.

In the simultaneous multiple species format, statistical analysis was similar to the individual species format. The overall test found *E. coli* O157:H7 inoculation level to be

highly significant ($p < 0.0001$) (**Table 6B**). Again, capture of *E. coli* O157:H7 was significantly more likely to occur at both the 2.0×10^7 and 2.0×10^5 inoculation levels ($p = 0.0031$) (**Table 7B**). In this format however, binding or capture was not statistically different for each of the GM1, GM3, and LN liposomes when compared to the control (**Tables 6B and 7B**).

Exact Analysis of *S. enteritidis* Capture. In the individual species capture format, the overall test found *S. enteritidis* inoculation level to be highly significant ($p < 0.0001$) (**Table 6A**). A pair-wise comparison was used to determine that inoculation levels of 2.0×10^3 CFU/ml were significantly different from 2.0×10^7 CFU/ml concentrations ($p < 0.0001$) (**Table 7A**). Capture of the bacterium was significantly more likely to occur at the higher concentration. Binding or capture was frequent and statistically similar for all liposome types when compared independently to the control liposomes in both the overall and individual effects tests (**Tables 6A and 7A**).

In the simultaneous multiple species format, statistical analysis was similar to the individual species format. Again, capture of *S. enteritidis* was significantly more likely to occur at the highest cell concentration ($p = 0.0002$) and capture was frequent and similar for all the liposome types including the control (**Tables 6B and 7B**).

Exact Analysis of *L. monocytogenes* Capture. In the individual species capture format, the three inoculation levels were not statistically different in the overall test or test for individual effects for *L. monocytogenes* (**Tables 6A and 7A**). Liposome type was significantly different in the overall test ($p = 0.0001$) (**Table 6A**) and the individual effects test showed that capture of *L. monocytogenes* was more likely to occur on LN liposomes than the control liposomes for all three inoculation levels ($p < 0.0001$) (**Table**

7A). There was only one capture on GM3 liposomes and zero on GM1 liposomes (Table 4A). Therefore, the probability of capture on these liposomes compared to the control was not able to be determined statistically.

In the simultaneous multiple species format, inoculation level and liposome type were statistically different for *L. monocytogenes* ($p = 0.0022$ and $p = 0.0196$, respectively in the overall test) (Table 6B). The inoculation level of 2×10^7 CFU/ml was statistically more likely to result in capture when compared to the lowest cell concentration tested ($p = 0.0096$) (Table 7B). The test for individual effects found that capture of *L. monocytogenes* was more likely to occur on LN liposomes compared to control liposomes ($p = 0.0073$) (Table 7B). Capture of *L. monocytogenes* on GM1 and GM3 liposomes was nearly identical to the control liposomes (Table 4B).

Exact Analysis of *L. innocua* Capture. In the individual species capture format, the three inoculation levels were not statistically different in the overall test or the individual effects test for *L. innocua* (Tables 6A and 7A). Liposome type was significantly different in the overall test ($p = 0.0019$) (Table 6A) and the individual effects test showed that capture of *L. innocua* was more likely to occur on LN liposomes than the control liposomes for all three inoculation levels ($p < 0.0001$) (Table 7A). Capture was infrequent on GM1 and GM3 liposomes (Table 4A) and statistically insignificant when compared to control liposomes (Table 7A).

In the simultaneous multiple species format, inoculation level and liposome type were statistically different in the overall test for *L. innocua* ($p = 0.0107$ and $p = 0.0283$, respectively) (Table 6B). The test for individual effects determined that capture was more likely to occur at the 2×10^7 CFU/ml than the 2×10^3 CFU/ml inoculation level ($p =$

0.0031) (**Table 7B**). Capture of *L. innocua* was more likely to occur on LN liposomes compared to control liposomes but the probability could not be statistically determined because the PCR product was present for each replicate (**Table 4B**). All other liposome types were statistically similar to the control.

Simultaneous Capture of *E. coli* O157:H7 and *S. enteritidis*. In the simultaneous capture format of *E. coli* O157:H7 and *S. enteritidis*, as in the above analyses, presence of a specific PCR product indicated the capture of cells on a given capture surface containing a biomolecule embedded in artificial membranes of immobilized liposomes (**Table 5**). Exact analysis was performed using the presence of the *E. coli* O157:H7 PCR product as the outcome variable (**Tables 8A and 9A**). Then, the same data set was subjected to exact analysis with the *S. enteritidis* PCR product as the outcome variable (**Tables 8B and 9B**).

Exact analysis of *E. coli* O157:H7 capture was performed for each of the inoculation levels and liposome types. The overall test found the inoculation level of *E. coli* O157:H7 highly significant ($p < 0.0001$) (**Table 8A**). *E. coli* O157:H7 was captured more frequently at inoculation levels of 2×10^7 than 2×10^3 CFU/ml ($p = 0.0446$) (**Table 9A**). The affect of *S. enteritidis* inoculation level on capture of *E. coli* O157:H7 appeared to be directly related to cell concentration (the species inoculated at the higher concentration was more frequently captured on biomimetic liposomes in most treatments) but was not statistically evident.

Liposome type was not found significant in the overall test (**Table 8A**) but the test for individual effects determined that *E. coli* O157:H7 capture was more likely to occur on GM1 liposomes when compared to liposomes lacking biomoleclues ($p = 0.0508$,

approaches significance) (**Table 9A**). The other biomimetic liposome types (GM3 and LN liposomes) were not similar to control liposomes with respect to *E. coli* O157:H7 capture (**Tables 5, 8A, and 9A**).

Exact analysis of *S. enteritidis* capture was performed for each of the inoculation levels and liposome types. The overall test found the concentration of *S. enteritidis* highly significant ($p < 0.0001$) (**Table 8B**). The individual effects test found that *S. enteritidis* was captured more frequently at inoculation levels of 2×10^7 than 2×10^5 and 2×10^3 CFU/ml ($p = 0.0792$ and 0.0801 , respectively) (**Table 9B**). These values approach statistical significance ($p > 0.05$). Again, the competitive affect of *E. coli* O157:H7 inoculation level on capture of *S. enteritidis* appeared to be directly related to cell concentration but was not statistically evident (**Table 8B**).

Liposome type was found significant in the overall test for *S. enteritidis* ($p = 0.0175$) (**Table 9A**), but the test for individual effects was unable to identify the specific type of liposome that differed compared to the control with respect to *S. enteritidis* capture (**Table 9B**) because the data set was simply too small.

CONCLUSIONS

Unilamellar immobilized microemulsified GM1, GM3, and LN biomimetic liposomes were used to capture *E. coli* O157:H7, *S. enteritidis*, *L. monocytogenes*, and *L. innocua*. Biological binding and capture of *E. coli* O157:H7, *S. enteritidis*, *L. monocytogenes*, and *L. innocua* on immobilized unilamellar liposomes containing GM1, GM3, or LN was confirmed using ELISAs and PCR techniques.

Individual species GM1 capture of *E. coli* O157:H7 and *S. enteritidis* was confirmed by ELISA at inoculation levels of 2×10^3 , 2×10^5 , or 2×10^7 CFU/ml only when GM1 was included at 8.9 molar percent in liposomes. ELISAs indicated the *Listeria* species were not captured on 8.9 molar percent GM1 liposomes. The ELISAs indicated a species-specific adhesion and binding to liposomes containing different biomolecules. PCR detection of captured bacteria was used to differentiate between species in individual and simultaneous multiple species inoculations and incubations with biomimetic liposomes.

Considering the ELISAs and PCR capture detections, *E. coli* O157:H7 was captured with GM1 liposomes more frequently than any of the other liposome types tested, indicating *in vitro* that GM1 is a receptor in specific adhesion for this pathogen *in vivo*. *S. enteritidis* capture was evident but not as discriminatory with respect to GM1, GM3, LN, or control liposomes. *L. monocytogenes* and *L. innocua* were captured more frequently on LN liposomes when compared to control liposomes, indicating *in vitro*, that the LN biomolecule is recognized and results in capture of both a pathogenic and non-pathogenic species. Capture of the *Listeria* species was less frequent on GM1 and GM3 liposomes than the control liposomes.

With respect to the simultaneous *E. coli* O157:H7 and *S. enteritidis* capture, compelling evidence of one bacterial species out competing another for receptors and ultimately adhesion was evident at 2×10^7 CFU/ml, the highest inoculation level tested. By inspection, a hundred fold excess of a competing species prevented capture of another species with the biomimetic liposomes whereas, in the absence of the competing species in the individual capture format, capture was evident.

REFERENCES

1. Burack W, Biltonen R. Lipid bilayer heterogeneities and modulation of phospholipase A2 activity. *Chem Phys Lipids* 1994; 73:209-222.
2. Huang H, Goldberg E, Zidovetzki R. Ceramides perturb the structure of phosphatidylcholine bilayers and modulate the activity of phospholipase A2. *Eur Biophys J* 1998; 27:361-366.
3. Mouritsen O, Biltonen R. Protein-lipid interactions and membrane heterogeneity, in protein-lipid interactions. A Wtts, Ed. Amsterdam, Netherlands: Elsevier, 1993.
4. Harris F, Smith S, Bell J. Physical properties of erythrocyte ghosts that determine susceptibility to secretory phospholipase A2. *J Biol Chem* 2001; 276:22722-22731.
5. Bangham A, Standish M, Watkins J. Diffusion of univalent ions across the lamellae of swollen phospholipids. *J Mol Biol* 1965; 13:238-252.
6. Frank JF. Confocal microscopy and microbial viability detection for food research. *J Food Prot* 2001; 64(12):2088-2102.
7. Sonnino S, Ghidoni R, Gazzotti G, Acquotti D, Tettamanti G. New trends in ganglioside chemistry. *Adv Exper Med Biol* 1988; 228:437-464.
8. Natomi H, Sugano K, Takaku F, Iwamori M. Glycosphingolipid composition of the gastric mucosa. *J Clin Gastroenterol* 1990; 12(Suppl. 1):S52-S57.
9. Finlay BB. Cracking *Listeria's* password. *Science* 2001; 292(5522):1665-1666.
10. Finlay BB, Cossart P. Exploitation of mammalian host cell functions by bacterial pathogens. *Science* 1997; 276(5313):718-725.
11. Brown E, Dejana E. Cell-to-cell contact and extracellular matrix. Editorial overview: Cell-cell and cell-matrix interactions-running, jumping, standing still. *Curr Opin Cell Biol* 2003; 15:505-508.
12. Cossart P. Met, the HGF-SF receptor: another receptor for *Listeria monocytogenes*. *Trends Microbiol* 2001; 9(3):105-107.
13. Marcus SL, Wenk MR, Steele-Mortimer O, Finlay BB. A synaptojanin-homologous region of *Salmonella typhimurium* SigD is essential for inositol phosphatase activity and Akt activation. *FEBS Lett* 2001; 494:201-207.

14. Boyle EC, Finlay BB. Bacterial pathogenesis: exploiting cellular adherence. *Curr Opin Cell Biol* 2003; 15:633-639.
15. Hazlett LD, Masinick S, Barrett R, Rosol K. Evidence for asialo GM1 as a corneal glycolipid receptor for *Pseudomonas aeruginosa* adhesion. *Infect Immun* 1993; 61(12):5164-5173.
16. Maloney MD, Lingwood CA. CD19 has a potential CD77 (globotriaosyl ceramide)-binding site with sequence similarity to verotoxin B-subunits: implications of molecular mimicry for B cell adhesion and enterohemorrhagic *Escherichia coli* pathogenesis. *J Exp Med* 1994; 180:191-201.
17. Mulvey MA, Huntgren SJ. Bacterial spelunkers. *Science* 2000; 289: 732-733.
18. Hultgren SJ, Jones CH. Utility of immunoglobulin-like fold of chaperones in shaping organelles of attachment in pathogenic bacteria. *ASM News* 1995; 61(9):457-64.
19. Bendas G, Vogel J, Bakowski U, Krause A, Muller J, Rothe U. A liposome-based model system for the simulation of lectin-induced cell adhesion. *Biochim Biophys Acta* 1997; 1325:297-308.
20. Colin M, Maurice M, Trugnan G, Kornprobst M, Harbottle RP, Knight A, Cooper RG, Miller AD, Capeau J, Coutelle C, Brahimi-Horn MC. Cell delivery, intracellular trafficking and expression of an integrin-mediated gene transfer vector in tracheal epithelial cells. *Gene Ther* 2000(7):139-152.
21. Knodler LA, Celli J, Finlay BB. Pathogenic trickery: Deception of host cell processes. *Nat Rev Mol Cell Biol* 2001; 2(8):578-588.
22. Qiu C, Young MBD, Finn A, Dichek DA. Cationic liposomes enhance adenovirus entry via a pathway independent of the fiber receptor and alpha v-integrins. *Hum Gene Ther* 1998; 9:507-520.
23. Deshpande SS. *Handbook of Food Toxicology*. New York: Marcel Dekkar, Inc., 2002.
24. Pizarro-Cerda J, Moreno E, Desjardins M, Gorvel JP. When intracellular pathogens invade the frontiers of cell biology and immunology. *Histol Histopathol* 1997; 12:1027-1038.
25. Steele-Mortimer O, Meresse S, Gorvel J-P, Toh B-H, Finlay BB. Biogenesis of *Salmonella typhimurium*-containing vacuoles in epithelial cells involves interactions with the early endocytic pathway. *Cell Microbiol* 1999; 1(1):33-49.

26. Ferrando M, Spiess WEL. Review: confocal scanning laser microscopy. A powerful tool in food science. *Food Sci Technol Int London* 2000; 6(4):267-284.
27. Frank JF. Microbial attachment to food and food contact surfaces. *Adv Food Nutr Res* 2001; 43:319-370.
28. Weimer BC, Walsh MK, Beer C, Koka R, Wang X. Solid-phase capture of proteins, spores, and bacteria. *Appl Environ Microbiol* 2001; 67(3):1300-1307.
29. Lippens W. Thesis: Rapid detection of *Listeria monocytogenes*, Nutrition and Food Science. Utah State University: Logan, UT, 2003.
30. Harrington E. Thesis: Rapid detection of *Salmonella enteritidis*, Nutrition and Food Science. Utah State University: Logan, UT, 2004.
31. Maurer J, Schmidt D, Petrosko P, Sanchez S, Bolton L, Lee M. Development of primers to O-antigen biosynthesis genes for specific detection of *Escherichia coli* O157 by PCR. *Appl Environ Microbiol* 1999; 65(7):2954-2960.
32. Osek J. Rapid and specific identification of Shiga toxin-producing *Escherichia coli* in faeces by multiplex PCR. *Lett Appl Microbiol* 2002; 34:304-310.
33. Bubert A, Hein I, Rauch M, Lehner A, Yoon B, Goebel W, Wagner M. Detection and differentiation of *Listeria* spp. by a single reaction based on multiplex PCR. *Appl Environ Microbiol* 1999; 65:4688-4692.
34. Malorny B, Hoorfar J, Bunge C, Helmuth R. Multicenter validation of the analytical accuracy of *Salmonella* PCR: towards an International standard. *Appl Environ Microbiol* 2003; 69(1):290-296.
35. Rahn K, Grandis SD, Clarke R, McEwen S, Galan J, Ginocchio C, III RC, Gyles C. Amplification of an *invA* gene sequence of *Salmonella typhimurium* by polymerase chain reaction as a specific method of detection of *Salmonella*. *Mol Cell Probes* 1992; 6:271-279.
36. Scholz H, Arnold T, Marg H, Rosler U, Hensel A. Improvement of an *invA*-based PCR for the specific detection of *Salmonella typhimurium* in organs of pigs. *Berl Munch Teirarztl Wochenschr* 2001; 114(9-10):401-403.
37. Atlamazoglou V, Yova D, Kavantzias N, Loukas S. Microscopical examination of the localization patterns of two novel rhodamine derivatives in normal and neoplastic colonic mucosa. *Lasers Med Sci* 2001; 16(4):253-259.

38. Aznar R, Alarcon B, On the specificity of PCR detection of *Listeria monocytogenes* in food: comparison of published primers. *System Appl Microbiol* 2002; 25:109-119.
39. Hosmer DW, Lemeshow S, *Applied Logistic Regression*. Second ed., New York: John Wiley & Sons, Inc., 2000.

Table 4. Individual species and simultaneous multiple species capture verified by PCR

A

	Individual Species Capture ¹											
	Control Liposomes			GM1 Liposomes			GM3 Liposomes			Laminin Liposomes		
	Inoculation Level			Inoculation Level			Inoculation Level			Inoculation Level		
	(CFU/ml)			(CFU/ml)			(CFU/ml)			(CFU/ml)		
	2 x 10 ³	2 x 10 ⁵	2 x 10 ⁷	2 x 10 ³	2 x 10 ⁵	2 x 10 ⁷	2 x 10 ³	2 x 10 ⁵	2 x 10 ⁷	2 x 10 ³	2 x 10 ⁵	2 x 10 ⁷
<i>E. coli</i> O157:H7	----	+----	++++	-+---	++++	++++	----	-+++	++++	----	----	-+++
<i>S. enteritidis</i>	----	-+--	-+++	----	++++	++++	----	+---	++++	----	+--	++++
<i>L. monocytogenes</i>	----	-+++	-+++	----	----	----	----	----	+	----	++++	++++
<i>L. innocua</i>	----	-+--	+++	----	----	----	----	----	-+--	++++	++++	++++

B

	Simultaneous Multiple Species Capture ²											
	Control Liposomes			GM1 Liposomes			GM3 Liposomes			Laminin Liposomes		
	Inoculation Level			Inoculation Level			Inoculation Level			Inoculation Level		
	(CFU/ml)			(CFU/ml)			(CFU/ml)			(CFU/ml)		
	2 x 10 ³	2 x 10 ⁵	2 x 10 ⁷	2 x 10 ³	2 x 10 ⁵	2 x 10 ⁷	2 x 10 ³	2 x 10 ⁵	2 x 10 ⁷	2 x 10 ³	2 x 10 ⁵	2 x 10 ⁷
<i>E. coli</i> O157:H7	---	---	++-	---	++-	+++	---	+	+++	---	-+-	++-
<i>S. enteritidis</i>	---	+	++	---	+++	+++	+	++-	+++	---	++	++
<i>L. monocytogenes</i>	---	-+	++-	---	-+	++	---	+	++-	+	+++	+++
<i>L. innocua</i>	---	-+	++-	---	+	++-	---	---	++	+++	+++	+++

¹ Each species individually inoculated at each concentration and incubated with each biomimetic liposome type

² Each species simultaneously inoculated at equal concentration for each inoculation level and incubated with each biomimetic liposome type

(-) indicates the absence of species specific PCR product

(+) indicates the presence of species specific PCR product

Table 5. Simultaneous capture of *E. coli* O157:H7 and *S. enteritidis* verified by PCR

	Simultaneous Capture of <i>E. coli</i> O157:H7 and <i>S. enteritidis</i>¹											
	Inoculation Levels (CFU/ml)		Inoculation Levels (CFU/ml)		Inoculation Levels (CFU/ml)		Inoculation Levels (CFU/ml)		Inoculation Levels (CFU/ml)		Inoculation Levels (CFU/ml)	
	<i>E. coli</i> 2x10 ⁷	<i>S. enteritidis</i> 2x10 ³	<i>E. coli</i> 2x10 ³	<i>S. enteritidis</i> 2x10 ⁷	<i>E. coli</i> 2x10 ⁷	<i>S. enteritidis</i> 2x10 ⁵	<i>E. coli</i> 2x10 ⁵	<i>S. enteritidis</i> 2x10 ⁷	<i>E. coli</i> 2x10 ⁵	<i>S. enteritidis</i> 2x10 ³	<i>E. coli</i> 2x10 ³	<i>S. enteritidis</i> 2x10 ⁵
Control Liposomes	+++	---	---	+++	+++	---	---	+++	---	---	---	+++
GM1 Liposomes	+++	---	---	+++	+++	---	---	+++	+++	---	---	+++
GM3 Liposomes	+++	---	---	+++	+++	---	---	+++	---	---	---	+++
Laminin Liposomes	+++	---	---	+++	+++	---	---	+++	---	---	---	---

¹ Both species simultaneously inoculated at six combinations of each inoculation level (2 x 10³, 2 x 10⁵, and 2 x 10⁷ CFU/ml) and incubated with each biomimetic liposome type

(-) indicates the absence of species specific PCR product

(+) indicates the presence of species specific PCR product

Table 6. Exact analysis probability values for inoculation level and biomimetic liposome type in both the individual and simultaneous multiple species incubation format for the capture of *E. coli* O157:H7, *S. enteritidis*, *L. monocytogenes*, and *L. innocua* in an overall test for significance ($p < 0.05$).

	A Individual Species Capture¹		B Simultaneous Multiple Species Capture²	
	Inoculation level (CFU/ml)	Biomimetic liposome type	Inoculation level (CFU/ml)	Biomimetic liposome type
<i>E. coli</i> O157:H7	< 0.0001	0.4366	< 0.0001	1.000
<i>S. enteritidis</i>	< 0.0001	0.5105	< 0.0001	0.7028
<i>L. monocytogenes</i>	0.1445	0.0001	0.0022	0.0196
<i>L. innocua</i>	0.0818	0.0019	0.0107	0.0283

¹ Each species individually inoculated at each concentration and incubated with each biomimetic liposome type

² Each species simultaneously inoculated at equal concentration for each inoculation level and incubated with each biomimetic liposome type

Table 7. Exact analysis probability values for inoculation level and biomimetic liposomes in both the individual and simultaneous multiple species incubation format for the capture of *E. coli* O157:H7, *S. enteritidis*, *L. monocytogenes*, and *L. innocua* in testing for significance of individual effects ($p < 0.05$).

A

Individual Species Capture¹

	Inoculation level (CFU/ml)		Biomimetic liposomes		
	2×10^3	2×10^5	GM1	GM3	LN
	<i>E. coli</i> O157:H7	0.0009	1.000	0.0209	0.2669
<i>S. enteritidis</i>	< 0.0001	0.7534	1.000	1.000	1.000
<i>L. monocytogenes</i>	0.4317	1.000	ND ³	ND	< 0.0001
<i>L. innocua</i>	0.3451	1.000	0.1805	ND	< 0.0001

B

Simultaneous Multiple Species Capture²

	Inoculation level (CFU/ml)		Biomimetic liposomes		
	2×10^3	2×10^5	GM1	GM3	LN
	<i>E. coli</i> O157:H7	0.0031	1.000	1.000	1.000
<i>S. enteritidis</i>	0.0002	0.5665	1.000	1.000	1.000
<i>L. monocytogenes</i>	0.0096	0.9455	ND	ND	0.0073
<i>L. innocua</i>	0.0031	1.000	1.000	1.000	ND

¹ Each species individually inoculated at each level and incubated with each biomimetic liposome type

² Each species simultaneously inoculated at equal concentration for each level and incubated with each biomimetic liposome type

³ **ND** = Not able to be determined because the conditional distribution was degenerate

Note: Inoculation level statistical probabilities independently compared 2×10^3 CFU/ml and 2×10^5 CFU/ml to 2×10^7 CFU/ml.

Biomimetic liposome statistical probabilities independently compared control liposomes to GM1, GM3, and LN liposomes

Table 8. Exact analysis probability values for inoculation level of *E. coli* O157:H7, biomimetic liposome type, and inoculation level of *S. enteritidis* in the simultaneous species incubation format for the capture of *E. coli* O157:H7 or *S. enteritidis* in an overall test of significance ($p < 0.05$).

Factorial Simultaneous Capture of *E. coli* O157:H7 and *S. enteritidis*¹

A <i>E. coli</i> O157:H7 Capture			B <i>S. enteritidis</i> Capture		
Inoculation level <i>E. coli</i> O157:H7	Biomimetic liposome type	Inoculation level <i>S. enteritidis</i>	Inoculation level <i>S. enteritidis</i>	Biomimetic liposome type	Inoculation level <i>E. coli</i> O157:H7
< 0.0001	0.2813	0.3558	< 0.0001	0.0175	0.7214

¹ Both species simultaneously inoculated at six combinations of each inoculation level (2×10^3 , 2×10^5 , and 2×10^7 CFU/ml) and incubated with each biomimetic liposome type

Table 9. Exact analysis probability values for inoculation level of *E. coli* O157:H7, biomimetic liposome type, and inoculation level of *S. enteritidis* in the simultaneous species incubation format for the capture of *E. coli* O157:H7 and *S. enteritidis* in testing for significance of individual effects ($p < 0.05$).

Factorial Simultaneous Capture of *E. coli* O157:H7 and *S. enteritidis*¹

A <i>E. coli</i> O157:H7 Capture							B <i>S. enteritidis</i> Capture						
Inoculation level <i>E. coli</i> O157:H7		Biomimetic liposomes			Inoculation level <i>S. enteritidis</i>		Inoculation level <i>S. enteritidis</i>		Biomimetic liposomes			Inoculation level <i>E. coli</i> O157:H7	
2x10 ³	2x10 ⁵	GM1	GM3	LN	2x10 ³	2x10 ⁵	2x10 ³	2x10 ⁵	GM1	GM3	LN	2x10 ³	2x10 ⁵
0.0446	1.000	0.0508	0.5992	ND ²	ND	0.0372	0.0792	0.0801	1.000	1.000	1.000	1.000	1.000

¹ Both species simultaneously inoculated at six combinations of each inoculation level (2×10^3 , 2×10^5 , and 2×10^7 CFU/ml) and incubated with each biomimetic liposome type

² **ND** = Not able to be determined because the conditional distribution was degenerate

Note: Inoculation level statistical probabilities independently compared 2×10^3 CFU/ml and 2×10^5 CFU/ml to 2×10^7 CFU/ml. Biomimetic liposome statistical probabilities independently compared control liposomes to GM1, GM3, and LN liposomes

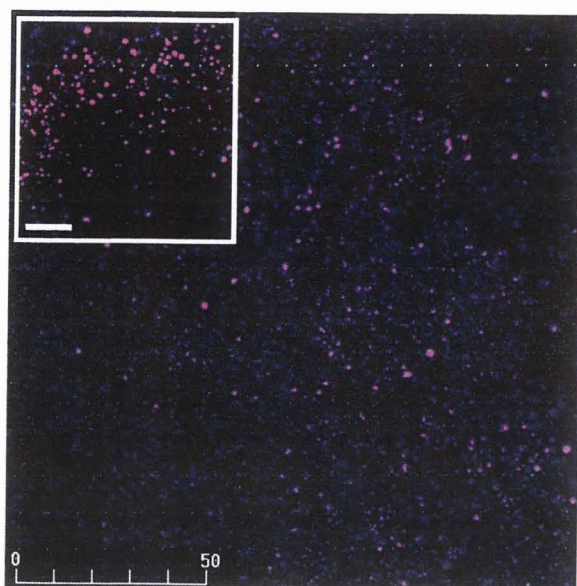


Figure 16. Field of DiD oil labeled immobilized unilamellar microemulsified GM3 liposomes immobilized directly after microemulsification. Liposomes immobilized via biotinylated phospholipids on coverslips containing covalently bound avidin. DiD oil (blue) labeled the artificial bilayers and encapsulated sulforhodamine B (red) was localized in the liposomal lumen. Co-localization of blue and red probes resulted in magenta coloration. Scale values represent μm . Inset: cross-section of GM3 liposomes at increased magnification. Bar = $10 \mu\text{m}$.

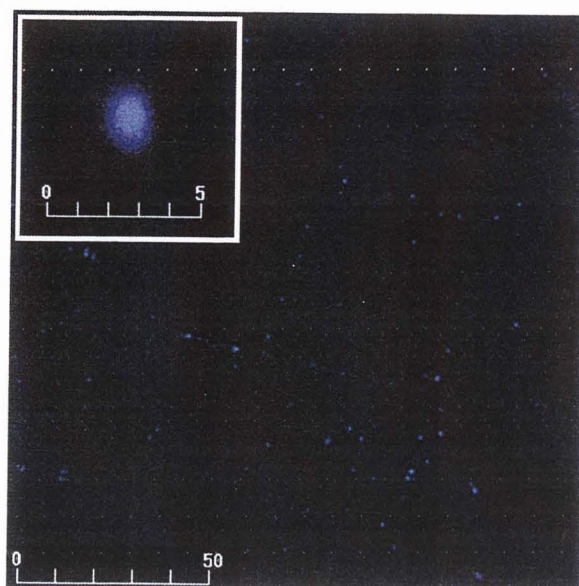


Figure 17. Field of immobilized GM3 unilamellar microemulsified liposomes immobilized directly after microemulsification labeled with WGA conjugated Alexa Fluor® 660 (blue). Liposomes immobilized via biotinylated phospholipids on coverslips containing covalently bound avidin. Inset: one representative GM3 liposome. Wheat germ agglutinin conjugated Alexa Fluor® 660 specifically labeled sialic acid residues of ganglioside molecules. Scale values represent μm .

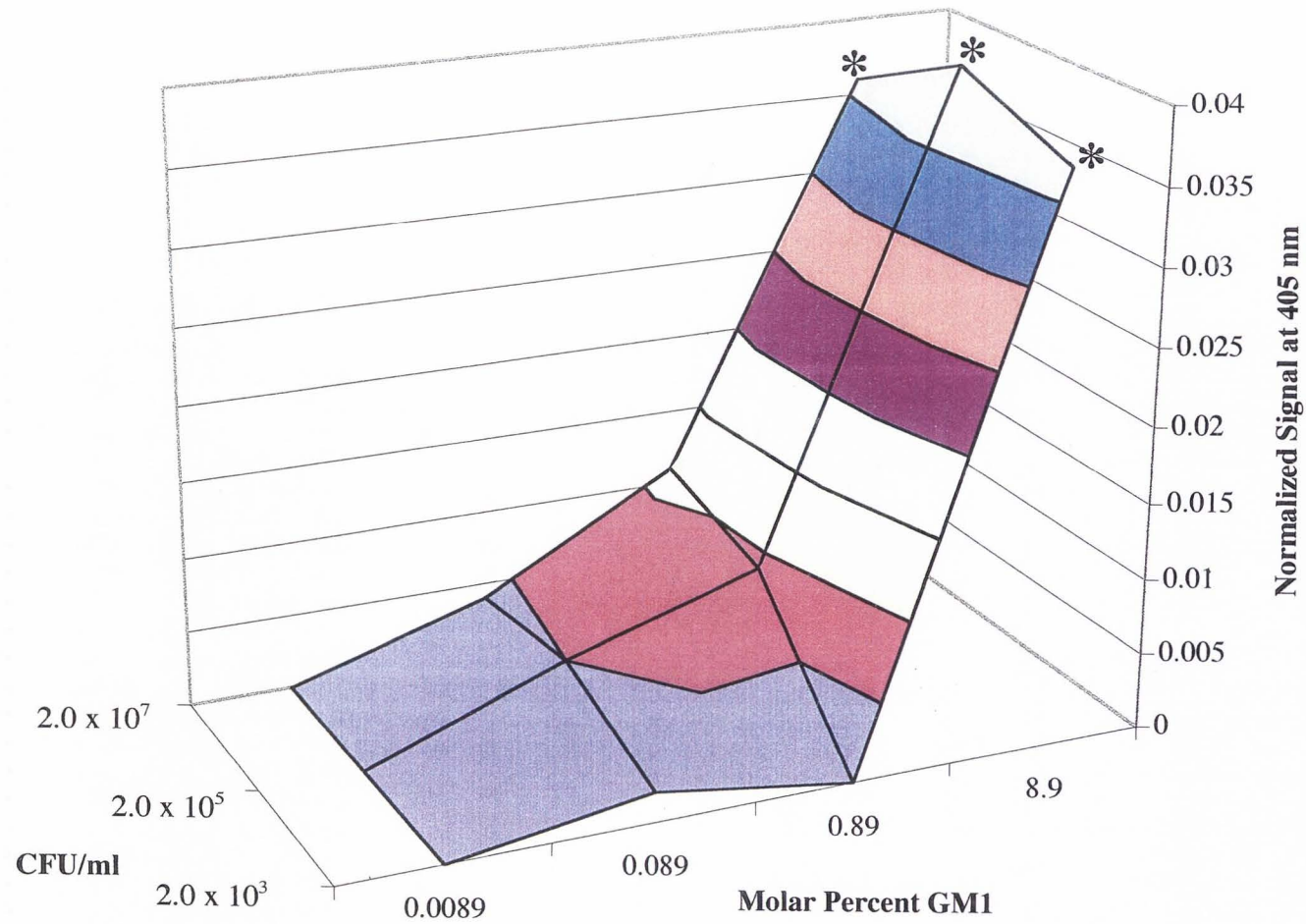


Figure 18. Individual species capture of *E. coli* O157:H7 with GM1 liposomes verified by ELISA. X-axis represents molar percent of GM1 compared to total lipid in formulation. Y-axis represents normalized signal (mean absorbance) at 405 nm. Z-axis represents inoculation levels as colony forming units per ml (CFU/ml). Treatments of significance ($p \leq 0.05$) using paired-comparison of GM1 liposomes and control liposomes are indicated by *.

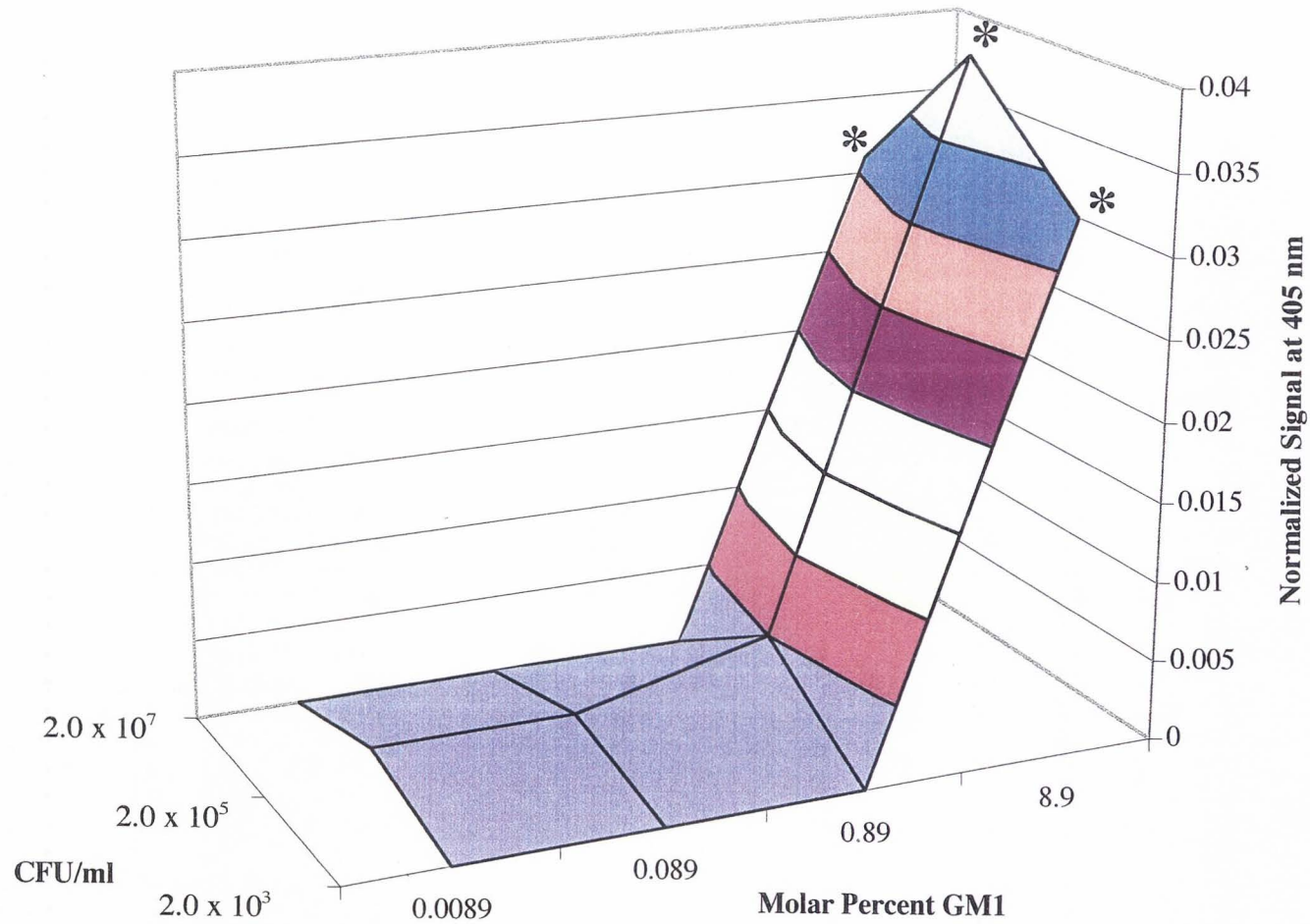


Figure 19. Individual species capture of *S. enteritidis* with GM1 liposomes verified by ELISA. X-axis represents molar percent of GM1 compared to total lipid in formulation. Y-axis represents normalized signal (mean absorbance) at 405 nm. Z-axis represents inoculation levels as colony forming units per ml (CFU/ml). Treatments of significance ($p \leq 0.05$) using paired-comparison of GM1 liposomes and control liposomes are indicated by *.

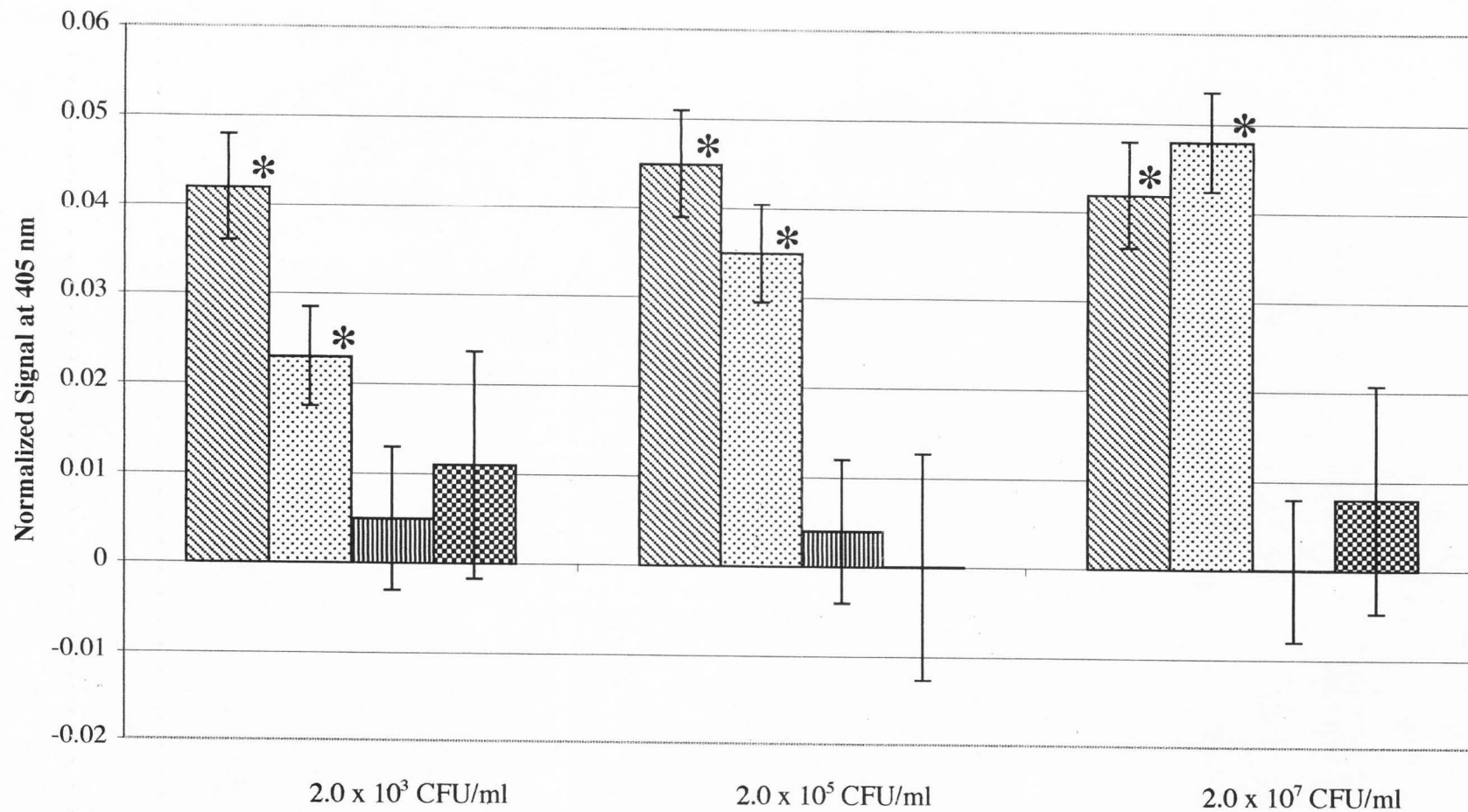


Figure 20. Individual species capture of *E. coli* O157:H7, *S. enteritidis*, *L. monocytogenes*, and *L. innocua* with GM1 liposomes verified by ELISA. X-axis represents inoculation levels as colony forming units per ml (CFU/ml). Y-axis represents normalized signal (mean absorbance) at 405 nm. Treatments of significance ($p \leq 0.05$) using paired-comparison of GM1 liposomes and control liposomes are indicated by *.

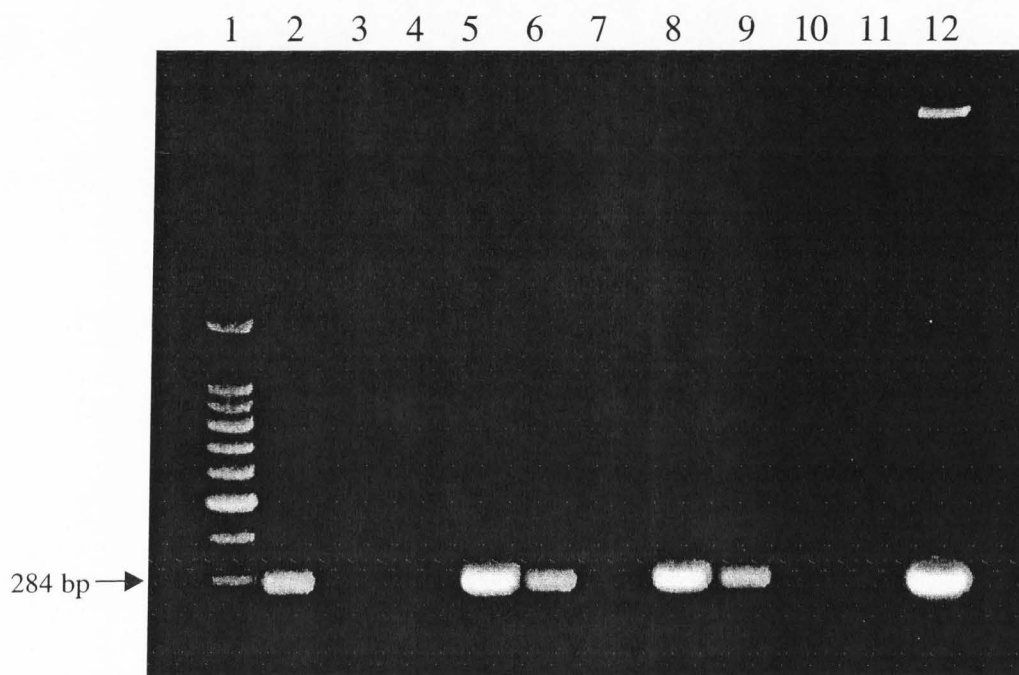


Figure 21. Capture of *S. enteritidis* with laminin, GM1 or GM3 liposomes. Lane 1) DNA ladder (from top to bottom: 1,500 1,000, 900, 800, 700, 600, 500, 400, and 300), Lanes 2-4) Laminin liposomes inoculated with 2.0×10^7 , 2.0×10^5 , or 2.0×10^3 CFU/ml, respectively, Lanes 5-7) GM1 liposomes 2.0×10^7 , 2.0×10^5 , or 2.0×10^3 CFU/ml, respectively, Lanes 8-10) GM3 liposomes 2.0×10^7 , 2.0×10^5 , or 2.0×10^3 CFU/ml, respectively, Lane 11) negative, ddH₂O, Lane 12) positive control, 2.0×10^9 CFU/ml lysed via 10 min boil.

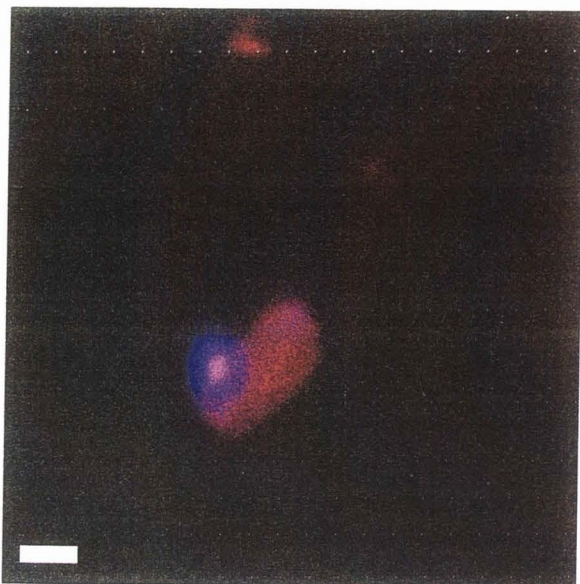


Figure 22. Captured *E. coli* O157:H7 bacterium (orange/red) on GM1 liposomes (blue/magenta). The bacterium and artificial membrane were probed by SYTOX[®] Orange and DiD oil, respectively. SRB was encapsulated in the liposomal lumen. Scale values represent μm . Bar = 1 μm .

CHAPTER V

SUMMARY AND CONCLUSIONS

NULL HYPOTHESIS

The reported molecular activity of biomolecules is not maintained *in vitro* when incorporated into immobilized liposomes.

Liposomes were produced to mimic cell surfaces by incorporating or embedding a variety of biomolecules including glycosphingolipids, a protein receptor and a channel protein. These biomimetic unilamellar liposomes were immobilized to solid surfaces in a manner that maintained the physical and chemical properties of the liposomes. Therefore, the molecular activity of biomolecules is maintained after incorporation into immobilized microemulsified biomimetic liposomes. Biomimetic liposomes may provide a system to study environmental influences and interactions between membrane bound biomolecules with soluble microorganisms and proteins.

Methodologies to produce and characterize immobilized liposomes were developed to examine the hypothesis by completing a series of objectives investigating liposomes formulated with biomolecules of well-characterized activity using two different approaches. A large transmembrane channel protein, EcoMscL, was incorporated into immobilized liposomes and activity was demonstrated under modulations corresponding to an osmotic event. Small membrane embedded surface receptors were incorporated into immobilized liposomes and retained their biological activity of binding proteins, toxins, or bacteria.

OBJECTIVES

Objective 1. To verify biological activity of liposomes containing a mechanosensitive channel from *Escherichia coli* (EcoMscL). The artificial membrane bilayers (liposomes) were immobilized onto a glass surface and observed for channel opening with confocal microscopy. This information is of interest to biological scientists and microscopists.

The aim of this study was to investigate the influence of osmotic stress on liposomes containing membrane bound mechanosensitive channel protein (EcoMscL) pentamers. Liposomes composed of phospholipids, cholesterol, proteins and *N*-biotinyl phosphatidylethanolamine were formulated, microemulsified and immobilized on glass coverslips containing covalently immobilized avidin. EcoMscL was cloned, expressed, labeled with 5-(and-6) carboxynaphthofluorescein (CNF), and incorporated as a membrane protein in the bilayer during the production of liposomes. Liposomes mimicked analogous larger cells (i.e., bacteria) known to rely on mechanosensitive channels for survival during osmotic shock.

Immobilized liposomes of various compositions were monitored using CLSM and maintained their integrity while the osmotics of the immersing solution were modified to simulate hypo-, and hyperosmotic shock. It was hypothesized that if the recombinantly expressed and partially purified EcoMscL protein retained its biological activity when labeled and incorporated into liposomes, it would open during an osmotic treatment and this opening would be observable as a change in fluorescence. The described methods allowed active monitoring of liposomes during osmotic events *in vitro* using CLSM as a

new approach to compliment and confirm reports of functional reconstitution of mechanosensitive proteins in liposomes.

Monitoring the diffusion and release of an encapsulated polar-tracing probe, sulforhodamine B (SRB), during osmotic modulation found significant probe quenching during the 0-4 M NaCl gradient compared to the control liposomes. We were unable to determine if this was due to cell puckering or the opening of the EcoMscL channel allowing the release of internalized SRB but the dramatic change in pixel intensity indicates that there was a biological response in EcoMscL liposomes when compared to the control liposomes. Other gradient treatments (0-300 mM NaCl and 0-200 mM EDTA) resulted in no difference in red channel reduction for any of the immobilized liposome types tested.

The stability of liposomes containing membrane proteins and recombinant EcoMscL from *E. coli* was estimated with respect to the liposomes' relative ability to encapsulate SRB in a dry-state. The immobilized liposome system was stable for a long period of time (approximately four months stored dry at refrigeration temperatures). The liposomes' composition and dimensions were suitable for monitoring and imaging using CLSM. EcoMscL has physical dimensions large enough that when opened allows encapsulated water soluble SRB to be released from the liposomal lumen to the immersing solution but we were unable to determine the source of release or quenching of the probe using CLSM alone. We are the first group to immobilize unilamellar liposomes on glass and study reconstituted EcoMscL, liposome functionality and bilayer encapsulation and integrity using CLSM. This study showed the stability and flexibility

of immobilized liposomes embedding a large membrane protein under various osmotic conditions.

Objective 2. To verify biological activity of liposomes containing glycosphingolipids (GM1 or GM3). The liposomes were immobilized onto a glass surface and challenged with bacteria and proteins (including cholera toxin). The *in vitro* assay used confocal microscopy, ELISA, or genetic-based detection systems to determine bacterial and toxin interactions.

A stable biomimetic system consisting of immobilized microemulsified liposomes containing embedded GM1 or GM3 on a solid glass support was developed. Our immobilization procedure did not alter the composition or dimensions of the liposomes but presented several advantages to alternative strategies. Immobilization affords an important element of spatial control. Immobilized liposomes were located in relatively the same *xy* plane equidistant from the glass surface and increasing the amount of avidin resulted in a greater immobilized liposome population on the solid support. Therefore using our methods, multiple immobilized liposomes can be observed in a single field under a host of treatments and potential binding sites were not limiting. Avidin-biotin immobilization is advantageous because nonspecifically bound molecules can be removed by washing the immobilized liposomes with buffer.

The stability of immobilized microemulsified liposomes containing membrane-embedded or encapsulated biomolecules was monitored over time using SRB. Our liposomes, labeled with appropriate fluorophores, have the advantage of direct monitoring over a long period of time. Stabilities of GM1 and control liposomes were compared over weeks and months rather than a period of minutes or hours as previously

reported with soluble liposomes. CNF-BSA liposomes that encapsulated SRB were stable for approximately two months while GM1 and control liposomes that encapsulated SRB were stable for at least four and a half months.

An application investigating the interactions between CNF labeled soluble proteins (cholera toxin, bovine lactoferrin, bovine serum albumin, and ovalbumin) and GM1 liposomes were characterized by the presence of the amine reactive probe, CNF. After incubation with the labeled proteins in solution, specific interactions between GM1 liposomes were observed with confocal microscopy. Cholera toxin (beta-subunit) (CTB) and bovine lactoferrin (BLF) were co-localized proximate to GM1 liposomes. CTB, BLF and ovalbumin were not associated with control liposomes lacking GM1.

In another application, *in vitro* capture of *Escherichia coli* O157:H7, *Salmonella enteritidis*, *Listeria monocytogenes*, and *Listeria innocua* with GM1 or GM3 liposomes was investigated using ELISAs and confirmed by PCR analysis. Individual and simultaneous species inoculations and incubations with GM1 and GM3 liposomes resulted in adhesion and capture of *E. coli* O157:H7 and *S. enteritidis*. This capture was investigated using ELISAs, with the capture evident with GM1 molar percent levels of 8.9. *L. monocytogenes* and *L. innocua* were not captured on GM1 liposomes. *S. enteritidis* was captured with GM1 and GM3 liposomes but also with the control liposomes lacking receptor molecules. *E. coli* O157:H7 capture with GM1 liposomes was more frequent and significantly different when compared to control liposomes. Biological capture of *E. coli* O157:H7 was investigated using CLSM showing that the organisms specifically co-localized with GM1 liposomes. Considering the results of the ELISAs and PCR capture detections, *E. coli* O157:H7 was captured with GM1 liposomes

more frequently than the other biomimetic liposomes tested, indicating *in vitro* that GM1 is a specific biological adhesion receptor for this pathogen *in vivo*. *L. monocytogenes*, and *L. innocua* were not frequently captured on GM1 or GM3 liposomes or the control liposomes indicating that GM1 is not a specific receptor for these organisms.

Objective 3. To verify biological activity of liposomes containing laminin, a eukaryotic protein receptor for bacteria. The liposomes were immobilized onto a glass surface and challenged with bacteria and proteins (including cholera toxin). The *in vitro* assay used confocal microscopy, ELISA, or genetic-based detection systems to determine bacterial and toxin interactions.

Microemulsified liposomes were effective biomembrane models for studying cellular interactions. The eukaryotic receptor biomolecule laminin (LN), a glycoprotein, was incorporated into unilamellar biotinylated liposomes. LN liposomes were stable for approximately four months. After incubation with the labeled proteins in solution, specific interactions between LN liposomes were observed with CLSM. CNF-CTB was co-localized proximate to LN liposomes while co-localization was absent with CNF-BLF, CNF-BSA, and CNF-OVA samples.

Again, *in vitro* capture of *E. coli* O157:H7, *S. enteritidis*, *L. monocytogenes*, and *L. innocua* with LN liposomes was investigated using ELISAs and confirmed by PCR analysis, as was described with GM1 and GM3 liposomes. Capture of individual species with LN liposomes was determined in the absence and presence of other species at the same inoculation level. Specific adhesion and capture of both of the *Listeria* species was evidenced on LN liposomes when compared to control liposomes lacking the glycoprotein.

Considering the ELISAs and PCR capture detections, *L. monocytogenes* and *L. innocua* were captured more frequently on LN liposomes when compared to liposomes, indicating *in vitro* that these organisms interact with this glycoprotein *in vivo*. *E. coli* O157:H7 and *S. enteritidis* were not discriminately captured with LN liposomes compared to the control liposomes.

For all species, inoculation levels were correlated to capture when the organism exhibited an interaction to biomimetic liposomes (GM1, GM3, or LN liposomes). Also, with respect to the simultaneous multiple species capture, evidence of a bacterial competition for receptors and ultimately adhesion was evident. A hundred fold excess of a competing species prevented capture of another species with the biomimetic liposomes whereas, in the absence of the competing species, capture was evident. In mixed populations inoculated at equal concentrations, biomimetic liposome binding and capture was nearly identical to that found in the absence of competing organisms.

CONCLUSIONS

It was hypothesized that known receptor biomolecules could be embedded or associated with the artificial bilayers of immobilized microemulsified liposomes to determine bioactivity *in vitro*. Methods were developed, resulting in the immobilization of stable, unilamellar liposomes on glass, to observe bilayer encapsulation or probes and specific interactions of proteins and bacteria with receptor molecules embedded in artificial bilayers using CLSM, ELISA, and PCR detection. The liposomes interacted with and captured proteins and bacteria from solution. CTB, BLF and *E. coli* O157:H7

specifically bound GM1 liposomes. *L. monocytogenes* and *L. innocua* bound LN liposomes. *S. enteritidis* nonspecifically bound to all liposome types. Simultaneous assays with multiple species found that the receptor associated captures were relatively independent of competitive microorganisms, when inoculated at equal concentration. Bacterial capture of all species with GM1 liposomes was initially detected using ELISAs. This was confirmed with extensive statistical analysis of PCR products, and for *E. coli* O157:H7, with microscopy. PCR and exact analysis clearly identified differences in capture among the various inoculation levels (2×10^3 , 2×10^5 , or 2×10^7 CFU/ml) and biomimetic liposomes. These results prove that the receptor molecules investigated retained their *in vivo* biological activity embedded in the artificial membranes of liposomes, and illustrates the potential of using immobilized liposomes as biomimetics to study molecular interactions using a variety of research techniques.

FUTURE RESEARCH

To extend the presented work, technologies such as a fluidized bed or flow system should be incorporated into the capture of organisms with liposomes containing gangliosides or LN. A variety of surfaces could be investigated for improving the efficiency of immobilization of liposomes and sensitivity of bacterial or protein capture. In substitution for endpoint PCR detection, real-time PCR would present an entirely new prospective on surface adhesion and capture of organisms especially at lower inoculation levels than those used in this study. Receptors could be enzymatically modified for capture inhibition studies to investigate adhesion specificity.

Molecular probes are constantly being developed and marketed for specific applications and techniques. There is no doubt that superior probes with greater sensitivity and specificity for either the aqueous lumen or lipid bilayer of liposomes will be available in the future. Probes were selected specific for these applications and the microscopy system using what was available at the onset of the study. Future probes will likely be sensitive to adhesion events and should be investigated for possible signal generation after a binding or capture event.

Additionally, each of the organisms in the study should be monitored before and after capture events. Adhesion resulting in possible rupture of liposomes would be of particular interest for a biosensor platform. Also, the biomolecule containing liposomes constituted an effective, discriminatory capture platform but more work needs to be performed to determine how capture is effected in simultaneous inoculations of multiple species. The number of samples presented in this study is simply too small to accurately describe a competitive effect.

This exploratory work represents only a small cross-section of proteins, toxins, and bacteria that could be similarly investigated using the developed techniques. Bacterial capture with liposomes should be further investigated by incorporating known and theorized receptor biomolecules into artificial membranes. The possibilities for receptor biomolecules and interactants are only limited by the imagination.

APPENDICES

APPENDIX A

LIPOSOME IDENTIFICATION LEGEND

Table A. Guide to identification of microemulsified liposomes listed by liposome type, probed component, fluorescent probe, and monitor channel (red, green, blue). Co-localization of probes indicated by channel mixing (yellow, magenta).

Liposome Type	Probed Component	Fluorescent Probes	Coloration
Control Liposomes	Lipid Bilayer	Fluorescein-PE & NBD-PE	Green
Ganglioside GM1 Liposomes	Lipid Bilayer	Fluorescein-PE & NBD-PE	Green
Liposomes Encapsulated SRB	Aqueous Lumen	Sulforhodamine B	Red
CNF-LN or CNF-EcoMscL Liposomes	Membrane Protein in Bilayer	5-(and-6) Carboxynaphthofluorescein	Blue
CNF-BSA Liposomes	Soluble Protein in Lumen	5-(and-6) Carboxynaphthofluorescein	Blue
Control & GM1 Liposomes Head-Group Labeled Lipid Bilayer Encapsulated SRB Lumen	Lipid Bilayer Aqueous Lumen	Fluorescein-PE & NBD-PE Sulforhodamine B	Yellow (Co-localization)
CNF-LN or CNF-EcoMscL Liposomes Encapsulated SRB Lumen	Membrane Protein in Bilayer Aqueous Lumen	5-(and-6) Carboxynaphthofluorescein Sulforhodamine B	Magenta (Co-localization)
CNF-BSA Liposomes Encapsulated SRB Lumen	Soluble Protein in Lumen Aqueous Lumen	5-(and-6) Carboxynaphthofluorescein Sulforhodamine B	Magenta (Co-localization)

APPENDIX B

PRIMERS FOR PCR IDENTIFICATION IN CHAPTER IV

Table B. Selected primers used in PCR identification

Sequence name	Sequence 5' to 3'	PCR product (bp)	Organisim	References
PF8 PR8	CGTGATGATGTTGAGTTG AGATTGGTTGGCATTACTG	420	<i>E. coli</i> O157:H7	1-2
ino2 Lis1b	ACTAGCACTCCAGTTGTTAAAC TTATACGCGACCGAAGCCAAC	870	<i>L. innocua</i>	3-4
Lis1b MonoA	TTATACGCGACCGAAGCCAAC CAAACGTGCTAACACAGCTACT	660	<i>L. monocytogenes</i>	3-4
139 141	GTGAAATTATCGCCACGTTTCGGGCAA TCATCGCACCGTCAAAGGAACC	284	<i>S. enteritidis</i>	5-8

1. Maurer J, Schmidt D, Petrosko P, Sanchez S, Bolton L, Lee M. Development of primers to O-antigen biosynthesis genes for specific detection of *Escherichia coli* O157 by PCR. Appl Environ Microbiol 1999; 65(7):2954-2960.
2. Osek J. Rapid and specific identification of Shiga toxin-producing *Escherichia coli* in faeces by multiplex PCR. Lett Appl Microbiol 2002; 34:304-310.
3. Lippens W. Thesis: Rapid detection of *Listeria monocytogenes*, Nutrition and Food Science. Utah State University: Logan, UT 2003.
4. Bubert A, Hein I, Rauch M, Lehner A, Yoon B, Goebel W, Wagner M. Detection and differentiation of *Listeria* spp. by a single reaction based on multiplex PCR. Appl Environ Microbiol 1999; 65:4688-4692.
5. Harrington E. Thesis: Rapid detection of *Salmonella enteritidis*, Nutrition and Food Science. Utah State University: Logan, UT 2004.
6. Malorny B, Hoorfar J, Bunge C, Helmuth R. Multicenter validation of the analytical accuracy of *Salmonella* PCR: towards an International standard. Appl Environ Microbiol 2003; 69(1):290-296.
7. Rahn K, Grandis SD, Clarke R, McEwen S, Galan J, Ginocchio C, III RC, Gyles C. Amplification of an *invA* gene sequence of *Salmonella typhimurium* by polymerase chain reaction as a specific method of detection of *Salmonella*. Mol Cell Probes 1992; 6:271-279.
8. Scholz H, Arnold T, Marg H, Rosler U, Hensel A. Improvement of an *invA*-based PCR for the specific detection of *Salmonella typhimurium* in organs of pigs. Berl Munch Teirarztl Wochenschr 2001; 114(9-10):401-403.

APPENDIX C

ELISA ABSORBANCE VALUES FOR
CHAPTER IV STATISTICAL ANALYSIS (T-TESTS)**Table C-1.** Individual species capture of *E. coli* O157:H7 with GM1 liposomes verified by ELISA

Molar percent GM1	<i>E. coli</i> O157:H7 inoculation level	Absorbance at 405 nm			Mean absorbance \pm SD	p-value ¹
0.0%	0.0 x 10 ⁰	0.053	0.062	0.052	0.056 \pm 0.006	
0.0%	2.0 x 10 ³	0.062	0.071	0.060	0.064 \pm 0.006	0.0015
0.0%	0.0 x 10 ⁰	0.041	0.050	0.056	0.049 \pm 0.008	
0.0%	2.0 x 10 ⁵	0.046	0.043	0.046	0.045 \pm 0.002	0.4748
0.0%	0.0 x 10 ⁰	0.048	0.043	0.049	0.047 \pm 0.003	
0.0%	2.0 x 10 ⁷	0.046	0.035	0.054	0.045 \pm 0.010	0.7007
0.0089%	0.0 x 10 ⁰	0.061	0.052	0.066	0.060 \pm 0.007	
0.0089%	2.0 x 10 ³	0.048	0.042	0.050	0.047 \pm 0.004	0.0173
0.0089%	0.0 x 10 ⁰	0.043	0.050	0.047	0.047 \pm 0.004	
0.0089%	2.0 x 10 ⁵	0.042	0.041	0.039	0.041 \pm 0.002	0.1399
0.0089%	0.0 x 10 ⁰	0.052	0.048	0.050	0.050 \pm 0.002	
0.0089%	2.0 x 10 ⁷	0.042	0.039	0.041	0.041 \pm 0.002	0.0013
0.089%	0.0 x 10 ⁰	0.045	0.041	0.044	0.043 \pm 0.002	
0.089%	2.0 x 10 ³	0.052	0.048	0.059	0.053 \pm 0.006	0.0684
0.089%	0.0 x 10 ⁰	0.051	0.055	0.049	0.052 \pm 0.003	
0.089%	2.0 x 10 ⁵	0.052	0.057	0.049	0.053 \pm 0.004	0.2254
0.089%	0.0 x 10 ⁰	0.049	0.048	0.049	0.049 \pm 0.001	
0.089%	2.0 x 10 ⁷	0.052	0.049	0.053	0.051 \pm 0.002	0.0942
0.89%	0.0 x 10 ⁰	0.047	0.048	0.052	0.049 \pm 0.003	
0.89%	2.0 x 10 ³	0.049	0.044	0.064	0.052 \pm 0.010	0.5492
0.89%	0.0 x 10 ⁰	0.060	0.058	0.061	0.060 \pm 0.002	
0.89%	2.0 x 10 ⁵	0.045	0.061	0.058	0.055 \pm 0.009	0.4444
0.89%	0.0 x 10 ⁰	0.053	0.061	0.055	0.056 \pm 0.004	
0.89%	2.0 x 10 ⁷	0.045	0.045	0.051	0.047 \pm 0.003	0.1181
8.9%	0.0 x 10 ⁰	0.066	0.065	0.070	0.067 \pm 0.003	
8.9%	2.0 x 10 ³	0.107	0.119	0.110	0.112 \pm 0.006	0.0099
8.9%	0.0 x 10 ⁰	0.073	0.062	0.077	0.071 \pm 0.008	
8.9%	2.0 x 10 ⁵	0.104	0.114	0.108	0.109 \pm 0.005	0.0323
8.9%	0.0 x 10 ⁰	0.076	0.082	0.072	0.077 \pm 0.005	
8.9%	2.0 x 10 ⁷	0.105	0.116	0.112	0.111 \pm 0.006	0.0085

¹ Pairwise comparison of absorbance values of inoculated and uninoculated control on same plate

Table C-2. Individual species capture of *S. enteritidis* with GM1 liposomes verified by ELISA

Molar percent GM1	<i>S. enteritidis</i> inoculation level	Absorbance at 405 nm			Mean absorbance ± SD	p-value ¹
0.0%	0.0 x 10 ⁰	0.055	0.072	0.058	0.062 ± 0.009	
0.0%	2.0 x 10 ³	0.065	0.087	0.060	0.071 ± 0.014	0.1406
0.0%	0.0 x 10 ⁰	0.065	0.062	0.073	0.067 ± 0.006	
0.0%	2.0 x 10 ⁵	0.058	0.057	0.059	0.058 ± 0.001	0.0865
0.0%	0.0 x 10 ⁰	0.048	0.051	0.052	0.050 ± 0.002	
0.0%	2.0 x 10 ⁷	0.047	0.047	0.057	0.050 ± 0.006	1.0000
0.0089%	0.0 x 10 ⁰	0.065	0.064	0.065	0.065 ± 0.001	
0.0089%	2.0 x 10 ³	0.052	0.065	0.057	0.058 ± 0.007	0.2451
0.0089%	0.0 x 10 ⁰	0.049	0.071	0.046	0.055 ± 0.014	
0.0089%	2.0 x 10 ⁵	0.041	0.062	0.042	0.048 ± 0.012	0.0445
0.0089%	0.0 x 10 ⁰	0.052	0.054	0.067	0.058 ± 0.008	
0.0089%	2.0 x 10 ⁷	0.043	0.053	0.051	0.049 ± 0.005	0.1835
0.089%	0.0 x 10 ⁰	0.052	0.061	0.052	0.055 ± 0.005	
0.089%	2.0 x 10 ³	0.060	0.067	0.061	0.063 ± 0.004	0.0130
0.089%	0.0 x 10 ⁰	0.049	0.071	0.046	0.055 ± 0.014	
0.089%	2.0 x 10 ⁵	0.041	0.062	0.042	0.048 ± 0.012	0.0445
0.089%	0.0 x 10 ⁰	0.052	0.054	0.067	0.058 ± 0.008	
0.089%	2.0 x 10 ⁷	0.043	0.053	0.051	0.049 ± 0.005	0.1835
0.89%	0.0 x 10 ⁰	0.049	0.042	0.058	0.050 ± 0.008	
0.89%	2.0 x 10 ³	0.029	0.027	0.037	0.031 ± 0.005	0.0097
0.89%	0.0 x 10 ⁰	0.051	0.061	0.064	0.059 ± 0.007	
0.89%	2.0 x 10 ⁵	0.048	0.056	0.061	0.055 ± 0.007	0.0315
0.89%	0.0 x 10 ⁰	0.053	0.076	0.049	0.059 ± 0.015	
0.89%	2.0 x 10 ⁷	0.046	0.073	0.045	0.055 ± 0.016	0.0604
8.9%	0.0 x 10 ⁰	0.053	0.063	0.062	0.059 ± 0.006	
8.9%	2.0 x 10 ³	0.086	0.115	0.103	0.101 ± 0.015	0.0168
8.9%	0.0 x 10 ⁰	0.068	0.058	0.075	0.067 ± 0.009	
8.9%	2.0 x 10 ⁵	0.111	0.081	0.101	0.098 ± 0.015	0.0388
8.9%	0.0 x 10 ⁰	0.076	0.074	0.067	0.072 ± 0.005	
8.9%	2.0 x 10 ⁷	0.104	0.094	0.111	0.103 ± 0.009	0.0491

¹ Pairwise comparison of absorbance values of inoculated and uninoculated control on same plate

Table C-3. Individual species capture of *E. coli* O157:H7 with GM1 liposomes verified by ELISA

Molar percent GM1	<i>E. coli</i> O157:H7 inoculation level	Absorbance at 405 nm			Mean absorbance ± SD	p-value ¹
0.0%	0.0 x 10 ⁰	0.058	0.046	0.055	0.062 ± 0.007	
0.0%	2.0 x 10 ³	0.055	0.062	0.068	0.061 ± 0.006	0.2794
0.0%	0.0 x 10 ⁰	0.043	0.052	0.055	0.050 ± 0.006	
0.0%	2.0 x 10 ⁵	0.041	0.059	0.053	0.051 ± 0.009	0.7706
0.0%	0.0 x 10 ⁰	0.066	0.048	0.053	0.056 ± 0.009	
0.0%	2.0 x 10 ⁷	0.060	0.051	0.047	0.053 ± 0.007	0.4223
8.9%	0.0 x 10 ⁰	0.077	0.070	0.063	0.070 ± 0.004	
8.9%	2.0 x 10 ³	0.108	0.115	0.111	0.111 ± 0.007	0.0169
8.9%	0.0 x 10 ⁰	0.064	0.066	0.071	0.067 ± 0.004	
8.9%	2.0 x 10 ⁵	0.110	0.118	0.112	0.113 ± 0.004	0.0047
8.9%	0.0 x 10 ⁰	0.068	0.071	0.074	0.071 ± 0.003	
8.9%	2.0 x 10 ⁷	0.102	0.114	0.114	0.110 ± 0.007	0.0045

¹ Pairwise comparison of absorbance values of inoculated and uninoculated control on same plate

Table C-4. Individual species capture of *S. enteritidis* with GM1 liposomes verified by ELISA

Molar percent GM1	<i>S. enteritidis</i> inoculation level	Absorbance at 405 nm			Mean absorbance ± SD	p-value ¹
0.0%	0.0 x 10 ⁰	0.055	0.041	0.059	0.052 ± 0.009	
0.0%	2.0 x 10 ³	0.061	0.069	0.053	0.061 ± 0.008	0.4475
0.0%	0.0 x 10 ⁰	0.056	0.048	0.052	0.052 ± 0.004	
0.0%	2.0 x 10 ⁵	0.051	0.053	0.046	0.050 ± 0.004	0.6265
0.0%	0.0 x 10 ⁰	0.051	0.055	0.060	0.055 ± 0.005	
0.0%	2.0 x 10 ⁷	0.046	0.045	0.056	0.049 ± 0.006	0.0762
8.9%	0.0 x 10 ⁰	0.058	0.061	0.057	0.059 ± 0.002	
8.9%	2.0 x 10 ³	0.093	0.096	0.084	0.091 ± 0.006	0.0067
8.9%	0.0 x 10 ⁰	0.063	0.061	0.058	0.061 ± 0.003	
8.9%	2.0 x 10 ⁵	0.101	0.090	0.092	0.094 ± 0.006	0.0059
8.9%	0.0 x 10 ⁰	0.064	0.059	0.065	0.063 ± 0.003	
8.9%	2.0 x 10 ⁷	0.109	0.094	0.113	0.105 ± 0.010	0.0084

¹ Pairwise comparison of absorbance values of inoculated and uninoculated control on same plate

Table C-5. Individual species capture of *L. monocytogenes* with GM1 liposomes verified by ELISA

Molar percent GM1	<i>L. monocytogenes</i> inoculation level	Absorbance at 405 nm			Mean absorbance \pm SD	p-value ¹
0.0%	0.0×10^0	0.068	0.067	0.051	0.062 ± 0.010	
0.0%	2.0×10^3	0.068	0.051	0.062	0.060 ± 0.009	0.8513
0.0%	0.0×10^0	0.046	0.059	0.061	0.055 ± 0.008	
0.0%	2.0×10^5	0.041	0.053	0.061	0.052 ± 0.010	0.1869
0.0%	0.0×10^0	0.071	0.048	0.061	0.060 ± 0.012	
0.0%	2.0×10^7	0.039	0.047	0.051	0.046 ± 0.006	0.2598
8.9%	0.0×10^0	0.068	0.074	0.068	0.070 ± 0.003	
8.9%	2.0×10^3	0.072	0.064	0.082	0.073 ± 0.009	0.7385
8.9%	0.0×10^0	0.072	0.066	0.065	0.068 ± 0.004	
8.9%	2.0×10^5	0.065	0.081	0.062	0.069 ± 0.010	0.8284
8.9%	0.0×10^0	0.073	0.055	0.081	0.070 ± 0.013	
8.9%	2.0×10^7	0.066	0.071	0.063	0.037 ± 0.004	0.7928

¹ Pairwise comparison of absorbance values of inoculated and uninoculated control on same plate

Table C-6. Individual species capture of *L. innocua* with GM1 liposomes verified by ELISA

Molar percent GM1	<i>L. innocua</i> inoculation level	Absorbance at 405 nm			Mean absorbance \pm SD	p-value ¹
0.0%	0.0×10^0	0.088	0.067	0.058	0.071 ± 0.015	
0.0%	2.0×10^3	0.065	0.051	0.069	0.062 ± 0.009	0.4629
0.0%	0.0×10^0	0.038	0.041	0.051	0.043 ± 0.007	
0.0%	2.0×10^5	0.041	0.053	0.083	0.059 ± 0.022	0.2091
0.0%	0.0×10^0	0.063	0.045	0.072	0.060 ± 0.014	
0.0%	2.0×10^7	0.063	0.048	0.061	0.057 ± 0.008	0.5949
8.9%	0.0×10^0	0.071	0.074	0.081	0.075 ± 0.005	
8.9%	2.0×10^3	0.088	0.090	0.082	0.087 ± 0.004	0.1599
8.9%	0.0×10^0	0.092	0.041	0.044	0.059 ± 0.029	
8.9%	2.0×10^5	0.071	0.068	0.056	0.065 ± 0.008	0.7133
8.9%	0.0×10^0	0.051	0.066	0.071	0.063 ± 0.010	
8.9%	2.0×10^7	0.091	0.062	0.051	0.068 ± 0.021	0.7943

¹ Pairwise comparison of absorbance values of inoculated and uninoculated control on same plate

CURRICULUM VITAE

Bradley Jay Taylor

555 North 300 East, Logan UT 84321

bjtaylorski@yahoo.com

435.787.1093

Academic Preparation:**Utah State University**

* Ph.D. Nutrition and Food Science 2004

Logan, UT

* GPA 3.92/4.00

Brigham Young University

* B.S. in Food Science 1999

Provo, UT

* Cum Laude

* GPA 3.79/4.00

Work Experience:**Food Chemistry and Microbiology Research Assistant/Lab Technician***Logan, Utah**Jan. '00 to May '04*

* Perform graduate research involving development of a liposome-based biomimetic capturing proteins and pathogenic microorganisms

* Perform dairy protein purification, analysis and test protein functionality in food systems

Quality Assurance Internship Nestle's Frozen Foods*Springville, Utah**Sept. '99 to Dec. '99*

* Performed microbiological sampling and to monitor contamination of processing equipment

* Enforced plant's HACCP program and performed QA audits

Sensory Lab/Research Assistant*Provo, Utah**May '98 to Dec. '99*

* Planed, organized, and ran taste panels conducted under Dr. Lynn Ogden's supervision at BYU's sensory facility

* Experiment with packaging, processing and formulation of patented carbonated "Sparkling" yogurt product

Quality Assurance Technician*Provo, Utah**Feb. '98 to May '98*

* Administered quality assurance tests on a variety of thermally processed food products produced throughout the U.S. and Canada

Laboratory Experience:

* ELISA & PCR detection

* Laser Scanning Confocal Microscopy

* Sensory Analysis

* Food Analysis

* Food Chemistry

* Protein Purification

* Dairy Processing

* Food Microbiology

Foreign Language Skills:

* Fluent in the Polish language

Activities:

- *Utah State University Graduate Student Senate Treasurer 2001-2002
- *Utah State University Graduate Student Senate Activities Chair 2000-2001
- *Utah State University Food Science Club Treasurer 2000-2003
- *Brigham Young University Food Science Club Treasurer 1999
- *Participated in the '98-'02 IFT Food Science College Bowl Competitions
- *Participated in the '98 IAFIS Collegiate Dairy Products Evaluation Contests

Honors and Awards:

- *Researcher of the Year, College of Agriculture, Utah State University '04
- *Utah State University Graduate Research Assistantship '01-'04
- *Recipient of the Ghandi Scholarship '00-'01
- *Academic University Scholarship Recipient '95, '97, '98, '99
- *Department of FSN Leadership Scholarship Recipient '98, '99
- *Deans List (multiple semesters at both universities)
- *Western Regional Champion IFTSA College Bowl '99 and '02
- *Most Creative DMI Product Development Competition, *Whey Krunchers* '00
- *Third place, IFT Product Development Competition, *Whey Krunchers* '00

Professional Memberships:

- *Institute of Food Technologists (IFT)

Publications:

- *Bunch, T.D., R.C. Evans, S. Wang, C.P. Brennan, D.R. Whittier, and B.J. Taylor. Lamb growth rates, feed efficiency, carcass evaluation, cholesterol level and sensory evaluation of various hair x wool sheep crosses. (accepted 2003) Small Ruminant Research.
- *Taylor, B.J. and M.K. Walsh. 2002. Development and sensory analysis of a textured whey protein meatless patty. *Journal of Food Science*. Vol. 67(4), 1555-1558

Presentations:

- *Poster Presentation: "*Escherichia coli* O157:H7 capture with GM1 containing liposomes verified by surface ELISA" B.J. Taylor, M.K. Walsh, and B.C. Weimer. (2003) National Meeting of the Institute of Food Technologists, Chicago, IL.
- *Poster Presentation: "Sensory Analysis of Whey Protein Patties" B.J. Taylor and M.K. Walsh. (2001) National Meeting of the Institute of Food Technologists, New Orleans, LA.

Press Releases:

- *No Whey! USU students create award-winning snack food. Salt Lake Tribune, July 2000.
- *New food solutions from extrusion. Prepared Foods. July 2000.
- *USU team puts food to the test. Utah Statesman. May 2002.